UNIVERSITÀ DEGLI STUDI FIRENZE
Da un secolo, oltre.

European Laboratory for Non-Linear Spectroscopy

International Doctorate in Atomic and Molecular Photonics
Ciclo XXXVIII

Terahertz Spectroscopy of Hydration Water in Crowded Protein Solutions

Candidate

Luigi Caminiti (ID number DT31601)

Thesis Advisors

Prof. Renato Torre

Firmato digitalmente da RENATO TORRE
Data: 09/02/2026 16:07:42 CET

Coordinator

Prof. Diederik Wiersma

Academic Year 2022/2025

Terahertz Spectroscopy of Hydration Water in Crowded Protein Solutions
PhD thesis. University of Florence

This thesis has been typeset by LaTeX and the UniFiTh class.

Author's email: caminiti@lens.unifi.it

Abstract

The dynamics of hydration water surrounding biomolecules play a crucial role in determining their structural stability, conformational flexibility, governing many of their interactions in the cellular environment. In crowded conditions, where high macromolecular concentrations prevail, water cannot be regarded as a passive solvent but instead acts as an active participant that mediates both intra- and intermolecular processes. Although the subject has been the focus of several studies, a clear description of how hydration water is affected by the presence of biomolecules has not been achieved. This thesis explores the structural and dynamical properties of hydration water in highly concentrated aqueous protein solutions, by combining a variety of optical and terahertz spectroscopic techniques spanning complementary frequency and time domains.

The first part of the work reports an Optical Kerr Effect spectroscopic study on water-lysozyme solutions at increasing concentrations. It was possible the direct separation of the contributions of bulk water, hydration water, and protein, revealing two distinct structural relaxation processes in the hydration shell. The faster process, occurring on a few-picosecond timescale, is associated with hydrogen-bond exchange dynamics, whereas the slower process, extending over tens of picoseconds, originates from water reorganization coupled to protein surface fluctuations. Two vibrational intermolecular modes of hydration water were also identified, corresponding to the bending and stretching vibrations of the hydrogen bond network. The amplitudes of both structural and vibrational components exhibit a marked discontinuity near the lysozyme concentration of 200–225 mg/mL, indicating a crossover in the hydration regime connected to the onset of protein clustering.

Terahertz time-domain spectroscopy investigation were conducted on the same water-lysozyme samples, in attenuated total reflection geometry. Absorption coefficients and the refractive index were measured in the 0.1–3 THz frequency range at temperatures between 4 and 35 °C. The results show that at lower temperatures, the absorption coefficient of hydration water strongly depends on protein concentration. At higher temperatures, this dependence weakens, suggesting effects of enhanced instability and polydispersity of clusters.

Measurements with a THz Fourier-transform infrared spectrometer were performed in the ZEMOS laboratory at Ruhr-Universität in Bochum (GER), enabled access to the full spectral range up to 18 THz. The analysis, based on the THz calorimetry framework, allowed the identification and quantification of two distinct hydration water populations: 'hydrophobic wrap' water, characterized by a red-shifted absorption band around 150 cm^{-1}, and 'hydrophilic bound' water, identified by the positive slope in the librational region (400–600 cm^{-1}). Complementary Dynamic Light Scattering measurements confirmed the presence of clusters of varying size, whose growth correlates with the redistribution of water between these two populations. By mapping the variations in the corresponding spectroscopic observables, a specific THz phase diagram for the cluster regime was constructed, clearly differentiating it from the regimes associated with liquid–liquid phase separation and liquid–solid phase separation.

Optical Pump–THz Probe spectroscopy was employed to investigate ultrafast

energy transport in heme proteins (myoglobin and cytochrome *c*). This technique directly tracks the flow of vibrational energy from the optically excited heme group through the protein matrix to the surrounding solvent. By characterising the THz spectrum of hydration water, it was possible to obtain the relaxation times, ranging from 6 to 10 ps and showing a clear isotope effect between H_2O and D_2O, are in excellent agreement with diffusive energy transfer models. These results reveal that thermal energy dissipation occurs predominantly through vibrational diffusion within the protein matrix, followed by coupling to the hydration shell, which strongly influences the characteristic time of this process.

Overall, this study provides new insights into how hydration water reorganizes and mediates the collective behaviour of proteins. The results contribute to the understanding of fundamental mechanisms governing biomolecular hydration, clustering, and phase transitions, and establish terahertz spectroscopy as a powerful tool for probing complex aqueous biological systems.

Contents

Chapter 1

Introduction

Over the years, water has been the focus of extensive investigation. Both theoretical and experimental studies have provided detailed insights into its structural and vibrational dynamics across its different phases. [1–7]. At room temperature, it can be described as a liquid composed of H_2O molecules that form a network through Hydrogen Bonds (HBs). A water molecule forms four HBs with neighbouring molecules. These bonds break and reform on a picoseconds timescale due to thermal fluctuations arising from the excitation of low-frequency modes [8]. The network created by HBs influences and determines the intra- and intermolecular vibrational spectrum of liquid water. Analysis of the higher frequencies, between 1000 and 4000 cm^{-1}, provides information on the dynamics related to intramolecular vibrations, while the spectrum lower than 1000 cm^{-1}, gives us info on the intermolecular dynamics of water.

At room temperature the vibrational spectrum of water in the low-frequency region exhibits two spectral peaks at approximately 50 and 175 cm^{-1}, which are typically ascribed to the bending and stretching vibrations of hydrogen bonds, respectively. A low-frequency component below 10 cm^{-1}corresponds to structural relaxation processes [9], and libration modes are observed above 300 cm^{-1} [10]. The dynamics described are summarised in Figure 1.1.

The importance and the role of water in the development of life is strongly linked to its influence on the myriad biological processes that take place in an aqueous environment. Water is not merely a passive solvent but an active participant in biological processes, modulating biomolecular structure, dynamics, and interactions [11]. Interactions between water molecules and biomolecules occur mainly through hydrogen bonding, with Coulomb forces and hydrophobic interactions playing a less dominant role. All these processes are involved in the structure and folding of the biomolecule and consequently also to the formation of aggregates and other critical phenomena [10–12]. Recent years have seen the development of novel experimental approaches and significant advances in established techniques, enabling investigations across complementary time and length scales [11, 13, 14]. The term *hydration water* or *hydration shell* is employed to denote the aqueous layers that envelop a single protein molecule and interact with it. The component of water that is not influenced by the presence of the molecule is termed *bulk water*. In Figure 1.2 a graphic representation of the results of a molecular dynamic simulation is reported.

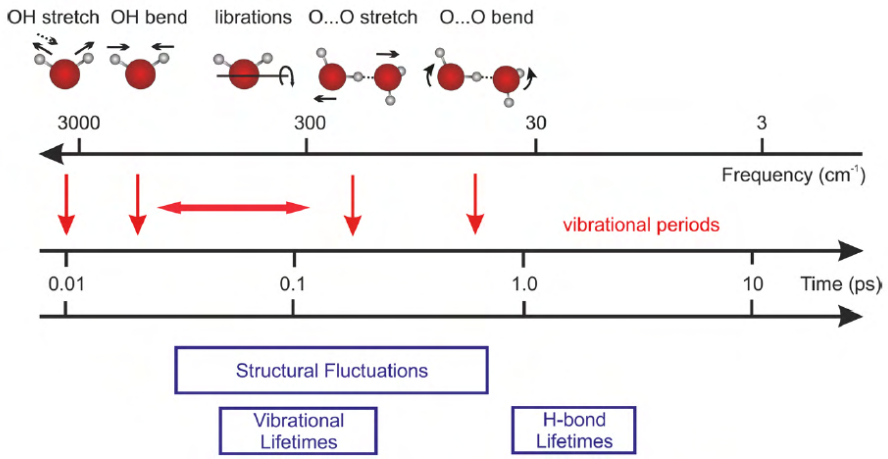

Figure 1.1. *Graphical representation of the characteristic time scales of the intra- and intermolecular dynamics of bulk water. Intramolecular dynamics occupy the high-frequency spectrum, while intermolecular dynamics occupy the low-frequency spectrum. Figure from [10].*

The image shows a lysozyme protein surrounded by hydration water molecules (red) and bulk water molecules (blue).

Changes in the properties of water molecules due to the presence of the biomolecule determines which molecules are classified as hydration molecules and which as bulk molecules. For this reason, there is no universal definition of hydration water, and the interpretation of what constitutes the hydration shell of a biomolecule typically depends on the nature of the technique used to probe the structural and dynamic properties of the system. [11].

Topic of debate concern the thickness of the hydration shell, with reported estimates ranging from a single water layer to more than 20 Å[16]. Most experimental techniques, particularly those probing structural properties or single-particle dynamics on picosecond or longer timescales, such as X-ray and neutron scattering [17], nuclear magnetic relaxation dispersion (NMRD) [18], and most molecular dynamics (MD) simulations [19], indicate that the influence of a biomolecule on surrounding water is short-ranged, yielding a hydration shell thickness of roughly one to two water molecules ($\sim$ 3–5 Å). In contrast, studies focusing on collective dynamics typically using terahertz spectroscopy [16, 20] or dielectric spectroscopy [21], along with some MD simulations [22, 23], report a much longer-range effect, estimating the average hydration shell thickness to exceed 10 Å, correspondingly approximately to 3–5 hydration layers. The quantitative definition of the hydration shell is challenging, as it is extremely difficult to establish the amount of water significantly influenced by the presence of the protein. It is reasonable to hypothesise that the shell consists of various layers of water molecules, which behave differently depending on their distance from the protein. The first layer is formed by water molecules that are in direct contact with the surface of the protein. Subsequent layers exhibit reduced sensitivity to the interaction with the protein until reaching layers of water that are distant from the surface. These layers possess a structure and

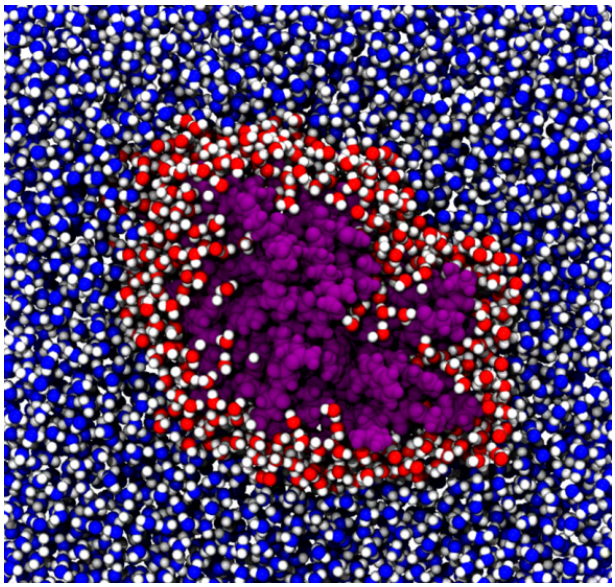

Figure 1.2. *Visual representation of the results of a Molecular Dynamic simulation of a water-protein system. The protein is a lysozyme (purple spheres), surrounded by water molecules: hydration water (in red) and bulk water (in blue). Figure from [15].*

dynamics that are analogous to those of bulk water [10]. Regarding the dynamics of hydration water, the hydration shells are often depicted as static arrangements of water molecules. In reality, these molecules do not freeze, instead their molecular dynamics are slowed down, extending the characteristic timescale from that of bulk water, on the order of a few picoseconds [24] to approximately 10–100 ps [25, 26], 1–10 ns [27], and in some cases even up to 1 μs [28], depending on the location and degree of binding to the biomolecule. The distribution of these characteristic timescales of water dynamics within the hydration shell represents one of the most critical parameters for describing biomolecular hydration [29].

The aim of this thesis is to deepen and improve our understanding of the profound mutual dependence between proteins and the hydration water that surrounds them when dissolved in aqueous solutions. The studies presented here primarily address the effects of protein crowding, serving as a basis to elucidate the mechanisms underlying critical phenomena such as liquid–liquid phase separation (LLPS), amyloid formation and related processes connected with the crowded environment. To achieve this goal, numerous investigations have been conducted on the spectroscopic properties of hydration water, combining various techniques to study water-protein solutions.

The protein mainly studied in this work is lysozyme, a globular protein whose characteristics are representative of several general biological phenomena involving proteins. Lysozyme from the white of hen eggs (HEWL), possesses a remarkably human-like tertiary structure and can easily form amyloid aggregates in vitro. This property is critical for understanding the molecular pathways leading to the formation of amyloid oligomers and mature amyloid fibrils [30–32], which are implicated in numerous degenerative diseases [33]. Furthermore, lysozyme is one of the few

basic proteins with a high isoelectric point (pH $\sim$ 11), which allows straightforward tuning of the surface charge by adjusting the pH, ionic strength, or protein concentration. This features makes lysozyme a valuable model system for investigating the role of excluded volume effects and interaction potentials in the formation of transient protein clusters [34–36].

Protein clustering in lysozyme–water solutions is closely connected to the phenomenon of liquid-liquid phase separation [37–39]. LLPS results in the coexistence of a dilute phase and a dense protein-rich phase, with different aggregate structures forming under slight variations of physical parameters such as ionic strength, concentration, and temperature. Hydration water plays a pivotal role in the regulation of these condensation phenomena, thereby unveiling a close correlation between the properties of water and the reorganization of proteins in solution. The process of condensate formation is accompanied by the release of the so called 'hydrophobic water' (i.e. molecules that hydrate non-polar moieties), while 'hydrophilic water' (i.e. molecules that hydrate polar moieties) remains within the condensate [12, 40–42]. The effect of protein crowding in aqueous solutions was the main focus of this study, with particular attention to how the resulting clusters impact the properties of hydration water. The techniques used are mainly using optical infrared and THz sources, both time-resolved ultrafast techniques such as the Optical Kerr Effect (OKE), THz-Time Domain Spectroscopy (THz-TDS), Optical Pump-THz Probe (OPTP), and frequency-resolved techniques such as THz-Fourier Transform FTIR in the THz region. The combined use of different spectroscopic techniques probing distinct physical observables, has provided a broader description of the properties of hydration water, revealing several effects that are not always detectable by individual techniques.

Optical Kerr effect measurements as a function of protein concentration are reported in the second chapter. In particular, varying the protein concentration allows to distinguish two distinct structural relaxation processes: hydrogen-bond exchange and water reorganization driven by protein surface fluctuations, in addition to sub-picosecond vibrational dynamics. Notably, a concentration-dependent crossover point was identified, marking a transition between two hydration clustering regimes and indicating a threshold for protein crowding. Part of this study was conducted during my Master's thesis work ("*Water-Protein Interaction Investigated by Ultra-Fast Non-Linear Spectroscopy*", University of Florence, 2020/2021) and finds a final comprehensive interpretation in this chapter and in the related publication [43].

The significant results of this study raised the question of whether similar critical effects on the characteristics of hydration water, as observed through OKE spectroscopy, could also be detected using other spectroscopic techniques. To address this question, the water-lysozyme samples studied in the OKE experiment, were further investigated using two additional techniques based on THz spectroscopy. The first experiment is a THz-Time Domain Spectroscopy study in the frequencies range between 0.1-3 THz. The results of these measurements are shown in the third chapter. These measurements revealed that the dependence on the concentration of hydration water absorption coefficients is also influenced by the temperature of the system. The variation in clusters structures with temperatures may explain the different behaviour observed.

The second technique involved a THz FTIR spectrometer, and the results are shown in the fourth chapter. These measurements were carried out at the Ruhr Universität in the ZEMOS center in Bochum (GER) during the abroad period of six months spent in the Professor Martina Havenith's research group. The results of these measurements allowed to distinguish the behaviour of the *hydrophobic* and *hydrophilic* components of hydration water and to interpret the thermodynamic properties of the samples as the lysozyme concentration varied.

The fifth chapter discusses the results of measurements carried out at the ZEMOS laboratories in Bochum. These measures investigated solutions of myoglobin and cytochrome *c* dissolved in H_2O and D_2O using an OPTP setup. This technique made it possible to extract the characteristic times of energy transport through the protein and its coupling with the solvent.

The sixth and last chapter of the thesis presents the conclusions and outlines future directions, regarding the possibility of introducing new techniques, as well as the application of those seen in the thesis on samples of different nature.

Chapter 2

Optical Kerr Effect spectroscopic investigation on water-lysozyme solutions

2.1 Introduction

The study presented in this chapter investigates lysozyme solutions in water at different concentrations using the non-linear spectroscopic technique of Heterodyne-Detected Optical Kerr Effect (HD-OKE).

A wide range of experimental approaches have been employed to study water–lysozyme solutions. However, only a limited number of techniques have specifically focused on the dynamics of hydration water, as separating its contribution from those of the protein and bulk solvent remains inherently challenging. Optical spectroscopic techniques have emerged as a promising means for probing ultrafast dynamics and thus capture the behaviour of hydration water. Both frequency-domain and time-domain spectroscopic studies have been reported, providing invaluable insights into the interactions and dynamics of lysozyme [44–50]. Nevertheless, these experiments have not yet fully resolved the detailed dynamics of hydration water. Earlier time-resolved measurements [47, 48] primarily focused on protein motions, without thoroughly addressing water dynamics. More recent studies in both the frequency domain [44, 45] and the time domain [49] have instead employed a simple exponential relaxation model associated with hydrogen-bond breaking and reformation within the water network to characterise structural dynamics. However, these analyses did not reveal the presence of the additional structural relaxation process predicted by simulations [15, 51, 52]. Moreover, the intermolecular vibrational modes of hydration water have not been characterised.

In this context, a comprehensive experimental spectroscopic study was carried out using time-resolved Optical Kerr Effect (OKE) measurements on water–lysozyme solutions. The aim of this study was to investigate the ultrafast dynamics of hydration water and to evaluate the effects of crowding as a function of protein concentration. The results provide detailed information on both the structural and vibrational dynamics of hydration water over a broad concentration range. The findings of the present study confirm the existence of two distinct relaxation processes:

one associated with hydrogen-bond exchange dynamics and the other with water reorganization driven by protein structural fluctuations. A thorough examination of the fast vibrational and slow structural components reveals that several measurable parameters undergo significant changes at a specific critical protein concentration. This observation suggests a potential correlation with the onset of cluster formation.

Heterodyne-Detected Optical Kerr Effect (HD-OKE) is a nonlinear time-domain spectroscopic technique [9, 53–55]. In this method, a non-resonant, linearly polarized pump pulse induces a transient anisotropy in the refractive index of an optically transparent, isotropic sample. The resulting material response is probed by a delayed, circularly polarized pulse, allowing direct measurement of the relaxation dynamics of the non-equilibrium coherent state generated by the pump pulse. The temporal that can be investigated spans from a few femtoseconds to several tens of picoseconds.

The signal measured in the HD-OKE experiment can be expressed as [55]:

$$S(t) \propto \int_{-\infty}^{+\infty} \left[\gamma\,\delta(t-t') + R(t-t')\right] G(t')\,dt' \tag{2.1}$$

where $\gamma\delta(t)$ is the instantaneous electronic response, $R(t)$ is the third-order nuclear response of the sample, and $G(t)$ is the instrumental function. The latter represents the temporal cross correlation of the pump and probe laser pulses. An accurate evaluation of the instrumental function is a critical element of an HD-OKE measurement for a correct extraction of the sample response function [55, 56]. A reliable procedure for extracting the instrumental function consists of performing a measurement on a calcium fluoride (CaF_2) plate placed inside the sample cuvette. The simple nuclear response of CaF_2 enables an accurate determination of the instrumental function [55]. However, this approach could not be implemented due to the limited size of the cuvette. In *C. Calvagna et al.* [56] it was demonstrated that an artificial instrumental function can be constructed by fitting the rising edge of the electronic peak with an analytical function, which, combined with its symmetric counterpart, generates a simulated instrumental response. Although this approach is less accurate than the procedure based on the CaF_2 reference, it provides the best compromise when the optimal method cannot be applied. For this reason, the instrumental function $G(t)$ was extracted using this procedure.

The response function $R(t)$ is directly related to the time derivative of the correlation function of first order equilibrium susceptibility $\chi(t)$:

$$R(t) \propto -\frac{\partial}{\partial t}\langle\chi(t)\chi(0)\rangle \tag{2.2}$$

The $\chi(t)$ is defined by the dynamics of the entire molecular system investigated and includes many intra- and inter-molecular motions; so, its expression can be very complex and can be hardly described by a rigorous molecular model. Nevertheless, in the case of protein-water solutions, a general separation of the dynamic time scales is present [57]; in the fast sub-picosecond time scale the dynamics are mainly due to the vibrational dynamics of intra-molecular modes of protein and inter-molecular HBs modes of water, while beyond the picosecond time scale, the dynamics are prevalently associated with the overall water structural relaxations.

The dynamics of the protein structural transitions and rotational diffusion are very slow and not accessible in the time window probed in the present experiment. The Fourier transform of the HD-OKE response function, $R(\omega)$, is directly connected with the spectrum measured in a Raman Depolarized Light-Scattering experiment. The imaginary part of $R(\omega)$, $\mathrm{Im}[R(\omega)]$, is obtained by Fourier transforming the measured HD-OKE signals after the deconvolution process from the instrumental function:

$$\mathrm{Im}[R(\omega)] = \mathrm{Im}\left[\frac{S(\omega)}{G(\omega)}\right] \tag{2.3}$$

2.2 Methods

2.2.1 Samples preparation

The HD-OKE measurements are performed on lysozyme water solutions at nine different concentrations (50, 100, 125, 150, 180, 200, 225, 250 and 300 mg/mL). The samples were prepared by dissolving the specified amount of dry powder of Hen Egg White Lysozyme (HEWL) obtained from Sigma Aldrich (L6876) in 1 mL of pure water (S.A.L.F. sterile and non-pyrogenic water for injections). We achieved the complete dissolution using Vortex mixing. All the samples were then filtered with a syringe filter (membrane 0.22 μm pore size) to avoid the introduction of dust. We checked the pH value of each sample with a pH Meter (istek 730P) to be around 4.8 as expected by the absence of any added acidic solution. The features of our samples ensure that the globular native shape of the protein is preserved, avoiding the formation of stable aggregates during measurements.

2.2.2 HD-OKE experimental setup

The experimental setup used for the OKE measurements is shown in Figure 2.1. The source used is a Ti:Sapphire laser (FUSION model by FEMTOLASER) operating in the mode-locking regime and producing pulses of 15 fs at a central wavelength of 780 nm. A laser pulse propagating in a material medium undergoes a time broadening due to dispersion effects in the material. For short pulses such as those considered here, this effect, due to the passage through lenses, polarisers, phase rotators, reflection on mirrors, and the air itself, is very significant. The first part of the apparatus therefore has the function of compensating for group delay dispersion (GDD), in order to obtain a pulse as close as possible to its Transform Limited in the sample area. The operating principle of this part of the setup is based on the multiple passage of the beam through two prisms so that a negative GDD is introduced into the system, which can be tuned for compensating the positive dispersion accumulated along the entire optical. The beam exiting the compression system is directed to a beam splitter (BS) which divides it into the pump beam and the probe beam. The pump beam is directed in a delay stage composed of a corner cube reflector mirror mounted on a mobile translator. In this way, a known time delay τ can be obtained between the pump pulse and the probe pulse. The pump beam is modulated by a chopper (C) which rotates at a frequency of 3 kHz allowing a Lock-In detection. The polarization of the pump beam is rotated by $\pi/4$ via a $\lambda/2$ plate. The pump is finally focalized by the AL1 lens on the sample.

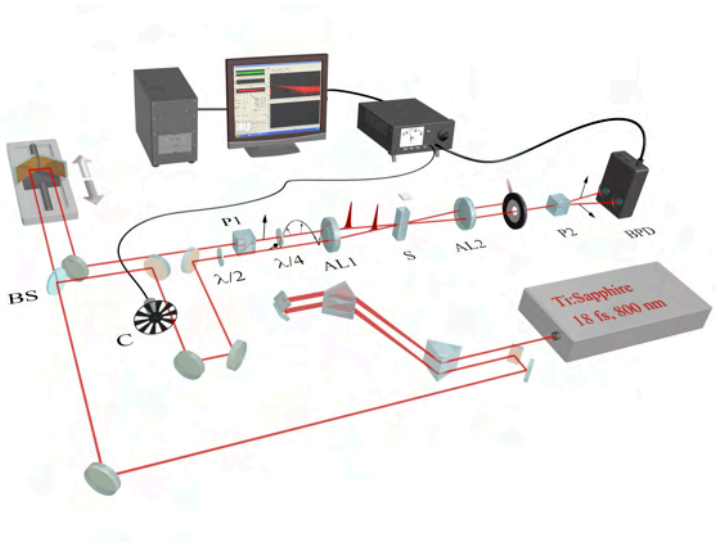

Figure 2.1. *Schematic representation of the experimental setup for the OKE measurements. A Ti:Sapphire laser (FEMTOLASER FUSION, 15 fs pulses at 780 nm) is used as light source. A prism compressor compensates for group delay dispersion (GDD), ensuring nearly transform-limited pulses. The beam is then divided by a beam splitter (BS) into pump and probe beams. The pump passes through a delay line, a chopper (C) for Lock-In detection, and a $\lambda/2$ plate for polarization rotation before being focused onto the sample by the lens AL1. The probe, after polarization control by the polariser P1 and a $\lambda/4$ plate, is focused onto the sample. After the sample, the lens AL2 collects the probe beam while the pump is blocked. The probe polarization components are separated by a Wollaston prism (P2) and detected with a balanced photodiode (BPD). The resulting differential signal is sent to a Lock-In amplifier for demodulation. Figure from [55].*

The probe beam follows a different optical path. After passing through the beam splitter it is directed towards the polarizing cube P1 from which it exits with horizontal polarization. The polarization then changes from linear to circular after passing through the $\lambda/4$ plate. The probe is now also focalized on the sample through the AL1 lens. The system is optimised to achieve spatial and temporal coincidence between pump and probe in the focus of AL1. The subsequent lens AL2 allows the two branches to be collinear again. The last part of the apparatus is dedicated to signal detection. The pump beam is no longer involved in following the system as it is blocked by a beam-stopper. The probe beam exiting AL2 is sent to a Wollaston polariser cube (P2) which divides it into its vertical and horizontal polarisation. At the exit of P2 the two polarization components are separated into two distinct beams with an exit angle of approximately 20°. These are now focalized on an balanced photodiode BPD. The output of this detector is a signal proportional to the difference between the intensities of vertical and horizontal components, which contains two heterodyne signal with opposite phase. The signal thus obtained is sent to the Lock-In amplifier, which renders the signal demodulated. The signal is recorded via an acquisition board, which simultaneously acquires the position of the delay line, so that the time dependence of the signal can be obtained.

The sample is contained within a fused quartz cell with dimensions $2 \times 10 \times$

30 mm^3. The measurements were all performed at a constant temperature of 25°C. To achieve this condition, the sample is placed in contact with a Peltier thermalization system, which allows the sample to be thermally stabilised with a stability better than 0.1 °C.

2.2.3 Normalization procedure

To enable a comparative analysis of vibrational and structural contributions, a normalization procedure was applied to account for signal intensity variations due to different protein concentrations. A reliable normalisation methodology should rely on the presence of clearly visible lines in the spectrum with an intensity and a shape essentially independent on the interaction solvent-solute. The intensity of these lines could be used to normalise the intensity of the electronic peak. The HD-OKE signal recorded for an aqueous lysozyme solution does not exhibit distinct bands, with the above stated features, for either the solute or the solvent within the frequency range typically accessible by these measurements. Thus, a direct normalization cannot be achieved.

A series of additional HD-OKE measurements on the water-protein solutions by introducing an external species with a well characterized and distinct signal relative to the water-lysozyme sample has been conducted. This approach allows to directly account for the intensity effect of concentration. Glycerol as a 10.74% molar fraction of water solvent has been added. Glycerol was chosen because of its low influence on the water-protein system [58] and it generates a contribution to the signal characterized by an intense oscillating pattern with a short time scale period. We acquired the HD-OKE signal at three concentrations of lysozyme in water-glycerol (100, 200 and 300 mg/mL). The first step of this procedure corresponds to the standard normalization in the time domain on the electronic peak. Next, we transitioned the data analysis to the frequency domain: the HD-OKE signals were Fourier transformed, and the instrumental function was deconvolved in the frequency domain. In the frequency domain it's selected a spectral region between 750 cm^{-1} and 1010 cm^{-1} in which only intramolecular vibrational bands of glycerol are present, which are expected to depend only on the glycerol concentration. The integral area of these bands is evaluated, and the result is proportional to the volume fraction of glycerol in solution and hence of the water-glycerol volume fraction. The HD-OKE signals for the water-glycerol-lysozyme samples were therefore normalised so that the integral of the selected glycerol bands decreases proportionally with the decrease in glycerol volume fraction as the lysozyme concentration increases. At this point, it is possible to establish a calibration line. The analysis was brought back to the time domain and the integrals of the signals were evaluated in this domain. The values obtained were plotted as a function of the lysozyme concentrations and, using the integral of the water-glycerol signal at 0 mg/mL lysozyme as a unitary reference value, a linear fitting procedure was performed to obtain the coefficients of the calibration line. It is then assumed that the signals obtained from the samples without glycerol also follow this calibration law. Finally, all nine HD-OKE water-lysozyme sample signals were normalised so that their time integral follows the calculated calibration line.

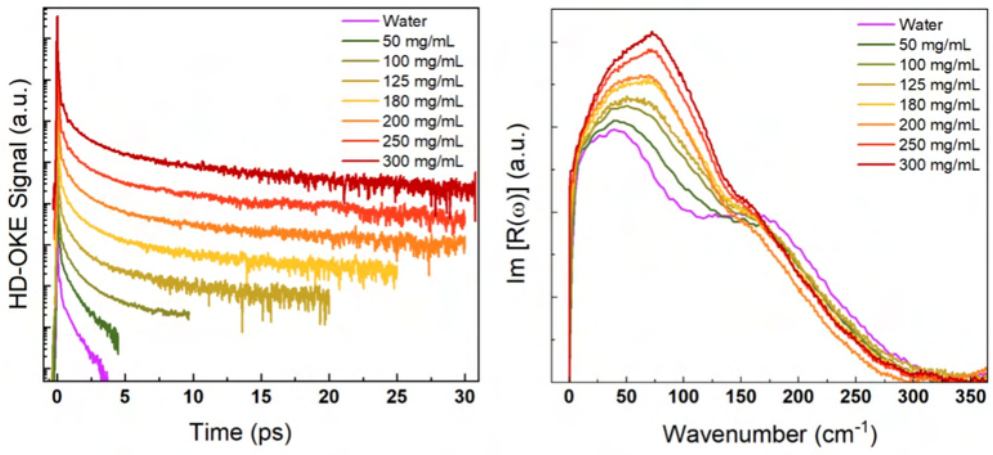

(a) (b)

Figure 2.2. (a) *HD-OKE experimental traces of lysozyme aqueous solutions at concentrations of 50, 100, 125, 180, 200, 250, and 300 mg/mL (from green to red), compared with pure water (purple). To facilitate comparison, each curve is scaled by an appropriate factor.* (b) *Spectra of the response functions corresponding to kinetics from panel A, obtained after removal of the instrumental contribution and applying the normalization procedure. Figure adapted from [43].*

2.3 Results

All measurements were acquired and analysed in the time domain. Figure 2.2(a) shows the OKE signals of selected lysozyme concentrations on a semi-log scale, while Figure 2.2(b) reports the Fourier transformed spectra of their response function obtained by the deconvolution from the instrumental function of the temporal signals. Each curve in Figure 2.2(a) is presented multiplied by an appropriate factor to avoid overlapping. The lysozyme concentration increase causes a grown in the signal intensity and a change in the spectral shape due to the structural and vibrational contributions. Figure 2.3(a) displays the HD-OKE signal and the corresponding fit for the sample at concentration 250 mg/mL. The signal exhibits a long structural relaxation on the ten of picoseconds timescale. The inset shows a zoom of the signal between 0 and 1.5 ps highlighting the fast oscillations due to intermolecular vibrational dynamics of protein and water.

The chosen approach allows disentangling the bulk water, hydration water, and protein contributions from the whole signal. The total HD-OKE response can be expressed as:

$$R(t) = F_{\text{bulk}} R_{\text{bulk}}(t) + R_{\text{h-ly}}(t). \tag{2.4}$$

The bulk water response, $R_{\text{bulk}}(t)$, is described by an analytical function derived from pure water OKE measurements [59] and weighted by the bulk water volume fraction F_{bulk}, estimated following *Camisasca et al.* [51]. Considering only the first hydration layer as hydration water is justified by molecular simulation work [13] showing that the protein perturbation decays rapidly with distance. The hydration water and protein response $R_{\text{h-ly}}(t)$ consists of a structural and a vibrational

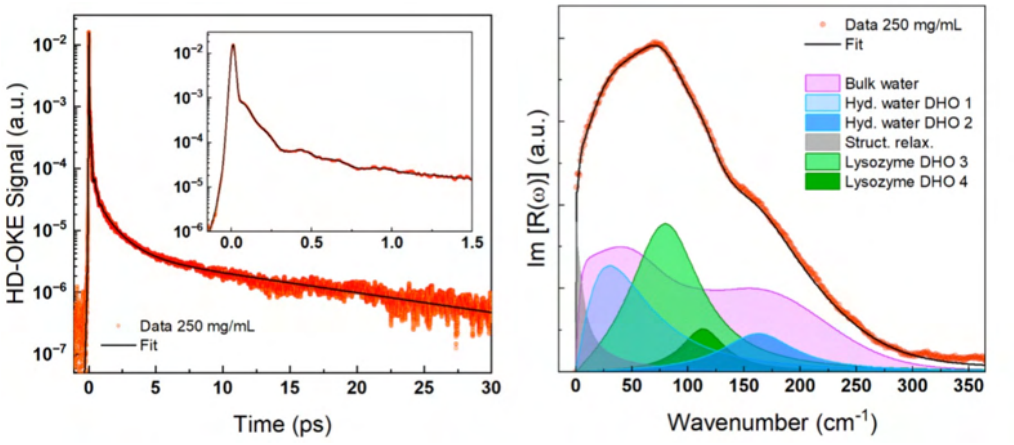

(a) (b)

Figure 2.3. (a) *Semi-logarithmic representation of the experimental signal for the 250 mg/mL solution (red markers) and the associated time-domain fit (black line). The inset emphasizes the oscillatory features due to vibrational dynamics observed within the first 2 ps.* (b) *Response function spectrum of the 250 mg/mL solution. Experimental data (red markers) and the corresponding fit (black line) are compared with the bulk water contribution (purple shaded curve) and the other components of the fit: a biexponential relaxation (grey area), two damped harmonic oscillators assigned to hydration water (blue areas), and two damped harmonic oscillators related to the protein response (green areas). Figure adapted from [43]*

contribution:

$$R_{\mathrm{h-ly}}(t) = R_{\mathrm{struct}}(t) + R_{\mathrm{osc}}(t) \tag{2.5}$$

The fitting functions reported in Eq 2.4 are modelled using a limited set of analytical expressions [56]. The structural relaxation, $R_{\mathrm{struct}}(t)$, is represented by two exponential decays combined with a fast rise term with a fixed parameter $\tau_R = 50$ fs, ensuring that the response function originates at zero:

$$R_{\mathrm{struct}}(t) = \frac{A_{\mathrm{exp1}}}{\tau_1}\left(1 - e^{-t/\tau_R}\right)e^{-t/\tau_1} + \frac{A_{\mathrm{exp2}}}{\tau_2}\left(1 - e^{-t/\tau_R}\right)e^{-t/\tau_2} \tag{2.6}$$

The inclusion of the rise term $\left(1 - e^{-t/\tau_R}\right)$ accounts for the actual growth of the signal, which deviates from an idealized Heaviside step-like behaviour. The vibrational response, $R_{\mathrm{osc}}(t)$, is described as the time derivative of a set of four damped harmonic oscillators (DHOs):

$$R_{\mathrm{osc}}(t) = \sum_{n=1}^{4} \frac{A_n}{\sqrt{\omega_n^2 - (\gamma_n^2/4)}} e^{-\frac{\gamma_n t}{2}} \sin\left(\sqrt{\omega_n^2 - \frac{\gamma_n^2}{4}}\, t\right) \tag{2.7}$$

These functions represent the minimal model required to reproduce the main dynamical features of the HD-OKE signal. Error estimates were obtained by evaluating the dispersion of parameters extracted from repeated measurements of the same sample. Figure 2.3(b) shows the experimental spectrum of the 250 mg/mL solution (red) together with the Fourier transform of the time-domain fit (black), as well as

its individual components: $R_{\text{bulk}}(t)$ scaled by F_{bulk}, the bi-exponential structural term (grey area), and the four DHOs (blue and green areas).

2.4 Discussion

2.4.1 Hydration water structural dynamics

The relaxation dynamics described by the $R_{\text{struct}}(t)$ fitting function are represented by a bi-exponential decay characterized by two structural relaxation times, τ_1 and τ_2. These processes occur on the tens of picoseconds timescale and can therefore be attributed exclusively to hydration water, since protein structural and rotational relaxations are associated with much slower timescales [57]. The HD-OKE data reveal that hydration water dynamics consist of two distinct relaxation processes operating on different timescales: one within a few picoseconds and the other extending over several tens of picoseconds. This result is consistent with predictions from simulations of the lysozyme–water system [15, 51] and with findings from time-resolved fluorescence spectroscopy on protein–water solutions [60, 61]. The faster process, with a characteristic time of approximately 1.6 ps, arises from the breaking and reforming of HBs networks through large-amplitude OH jumps [10, 15]. This mechanism resembles the α-relaxation observed in bulk water [15, 51], but is slowed by about a factor of three as a result of water binding to hydrophilic and hydrophobic protein residues [45, 51, 52]. The slower relaxation, ranging between 13 and 22 ps, corresponds to a structural rearrangement process driven by protein fluctuations, which does not occur in bulk water. Figure 2.4 reports τ_1 and τ_2 as a function of lysozyme concentration. Both values remain nearly constant within experimental uncertainties, indicating that the hydration water dynamics are only weakly dependent on protein concentration. The analysis of the amplitudes instead shows a peculiarity.

Figure 2.5 shows the sum of the amplitudes of the two relaxations as a function of concentration. A clear discontinuity appears at $\sim$ 200 mg/mL, more evident in the amplitudes than in the relaxation times. Protein aggregation is controlled by the balance between protein–protein and protein–water interactions. The interplay of short-range attractive potentials, long-range electrostatic repulsion, and hydrophobic/hydrophilic effects mediated by water results in the formation of transient clusters in dynamic equilibrium with isolated proteins. Such clusters are present even at low lysozyme concentrations, but above a critical concentration their formation becomes energetically favoured compared to maintaining a monodisperse solution [34, 36, 45, 62, 63]. The amplitude discontinuity observed, provides a clearer signature of a concentration-induced dynamical crossover, reflecting the onset of clustering phenomena that progressively alter the hydration environment of proteins.

2.4.2 Hydration water vibrational dynamics

The analysis of the vibrational dynamics region is inherently complex due to the overlap between the contributions of hydration water and bulk water, since the intermolecular HBs bands of hydration water occupy the same spectral region as those of bulk water [64]. In addition, certain protein modes exhibit vibrational fre-

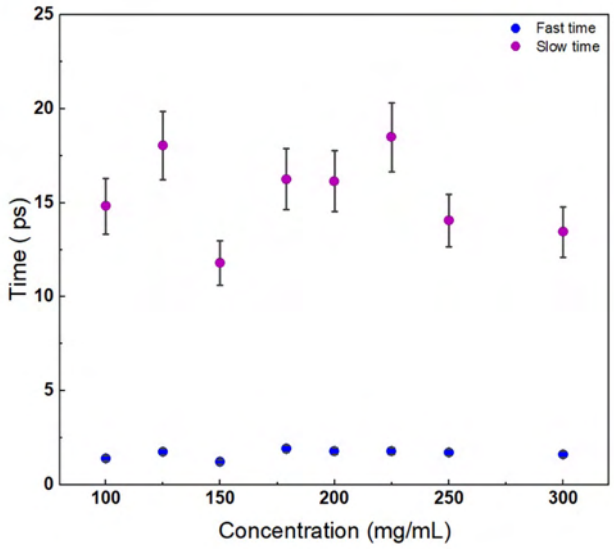

Figure 2.4. *Relaxation times τ_1 and τ_2, extracted from the bi-exponential fit function shown in Eq. 2.6. They highlight two distinct relaxation processes with well separated structural timescales. No significant variation with protein concentration is observed within the experimental uncertainties, indicating that these relaxation dynamics are only weakly affected by changes in lysozyme concentration or by clustering phenomena. For the 50 mg/mL lysozyme solution, the signal quality does not allow for a reliable determination of hydration water relaxation times, and therefore these values are not reported. Figure from [43].*

quencies similar to water modes. Consequently, the hydration water contribution has often been treated as part of the overall solvent spectrum [50] or incorporated into the hydrated protein response [44, 48]. In this investigation, after subtraction of the bulk water contribution, the sub-picosecond signal is characterized by two main vibrational components: hydration water modes and protein intramolecular modes, including structural vibrations and librations of lysozyme side chains [50]. The experimental signal in this regime can be fully reproduced by four DHOs (see Figure 2.3(b)). DHOs 3 and 4 are assigned to lysozyme librations, as supported by comparison with Raman spectra of protein crystals [65, 66]. While DHO 3 is unambiguously attributed to protein dynamics [61, 66], DHO 4 may also include a minor hydration water contribution. However, the inclusion of such a contribution would only rescale the relative amplitudes and would not alter the overall interpretation. Instead, DHOs 1 and 2 are reliably assigned to hydration water modes.

Figure 2.6(a) presents the hydration water spectrum extracted from the 250 mg/mL solution after subtraction of bulk water and lysozyme oscillators. The bulk water response is shown for comparison (purple curve). Further subtraction of the structural relaxation component (grey shaded curve) yields two distinct vibrational modes at 55 and 166 cm^{-1}, corresponding to DHOs 1 and 2 (blue curves). These modes are similar to those reported for hydration water confined in silica nanopores [64] and can be assigned to the intermolecular bending and stretching vibrations of the HBs network in the hydration shell surrounding the protein. The dependence

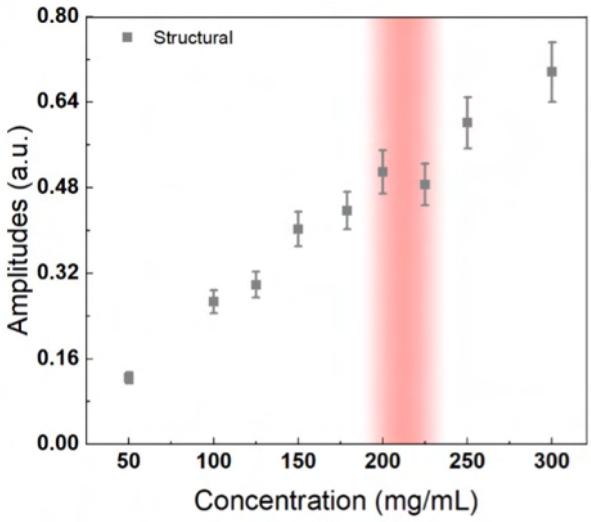

Figure 2.5. *Integrated amplitudes of the structural relaxation components as a function of lysozyme concentration. Amplitudes were obtained from the integral areas of the spectral contributions reported in* Figure 2.3(b)*, evaluated as the subtended area between 0 and infinite frequency. Figure from [43].*

of the hydration water spectrum on protein concentration was then analysed and compared with bulk water (see Figure 2.6(b)). The mode intensities exhibit a pronounced concentration dependence. The bending mode (DHO 1) increases almost monotonically with concentration, whereas the stretching mode (DHO 2) displays a discontinuity between 180 and 200 mg/mL. To emphasize this effect, Figure 2.7 reports the effective amplitudes of both vibrational modes, obtained by integrating the DHO contributions. Both bending and stretching amplitudes exhibit a sharp discontinuity at ∼200–225 mg/mL, coinciding with the concentration threshold previously identified in the structural relaxation amplitude analysis. Below this threshold, both amplitudes increase steadily with concentration, consistent with the growing hydration water content. At the threshold, all amplitudes, including the structural component, decrease abruptly, indicating a reduction in hydration water. Beyond the crossover, amplitudes increase again at comparable rates.

This behaviour suggests that clustering phenomena play a decisive role in modulating the hydration shell. The main effect is a reduction of the exposed protein surface area, which decreases the total hydration water content. However, this effect alone does not explain the different concentration dependence of the bending and stretching modes. The discrepancy is likely related to changes in intermolecular interactions among hydration water molecules under crowded conditions, which disproportionately affect the stretching mode. This interpretation is consistent with terahertz spectroscopy studies [12, 40–42], which reported that condensation phenomena associated with liquid–liquid phase separation (LLPS) reduce the population of hydration water near hydrophobic regions, while hydrophilic water remains largely unaffected. In such scenarios, clusters tend to retain hydrophilic water but release hydrophobic water into the bulk. This mechanism provides a plausible explanation for the observed crossover and the stronger suppression of the stretching

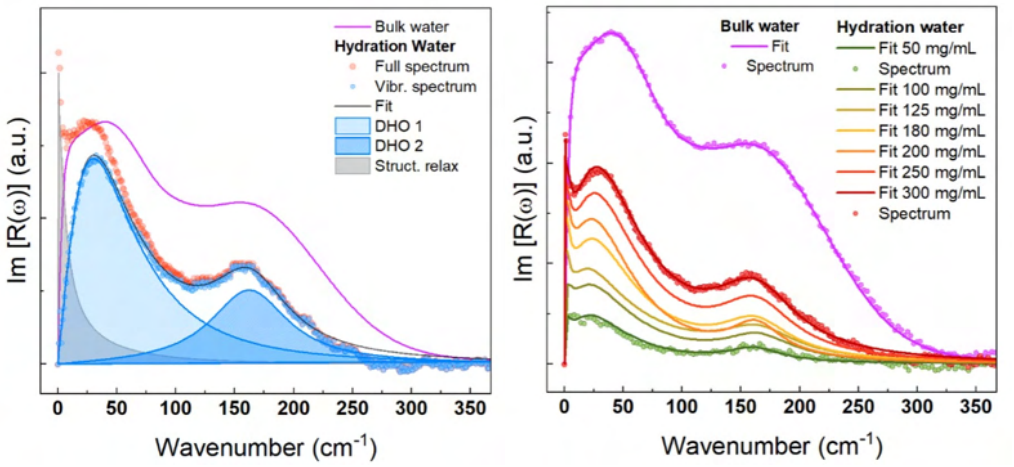

(a) **(b)**

Figure 2.6. (a) *Comparison between the full spectrum (red circles) and the vibrational spectrum (blue circles) of hydration water dynamics, both extracted from the 250 mg/mL lysozyme–water sample. For reference, the spectrum of the bulk water component weighted by its volume fraction is also shown (violet line). The fitted structural contribution (grey shaded line) and the two hydration water oscillators (blue shaded lines, DHOs 1 and 2) are reported.* (b) *Hydration water spectra obtained from lysozyme–water samples at concentrations ranging from 50 mg/mL (green) to 300 mg/mL (red), together with bulk water (violet). To avoid overcrowding, spectra at intermediate concentrations are not shown. Figure from [43].*

mode compared to the bending mode. Overall, clustering appears to modulate hydration shell composition but has little effect on relaxation times or vibrational frequencies.

2.5 Conclusion

In this HD-OKE investigation, the combination of high signal-to-noise data, rigorous fitting procedures, and a systematic concentration study enabled the clear differentiation and quantification of the dynamical processes in protein–water solutions, with particular focus on hydration water. Measurements over extended temporal windows revealed two distinct relaxation processes: a fast component associated with water α-relaxation and a slower component linked to structural reorganization of water coupled with protein fluctuations. This constitutes the first experimental confirmation of phenomena previously predicted by simulation studies [15, 51], offering critical insights into the debated nature of protein hydration dynamics.

The methodology used allowed the direct isolation of hydration water vibrational modes, which exhibit bending and stretching intermolecular bands similar to bulk water but with distinct amplitude behaviour as a function of protein concentration. A clear crossover was identified at ∼200–225 mg/mL, marked by a discontinuity in both structural relaxation and vibrational amplitudes. This crossover is interpreted as the onset of enhanced protein clustering under crowded conditions, leading to a

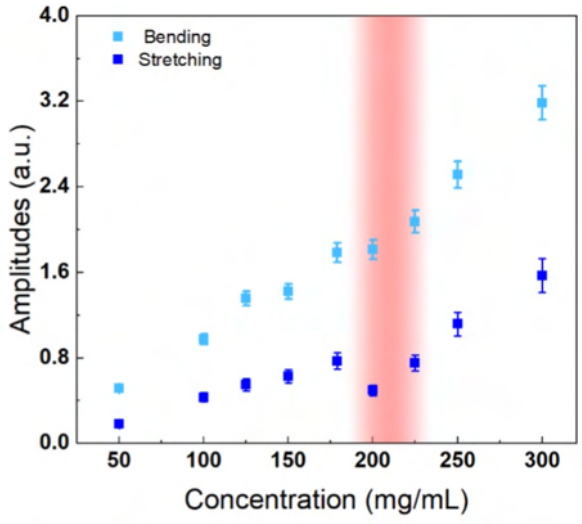

Figure 2.7. *Integrated amplitudes of the vibrational modes of hydration water as a function of concentration. Amplitudes were obtained from the integral areas of the spectral contributions reported in* Figure 2.3(b) *evaluated as the subtended area between 0 and infinite frequency. All amplitudes exhibit a marked change at ∼200–225 mg/mL, consistent with the concentration threshold where lysozyme cluster formation becomes energetically favoured over monomeric dispersion. Figure from [43].*

reduction in total hydration water, particularly hydrophobic hydration.

Comparison with the phase diagram of lysozyme solutions suggests a possible correlation with the critical point of LLPS [37, 38], indicating that critical phenomena may influence clustering even far from the coexistence region. Overall, these results highlight the unique capability of HD-OKE spectroscopy to resolve subtle biomolecular interactions and provide a powerful tool for probing hydration water dynamics and protein clustering phenomena.

Chapter 3

THz-Time Domain Spectroscopy study on water-lysozyme solutions

3.1 Introduction

The experiment presented in the previous chapter showed how studying the characteristic dynamics of hydration water can provide information on the overall properties of the solution and the conformations that the solute can assume within the solvent. As already discussed in the introduction to this thesis, however, the definition of hydration water may depend on the type of experimental technique used. It is therefore of interest to investigate the same solutions previously studied using different techniques. This allows us to understand whether the spectroscopic signatures linked to the presence of clusters in solution, observed in the properties of hydration water using the OKE technique, can be observed using different spectroscopic techniques.

This chapter reports and discusses the results of a spectroscopic investigation in the THz frequency range, performed using the time-resolved THz-TDS technique in Attenuated Total Reflection (ATR) geometry. The ATR configuration is ideally designed to be used with highly absorptive media, such as the aqueous solutions studied in this experiment. Further details on the optical setup are provided in the dedicated sections of this chapter (see sections 3.2.2 and 3.2.3). In this case, not only the properties of the samples were studied as the protein concentration in the solution varied, but their behaviour as a function of temperature was also investigated. The temperature range investigated spanned from 4°C to 35°C.

The presence of proteins can influence the surrounding water molecules and alters several of their experimentally measurable properties, particularly the relaxation and reorientation rates within the HBs network. These reorientations occur as the water molecules within the network continuously tumble and diffuse, undergoing cycles of HB formation and breaking. THz absorption spectroscopy is a powerful means of investigating such effects since the absorption coefficient depends sensitively on the collective dipolar fluctuations of the hydrogen-bond network on the picosecond timescale [67]. From the onset of its application, THz spectroscopy

has demonstrated exceptional sensitivity in the study of hydration shells [29]. In the specific case of protein hydration water, there are numerous studies demonstrating the high sensitivity of the technique. The extension of the hydration shell measured in these studies is significantly greater than that measurable with other techniques. To give a few examples, in the case of BSA, an extension of 1.5 nm is measured [20], in the case of ubiquitin 1.8 nm [67], reaching up to 4.2 nm in the case of human lysozyme [68].

A further advantage is that water is an extremely opaque medium in the THz region, so adding proteins to an aqueous solution generally leads to a decrease in the absorption of the solution. It is therefore possible to assume that the contribution of the protein to the absorption spectrum is practically negligible [69]. This implies that the differences between the absorption spectra of pure water and a water-protein solution are attributable either to a excluded volume effect or to modifications in the dynamical behaviour of water within the hydration shells.

The first hypothesis would imply that, for a study based on protein concentration (C) as in the case reported here, the absorption coefficients $\alpha(\nu, C)$ at various concentrations can be expressed as a linear combination of two contributions, corresponding to the absorption coefficient of the protein $\alpha_{\mathrm{P}}(\nu)$ and of the solvent $\alpha_{\mathrm{solv}}(\nu)$, weighted by the volume fraction ($\Phi_{\mathrm{P}}(C)$ and $\Phi_{\mathrm{solv}}(C)$), that they occupy in the system:

$$\begin{aligned}\alpha(\nu, C) &= \alpha_{\mathrm{P}}(\nu)\Phi_{\mathrm{P}}(C) + \alpha_{\mathrm{solv}}(\nu)\Phi_{\mathrm{solv}}(C) \\ &\approx \alpha_{\mathrm{solv}}(\nu)\left(1 - \Phi_{\mathrm{P}}(C)\right)\end{aligned} \tag{3.1}$$

However, this data modelling is not sufficient to justify the protein concentration behaviour of the absorption spectra [16, 67, 68, 70]. A model that takes into account a three-phase system, namely protein, bulk water and hydration water, is able to reproduce the data, thus supporting the second hypothesis [16, 67, 70]. The absorption coefficient in this model became:

$$\begin{aligned}\alpha(\nu, C) &= \alpha_{\mathrm{P}}(\nu)\Phi_{\mathrm{P}}(C) + \alpha_{\mathrm{H}}(\nu)\Phi_{\mathrm{H}} + \alpha_{\mathrm{B}}(\nu)\Phi_{\mathrm{B}}(C) \\ &\approx \alpha_{\mathrm{H}}(\nu)\Phi_{\mathrm{H}}(C) + \alpha_{\mathrm{B}}(\nu)\left(1 - \Phi_{\mathrm{P}}(C) - \Phi_{\mathrm{H}}(C)\right)\end{aligned} \tag{3.2}$$

where α_{H} and Φ_{H} are the absorption coefficient and volume fraction of hydration shells and α_{B} and Φ_{B} of the bulk water component.

In this model, hydration water is treated as an element independent of concentration and, above all, with well-defined contours, making it a rough approximation. However, this approximation is sufficient to extrapolate the extent of the hydration shell, showing the existence, in the case of THz, of an extraordinarily extended shell [16, 29, 67]. By studying solutions at different concentrations, the existence of 'terahertz excess' was observed, i.e., an initial increase in absorption compared to the expected decrease due to water removal linked to the increase in concentration, an effect that can only be explained by the presence of a hydration shell characterised by a higher absorption coefficient than bulk water. Once a critical concentration is exceeded, a reversal trend in the absorption coefficient is observed, which begins to decrease. This crossing point is associated with the intersection of the hydration shells of two distinct proteins, so this information can be used to estimate

the extent of the shell [16, 67]. In these works authors define a "dynamical hydration shell" strongly coupled to protein motion and extends across energetic barriers at the protein surface. They use "dynamical" to emphasise that this shell is not equivalent to the static hydration shell identified by X-ray crystallography or NMR, which involves sterically bound water molecules. Instead, it encompasses all water molecules exhibiting network dynamics that are distinct from those of bulk water and therefore exhibit distinct THz absorbance. The influence of the protein extends well beyond the static hydration radius as it modifies the dynamic behaviour of the water network without forming fixed hydrogen bonds with the protein [67].

A possible explanation for the differences in the absorption spectra of bulk water and hydration water was sought through theoretical works dealing with the standard electrostatics of the water-protein system when subjected to an electric field [69, 71]. It turns out that this effect cannot be justified by treating the protein within water simply as a spherical void in the medium, i.e. the variation is linked to the additional polarisation created to satisfy the boundary conditions between the void-medium interface. The scenario appears more complicated, suggesting the need to consider an effective-medium representation of the complex structure of the protein-water interface, which requires modification of the standard dielectric boundary-value problem.

3.2 Methods

3.2.1 The THz-TDS technique

The THz-TDS technique allows to probe the process associated with change in the dipole moment of a substance as in a standard absorption experiment. In short, the THz-TDS consists of a pump-probe technique that probe coherently the amplitude and phase of a THz pulse field, using a generation and detection system that employs an ultrafast mode-locked laser. In the specific case of the measurements reported here, two photoconductive antennas (PcAs) are used as source and detector of the THz beam. When excited by the optical radiation of the laser beam, these antennas are able to generate and detect THz pulses in a spectral range from approximately 0.1 THz to 4.5 THz. One of the advantages of using this method, compared to another frequency resolved technique such as FTIR, is the possibility of accessing not only the electric field modulus of the THz pulse but also its phase, thus obtaining directly information on the complex refractive index in both its real and imaginary parts [72]. Investigating samples dissolved in polar liquids, particularly water, has proven challenging due to the exceptionally high absorption of these liquids in the THz frequency range. A standard THz-TDS transmission setup is not ideal, as the maximum measurable absorption is limited by the system's dynamic range and it would require the use of an extremely thin sample, on the order of hundreds of μm, a condition that is not easy to achieve, particularly for water-protein solutions. For this reason, an ATR cell is used to position the sample. In the ATR geometry, the sample is placed on the surface of a prism with a constant refractive index over the probed frequency range. The prism is designed to ensure total reflection when the THz beam reaches the prism–sample interface. In this way, the beam cannot interact with the sample except through the propagation of the evanescent wave

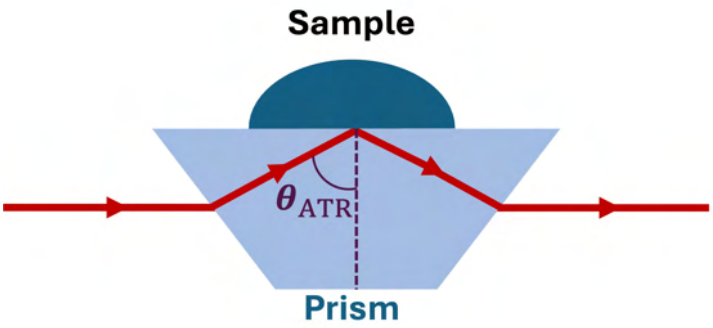

Figure 3.1. *Optical path of the THz beam under attenuated total reflection (ATR) conditions. The angle θ_{ATR} is the angle of reflection on the surface of the prism on which the sample stands.*

generated in the total reflection condition. The beam propagates within the sample over a distance on the order of the wavelength of the radiation used, thus solving the problem of sample thickness and maintaining a sufficient dynamic range to obtain the measurement.

For optical parameter extraction, it is possible to compare the signal detected with and without the sample on the prism surface. In this way, it is possible to obtain the complex transfer function $T(\omega)$ [72]:

$$T(\omega) = \frac{E_{\mathrm{sam}}(\omega)}{E_{\mathrm{ref}}(\omega)} = \frac{r_{\mathrm{sam}}(\omega)}{r_{\mathrm{air}}(\omega)} \tag{3.3}$$

where $E_{\mathrm{sam}}(\omega)$ and $E_{\mathrm{ref}}(\omega)$ are the Fourier transforms of the electric field measured with and without the sample on the prism respectively, $r_{\mathrm{sam}}(\omega)$ is the Fresnel reflection coefficient of the prism-sample interface and $r_{\mathrm{air}}(\omega)$ is that of the prism-air interface for p polarization. Starting from the definition of the two reflection coefficients it's possible to connect the transfer function to the complex refractive index of the sample $\tilde{n}_{\mathrm{sam}}(\omega)$ [73]. The reflection coefficient between the prism and the sample can be written as:

$$r_{\mathrm{sam}}(\omega) = \frac{\tilde{n}_{\mathrm{prism}}(\omega)C_{\mathrm{sam}}(\omega) - \tilde{n}_{\mathrm{sam}}(\omega)\cos\theta_{\mathrm{ATR}}}{\tilde{n}_{\mathrm{prism}}(\omega)C_{\mathrm{sam}}(\omega) + \tilde{n}_{\mathrm{sam}}(\omega)\cos\theta_{\mathrm{ATR}}} \tag{3.4}$$

where θ_{ATR} is the reflection angle on the internal surface of the prism (see Fig(3.1)), $\tilde{n}_{\mathrm{prism}}$ is the complex refractive index of the prism and

$$C_{\mathrm{sam}} = \sqrt{1 - \frac{\tilde{n}^2_{\mathrm{prism}}(\omega)}{\tilde{n}^2_{\mathrm{sam}}(\omega)}\sin^2\theta_{\mathrm{ATR}}} \tag{3.5}$$

The same relation is valid for $r_{\mathrm{air}}(\omega)$ by substituting the air parameters in place of those of the sample in the equation. By knowing the refractive index of air and prism, and by measuring the transfer function, the complex refractive index of the sample can be expressed as:

$$\tilde{n}_{\mathrm{sam}}(\omega) = \chi(\omega)\tilde{n}_{\mathrm{prism}}(\omega), \tag{3.6}$$

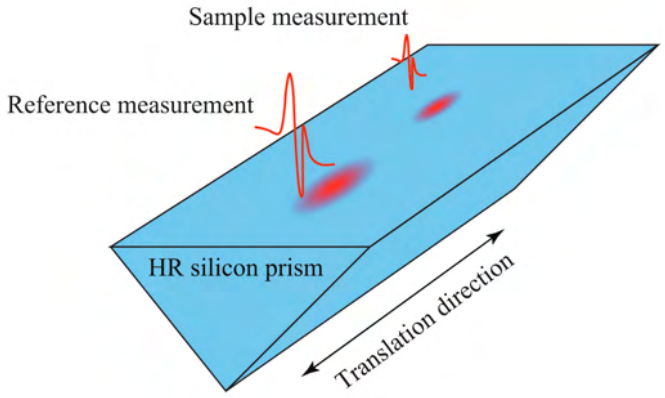

Figure 3.2. *Graphical representation of the configuration used for ATR spectroscopy. The prism is divided into two sections that can be moved orthogonally to the beam axis to take reference and sample measurements employing a motorised stage. Figure from [72]*

with

$$\chi(\omega) = \sqrt{\frac{-A^2(\omega) \pm \sqrt{A^4(\omega) - 4\sin^2\theta_{\mathrm{ATR}}}}{2}} \tag{3.7}$$

where $A(\omega)$ is:

$$A(\omega) = \frac{1 - r_{\mathrm{sam}}(\omega)}{1 + r_{\mathrm{sam}}(\omega)} \tag{3.8}$$

The sign of 3.7 should be chosen such that imaginary part of the refractive index remains negative in order to comply with energy conservation. The refractive index and the absorption coefficient of the sample are connected to the real and imaginary part of $\tilde{n}_{\mathrm{sam}}$:

$$n_{\mathrm{sam}}(\omega) = \mathrm{Re}(\tilde{n}_{\mathrm{sam}}(\omega)) \tag{3.9}$$

$$\alpha_{\mathrm{sam}}(\omega) = \frac{2\omega}{c}\,\mathrm{Im}(\tilde{n}_{\mathrm{sam}}(\omega)) \tag{3.10}$$

In this work has been used the calibration and analysis procedure reported in *Soltani et al.*[72]. They proposed a method to enhance the reliability of ATR THz-TDS measurements employing an elongated prism mounted on an optical translation stage. The upper surface of the prism is divided into two distinct areas: one dedicated to the sample measurement and the other to the reference acquisition (see figure 3.2). By laterally shifting the prism in a direction perpendicular to the beam axis, it becomes possible to alternate between reference and sample measurements. Because the sample is deposited onto the prism surface, this configuration helps to minimize errors arising from arbitrary tilting of the prism during sample placement. Moreover, without amplifying the influence of misalignment, this setup enables interleaved reference and sample scans over extended measurement periods, thereby reducing the impact of long-term signal drifts. It should be noted that translating the prism can still introduce a small angular misalignment, which may represent a significant source of measurement error. Nevertheless, in this configuration, the angular deviation is predetermined and can be corrected during data

post-processing. To further mitigate this issue, spectral calibration function for both phase and amplitude components can be established, allowing compensation for the residual misalignment effects. To obtain this calibration function $F_{\text{cal}}(\omega)$, it is necessary to measure the signal at the position of the prism where the sample is placed before it is positioned $E_{\text{sam}}^{\text{empty}}$. This result in:

$$F_{\text{cal}}(\omega) = \frac{E_{\text{sam}}^{\text{empty}}(\omega)}{E_{\text{ref}}(\omega)} \tag{3.11}$$

The reference measurement can be corrected as:

$$E_{\text{ref}}^{\text{cor}}(\omega) = E_{\text{ref}}(\omega) \cdot F_{\text{cal}}(\omega) \tag{3.12}$$

Applying the calibration function to the transfer function 3.3, it is finally found that:

$$T(\omega) = \frac{E_{\text{sam}}(\omega)}{E_{\text{ref}}(\omega)} \cdot \frac{1}{F_{\text{cal}}(\omega)} \tag{3.13}$$

By loading the sample onto one side of the prism, the relative misalignment between the sample and reference sides is maintained, and this correction factor remains valid.

3.2.2 THz-TDS setup

The figure 3.3 shows the optical setup for carrying out THz-TDS measurements. The experiment consists of a pump-probe technique, in which an ultrafast optical source is used to generate and detect a THz pulse by exploiting the properties of two photoconductive antennas (PcAs). The optical source is a Erbium based ultrafast laser (T-light fiber laser from MenloSystem), providing pulses of ∼120 fs duration, at 780 nm with energy of ∼ 1 nJ and at a repetition rate of 100 MHz.

The emitted optical beam is split into two branches, pump and probe, by the beamsplitter (BS). The pump beam is directed onto the generation PcA while the probe beam is redirected towards an optical delay line (a corner cube mirror (CC) positioned on a motorised stage) to introduce a time delay between the pump and probe pulses. At the output of the delay line, the probe beam arrives at the detection PcA. Details on the generation and detection of the THz beam through PcAs are provided in the dedicated section. The THz beam generated by the generation PcA is collected and directed onto the sample via a series of off-axis parabolic mirrors (PM). Using a hyper-hemispherical silicon lens attached to the PcA is possible improve the out-coupling of the THz radiation. After passing through the sample, the beam is finally focused onto the detection PcA. Another hyper-hemispherical lens is also attached to this PcA. The output signal from the latter is then sent to a lock-in amplifier (model UHF from Zurich Instrument) and recorded via an acquisition board. Lock-In detection is performed using a sinusoidal bias of the PcA emitter with voltage values oscillating between 0 and 30 Volt. The temporal waveform of the THz pulse is obtained by scanning the pump–probe delay. The entire THz system is contained within a chamber purged with nitrogen to prevent the effects of strong absorption linked to the presence of water vapour in the air.

To obtain the ATR measurement configuration, a custom ATR cell was made (figure 3.4). The main element of the cell is the 45° HR-Silicon prism, which allows

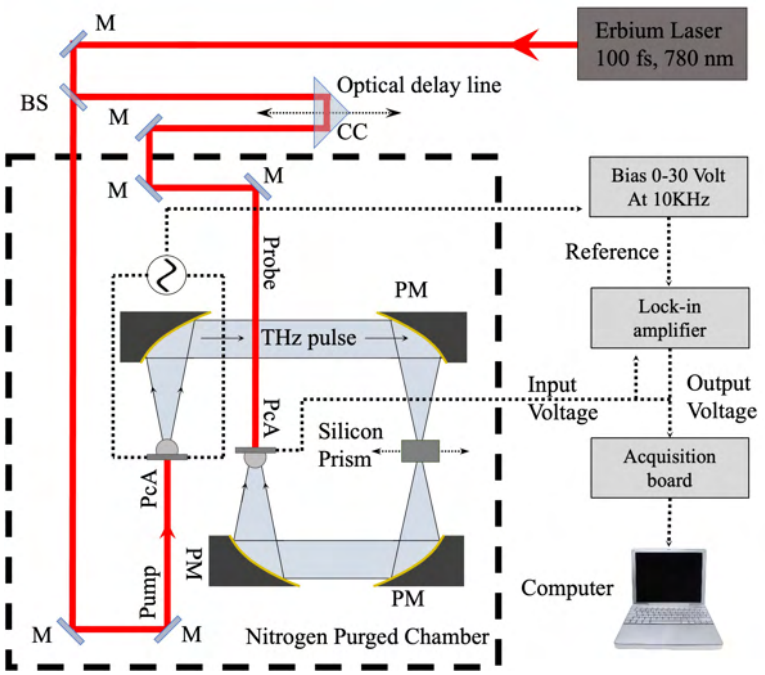

Figure 3.3. *Optical setup for the THz-TDS experiment. A 120 fs optical pulse generated by an erbium femtolaser is split into two paths, pump and probe, by a beam splitter (BS). The pump branch is used to excite a photoconductive antenna PcA for the generation of a THz pulse. The beam thus generated is collected and propagated by a series of off-axis parabolic mirrors (PM) until it is focused on the prism on which the sample for the ATR measurement is placed. At the output of the sample area, the THz beam is detected by a second PcA. A photocurrent is generated in the receiving antenna, which is biased by the electric field of the incoming THz pulse and triggered by the probe optical pulse. This is delayed in time with respect to the pump by means of a corner cube mirror (CC) mounted on a motorised stage. This allows measurements that depend on the time delay between the pump and probe pulses. The generating PcA is supplied with a bias current modulated sinusoidally in time to allow detection via a lock-in amplifier.*

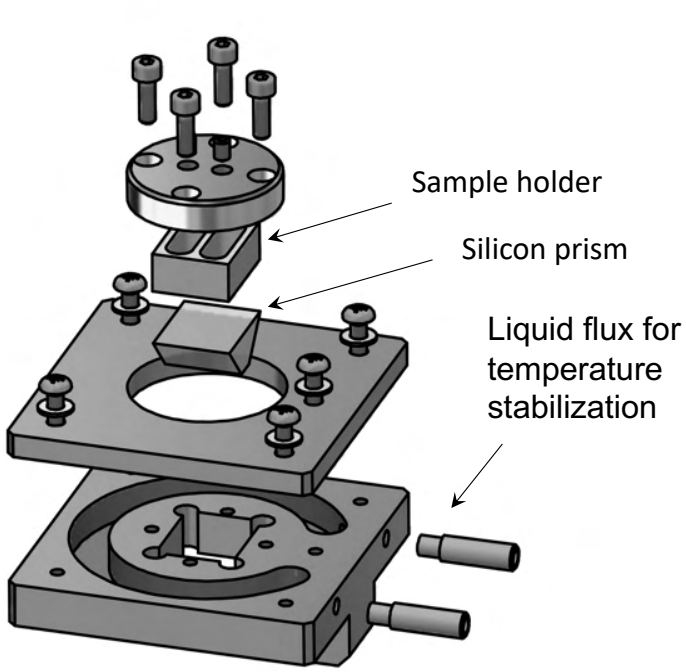

Figure 3.4. *Design of the ATR cell used for THz-TDS measurements. The Teflon sample holder is positioned on the silicon prism with two openings enabling the quick change from the sample position to the reference one by moving the cell transversely to the THz beam. The entire system is thermally controlled by a liquid flow from a electronically heat-controlled chiller.*

for attenuated total reflection. A Teflon insert is mounted on the prism to act as a sample holder. This has two chambers: the first is filled with the sample, while the second is always left empty to obtain the reference measurement. The ATR cell is mounted on a motorised stage to allow the signal to be acquired from either chamber (see previous section). An aluminium cap is used to close the system. Two holes are drilled in this cap to allow the sample to be inserted and removed without disassembling the entire cell. Two small screws can be used to close these two openings to prevent evaporation. The system is thermally controlled by a water flow from a thermoelectric liquid chiller. After a thorough calibration procedure, it was possible to evaluate the thermal stability of the system at $\pm$ 0.1 °C. The measurements were taken at temperatures ranging from 4 °C to 35 °C.

3.2.3 THz pulse generation and detection

For the generation and the detection of the THz pulses have been used two PcAs. A photoconductive antenna functions as an electrical switch that employs the enhanced conductivity observed in semiconductors and insulators upon illumination. This phenomenon, known as photoconductivity, arises from the increase in the number of free charge carriers, electrons and holes, generated by the absorption of photons. In order for this process to occur, it is necessary that the photon energy be sufficiently high to exceed the material's bandgap. The response of a PcA is

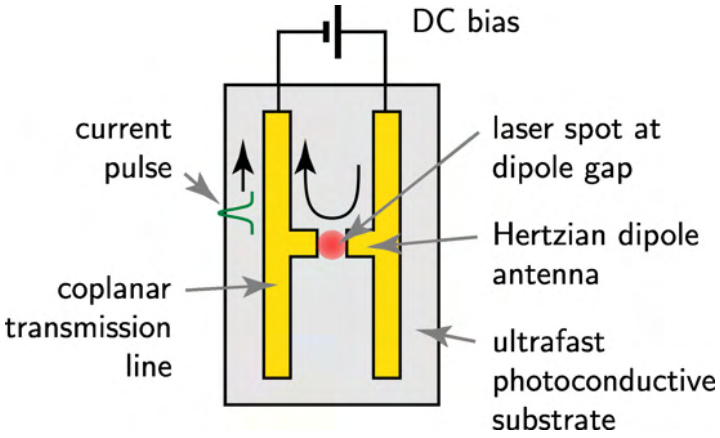

Figure 3.5. *Design of a photoconductive antenna. Two coplanar transmission lines used as electrodes are deposited in a semiconductor substrate. Figure adapted from [75].*

expected to occur within the sub-picosecond time range. The switch-on time is contingent on the duration of the laser pulse, whilst the switch-off time is primarily determined by the lifetime of photoexcited carriers within the semiconductor substrate of the antenna [74]. The PcA consist of two metal electrodes imprinted on a semiconductor photoconductive substrate (GaAs for the PcAs used in this work). In Figure 3.5 is reported the schematic diagram of a PcA with its components.

The photoinduced carriers are accelerated across the dipole gap under the influence of the bias electric field generated by the coplanar electrode lines, before recombination occurs. This motion gives rise to a transient photocurrent, which in turn leads to the emission of a coherent broadband THz pulse from the dipole. This transient current radiates a coherent electric E_{THz}, which, at the far field, is proportional to the first-order derivative of the photocurrent density $J(t)$ [76] :

$$E_{\mathrm{THz}}(t) \propto \frac{dJ(t)}{dt} \tag{3.14}$$

where

$$J(t) = P_{\mathrm{opt}}(t) \otimes (q\, n(t) v(t)) \tag{3.15}$$

Here the symbol $\otimes$ represent the convolution product, $P_{\mathrm{opt}}(t)$ is the intensity of the laser pump pulse, q the electron charge and $n(t)$ and $v(t)$ are respectively is the numerical density and the velocity of the photocarriers. To collect the dipole generated THz field, specific lenses in HR-Silicon are used. These lenses are characterized from a hyper-hemispherical shape. This design does not lead to spherical aberration [74]. The functioning of the detection PcA is very similar to what has been described so far. The main difference is that the detection antenna is not DC biased. In fact, the bias current is supplied by the electric field of the THz pulse that encounters the PcA. The optical probe pulse focused on the diode gap, as in the previous case, creates photocarriers which, driven by the electric field of the THz pulse, generate a current inside the antenna. The induced photocurrent is proportional to the field amplitude of the THz radiation focused on the photoconductive gap. This provides the time-resolved signal that allows the temporal shape of the

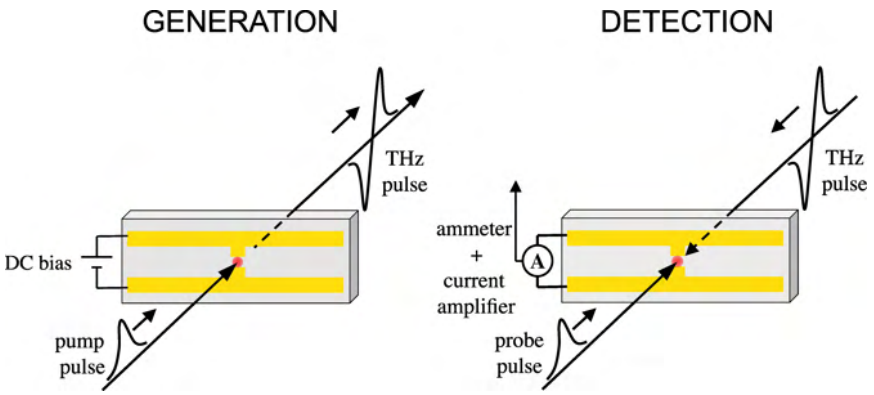

Figure 3.6. *Schematic representation of THz pulse generation and detection with a PcA. In the first case the optical laser beam is focalized at the centre of the dipole gap to create generation of photocarriers that under the effects of the bias voltage flow through the electrodes generating the THz electric field. In the case of detection, however, the bias field is provided by the electric field of the THz pulse, which combines with the photocarriers generated by the probe beam to create a current proportional to the amplitude of the THz electric field. Figure adapted from [74].*

THz pulse to be reconstructed. The signal is function of the time delay between the pump and probe pulses. In figure 3.6 is reported a schematic representation of THz pulse generation and detection with a PcA.

3.2.4 Sample Preparation

The measurements were conducted by preparing three stock solutions, which involved the dissolution of HEWL (L6876, Sigma-Aldrich) in ultra pure milliQ water. The samples, measured at various concentrations at different temperatures, were prepared by diluting the stock solutions. The measurements taken at 4°C and 9°C share the same set of sample, as well as those taken at 17°C and 35°C. A vortex is used to ensure the correct dissolution of the protein in the stock solutions. The solutions were filtered with a 0.22 μm Millipore syringe filter. Subsequent to filtration, the concentration was re-measured using a UV-VIS spectrophotometer by studying the intensity of the absorption peak characteristic of the protein at 281 nm. The concentration of the solutions was measured again at the conclusion of the measurements.

3.3 Results

Figure 3.7 (a) reports the measured time resolved signals in the reference (blue line) and sample (red line) of the 175 mg/mL concentration solution at 9°C. The traces shown are the averages of five measurements. Each measurement was obtained by averaging the signal from four scans of the delay line. A single scan enables probing of the signal over a time window of approximately 80 ps. The figure shows data up to 35 ps for better visualisation. The inset shows a shorter time window to highlight the temporal shape of the THz pulse. The measurements of the different samples

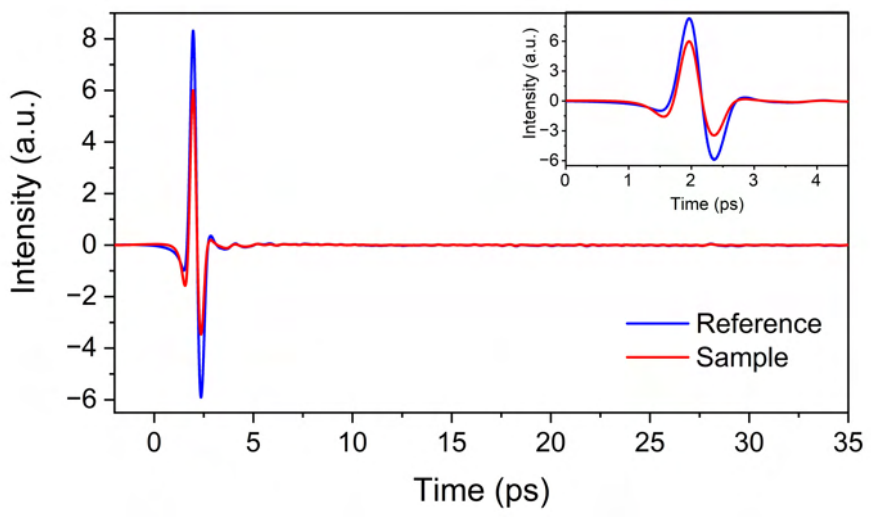

(a)

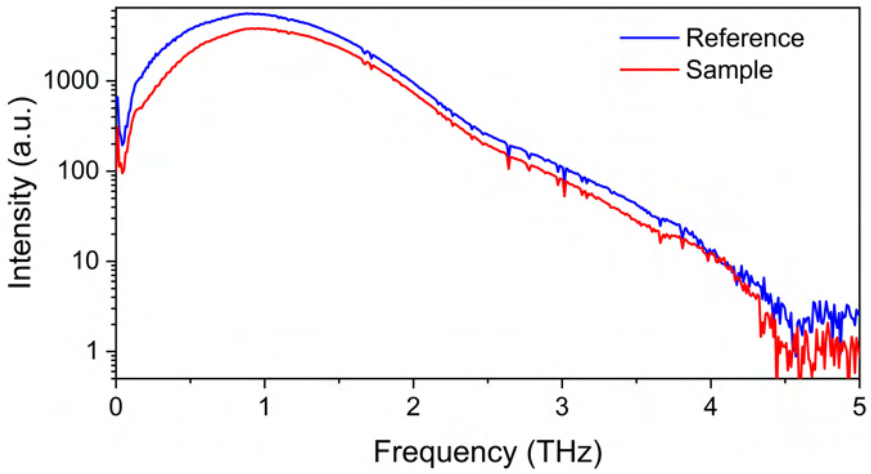

(b)

Figure 3.7. (a) *Time traces of the signal for the ATR cell in the "reference" (blue line) and "sample" (red line) positions, for the 175 mg/mL solution at 9°C. The averages of five measurements are shown here. The insert shows a detail between 0 and 4 ps to better visualise the temporal shape of the THz pulse.* (b) *Fourier transforms in logarithmic scale of the time traces reported in (a).*

were acquired by alternating the position of the ATR cell between the "reference" and "sample" positions. Before inserting the sample, a calibration measurement was performed in the same way to obtain the function used to correct the transfer function (see equation 3.13).

Comparison of the "reference" and "sample" signals reveals that the presence of the sample reduces the signal intensity by approximately 25%. This reduction is due to the absorption of the evanescent wave by the aqueous solution.

Figure 3.7 (b) shows the Fourier transforms of the two time signals shown in the figure 3.7 (a) on a semi-log scale. The THz pulse spectrum is approximately 4.5 THz wide (consistent with the maximum bandwidth obtainable from PcAs) and has a maximum at approximately 1 THz. The narrow lines visible on both spectra are due to the absorption of residual water vapour present inside the nitrogen-purged box containing the THz setup (see section 3.2.2). Comparing the two spectra, no significant changes in the spectral shape of the pulse are observed. These once again show the reduction in signal intensity due to absorption by the aqueous sample. Performing the analysis described in section 3.2.1 from the transfer function it's possible to extract the absorption coefficient α and the refractive index n of the investigated solutions. In figure 3.8 the absorption coefficients of the water lysozyme solutions with different concentrations are shown. The purple line refers to the pure water absorption coefficient. Here are reported the results at the lowest temperature 4°C (3.8(a)) and the highest 35°C (3.8(b)).

It can be observed that, above 2.5 THz, the signal-to-noise ratio is not sufficient to reliably discuss the spectral properties. At both temperatures, a clear decrease in the absorption coefficient is observed as the protein concentration increases, consistent with the findings of similar studies on highly concentrated samples [67, 68]. The decrease is more visible in measurements at higher temperatures. The increase in concentration does not show a significant variation in the shape of the spectra, which mainly appears to change in slope. It should be noted that the dynamics observed in this spectral region are mainly related to the low frequency tail of the intermolecular stretching band at 4-5 THz of the network of hydrogen bonds forming water [2, 10]. Comparing the two temperatures, the absorption coefficients appear greater at higher temperatures, as expected considering the higher absorption of water as the temperature increases. What is measured here is in agreement with the literature findings [77, 78].

Figure 3.9 shows the refractive index for the water-lysozyme solutions for the temperature of 4°C and 35°C. As for the absorption coefficients the refractive index decreases with concentration increasing but the effect is proportionally lower than that observed for absorption coefficients. Considering the measures at 35°C the α of water decreases of $\sim 25\%$ compared with the highest concentration solution, while for the refractive index a variation of $\sim 2\%$ is observed. The refractive index increase with temperature especially in lower frequencies region. Again, this behaviour is expected in water [77, 78]. The values obtained are consistent with previous work on lysozyme solutions [68].

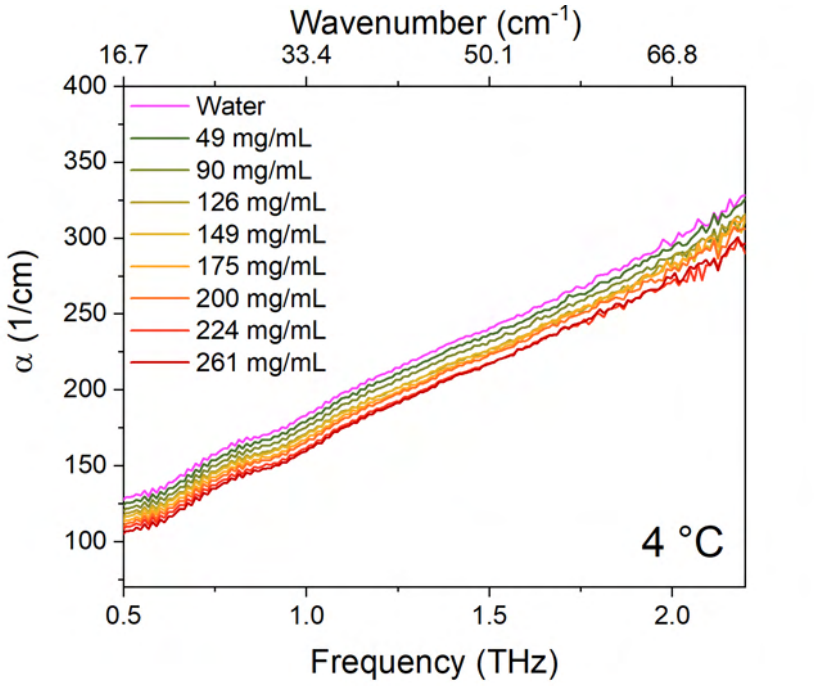

(a)

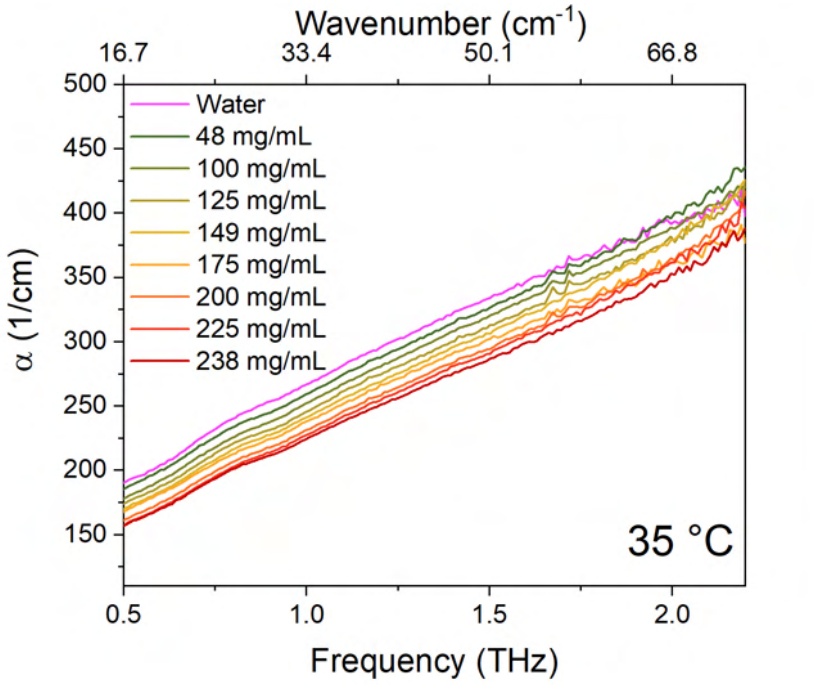

(b)

Figure 3.8. (a) *Absorption coefficients of water-lysozyme solutions in a concentration range between ∼ 50 mg/mL and ∼ 260 mg/mL at a temperature of 4°C.* (b) *Absorption coefficients of water-lysozyme solutions in a concentration range between ∼ 50 mg/mL and ∼ 240 mg/mL at a temperature of 35°C.*

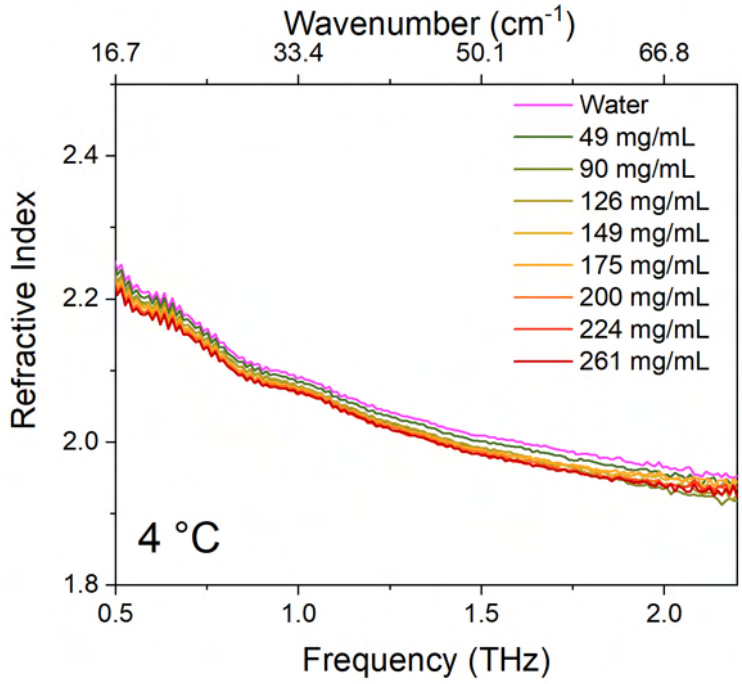

(a)

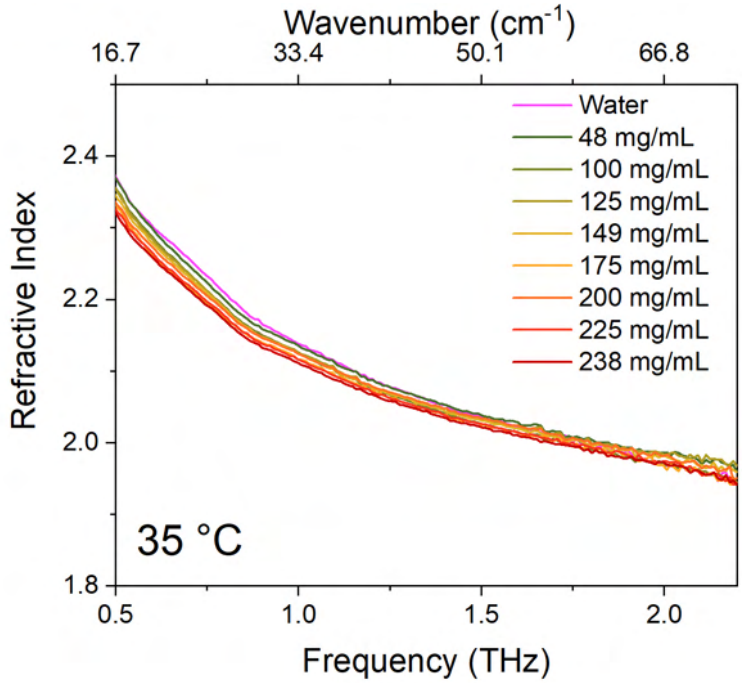

(b)

Figure 3.9. (a) *Refractive index of water-lysozyme solutions in a concentration range between ∼ 50 mg/mL and ∼ 260 mg/mL at a temperature of 4°C.* (b) *Absorption coefficients of water-lysozyme solutions in a concentration range between ∼ 50 mg/mL and ∼ 240 mg/mL at a temperature of 35°C.*

3.4 Discussion

As discussed in the introduction of this chapter, THz spectroscopy is highly sensitive to hydration water and can probe hydration shells extending up to 4.2 nm in the case of lysozyme [68]. Given the very high concentration range investigated in this study, it is possible to assume that the hydration shells of the individual proteins overlap with one another. To verify whether this assumption holds at all temperatures and across the entire concentration range, a system composed of bulk water, hydration water, and lysozyme molecules can be considered, and the variation of the volume fraction of each component can be evaluated. From the volumetric measurements of *J. Krakowiak et al.* [79] it is possible extrapolate the lysozyme specific volume as a function of concentration and temperature. Although these values were measured over concentration and temperature ranges different from those used in this work, the trends they found can be extrapolated to estimate the variation in specific volume at low temperature and high concentration. In this way, taking both variables into account, the maximum observable variation is found to be approximately 3%, variation that did not prove to be significant during analysis. For this reason, for evaluating of the volume fraction of lysozyme in solution, it is assumed that a single lysozyme molecule has a constant specific volume of 0.715, given by the average of the extrapolated values.

Once the specific volume has been defined, considering the number of lysozyme molecules at different concentrations and assuming a spherical hydration shell with a radius of 4.2 nm, it is found that the only samples in a condition where a bulk water residue is present are those with a concentration of $\sim$ 50 mg/mL. For these samples, it is found that bulk water should occupy approximately 38% of the total volume of the solution. In all other solutions at higher concentrations, the solvent can be considered to consist entirely of hydration water. The hydration shells in these solutions will therefore overlap more and more as the concentration increases. A graphical representation of the different low and high concentration regimes is shown in the figure 3.10. To provide this volume estimate, the water–protein system is evaluated as if it were homogeneous.

The saturation of the hydration water in the samples therefore does not allow the direct application of equation 3.1, in which the system is described as consisting solely of bulk water and protein, nor the application of equation 3.2, in which the solvent is considered as a combination of bulk water and hydration water. The absorption coefficients found can instead be treated as the linear combination of two components, one linked to hydration water and one to protein. Therefore, considering the absorption of protein to be negligible compared to the aqueous component, the absorption coefficient $\alpha(\nu, C)$ of the solutions is described as:

$$\begin{aligned} \alpha(\nu, C) &= \alpha_{\mathrm{H}}(\nu, C)\Phi_{\mathrm{H}}(C) + \alpha_{\mathrm{Lys}}(\nu)\Phi_{\mathrm{Lys}}(C) \\ &\approx \alpha_{\mathrm{H}}(\nu, C)(1 - \Phi_{\mathrm{Lys}}(C)) \end{aligned} \tag{3.16}$$

where $\alpha_{\nu,\mathrm{C}}$ is the absorption coefficient of the hydration water component and $\Phi_{\mathrm{Lys}}(C)$ is the volume fraction occupied by lysozyme. The variations in the absorption coefficient spectra at different concentrations are therefore attributable to two effects: the first is linked to an increase in excluded volume, the second to a

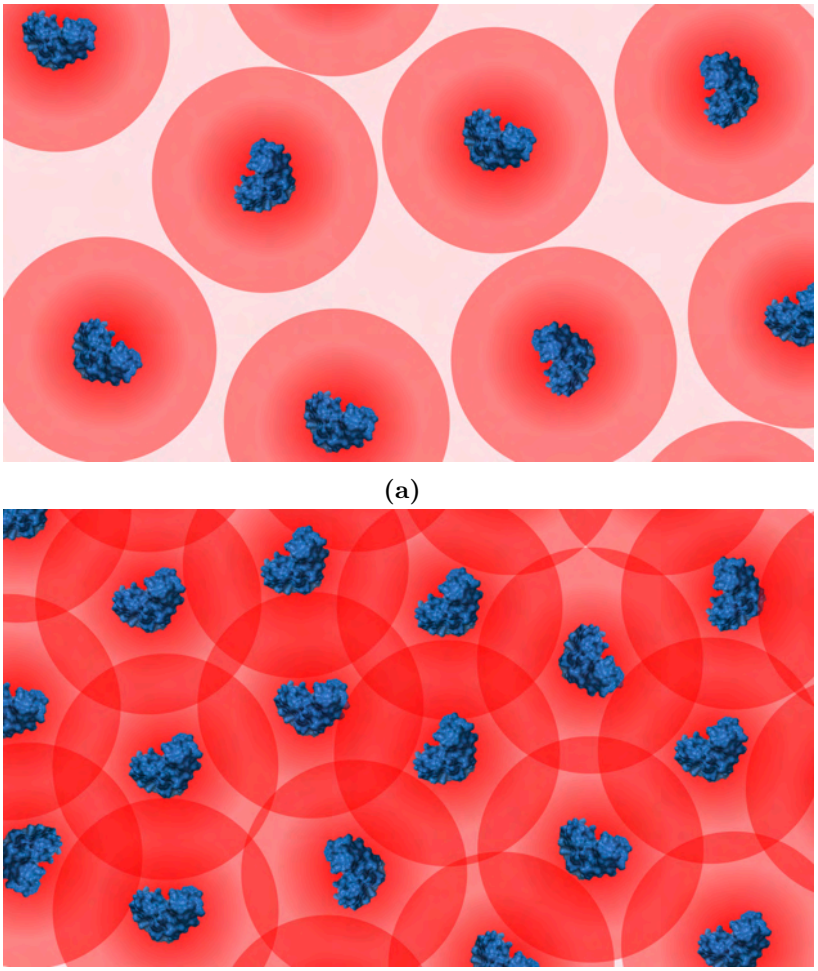

(a)

(b)

Figure 3.10. (a) *Sketch depicting what happens in a low-concentration lysozyme-water solution. Lysozyme molecules are surrounded by their hydration shell. The darker part of the shell represents the more strongly bound water, while the lighter part represents the less strongly bound water. It can be seen that the hydration shells do not overlap and a component of bulk water within the solution is still present (pink background).* (b) *High concentration scenario (> 50 mg/mL). Due to the high number of lysozyme molecules, the hydration shells are extremely overlapping. The solution no longer contains a bulk water component.*

dependence of the hydration water component on protein concentration. Although the solutions are saturated with hydration water, the extent to which the hydration shells of the individual proteins overlap will clearly depend on the amount of protein in solution. For this reason in the equation 3.16 the dependence of α_H from concentration is explicit, while in equation 3.2 α_H is considered concentration independent.

Based on these assumptions, α_H at different concentrations can be derived from experimental data by applying the relationship:

$$\alpha_H(\nu, C) = \frac{\alpha(\nu, C)}{1 - \Phi_{Lys}(C)} \tag{3.17}$$

The results for the 4°C and 35°C temperatures are reported in figure 3.11. The values for the others temperatures are reported in the appendix A. Comparing the results at the two most distant temperatures, a different dependence of α_H on concentration can be observed. At higher temperatures, all the spectra differ from the bulk water spectrum at 35°C in a similar way and do not seem to show a strong dependence on protein concentration. This implies that at higher temperatures, the variation in the absorption spectrum of the solutions is mainly related to an excluded volume effect. In contrast, at low temperatures, a strong dependence of α_H on concentration is observed. In fact, there is an overall increasing trend as the concentration rises, with hydration water appearing to differ more from bulk water at the highest concentrations. In general, at all temperatures and concentrations, the absorption coefficient associated with the hydration water component is higher than that measured for bulk water. This result is consistent with previous studies [16, 29, 67, 68].

To better visualise the effect of concentration and temperature variations on the hydration water absorption coefficients, figure 3.12 shows the average value of α_H evaluated between 0.5 THz and 2.0 THz at different temperatures as a function of concentration. The error bars associated with the measurements are evaluated by evaluating the standard deviation from the mean value, found by analysing the single measurements. The values found show an approximate linear increase with increasing concentration for all temperatures. However, the slope of this linear trend appears to depend on temperature. At lower temperatures, there is a greater slope, while a plateau appears at higher temperatures, particularly at concentrations above 50 mg/mL. Essentially, hydration water at lower temperatures behaves very differently from bulk water only at high concentrations.

One possible explanation for this effect is linked to the presence of clusters within the solutions. In the previous chapter, OKE spectroscopy data showed how hydration water is influenced by the presence of clusters in solutions. However, in the data analysis carried out so far, the system has always been treated as homogeneous, even though it is not. In the simulative work of *A. Baumketner and W. Cai* [63], the strong dependence of the cluster structure on temperature is shown. Specifically, they demonstrated how, once a certain critical concentration is exceeded, the number of molecules that constitute a single cluster tends to become constant, so within the solution there is a homogeneous distribution of macroparticles (the clusters) of approximately the same size. It was found that the critical concentration at

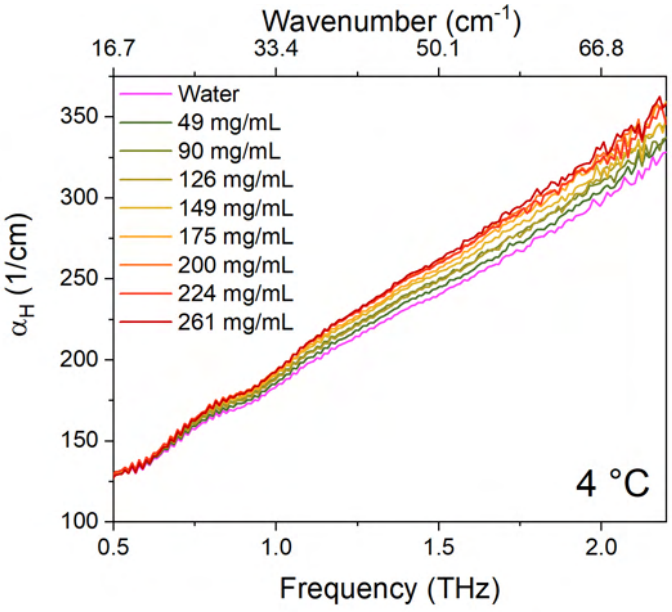

(a)

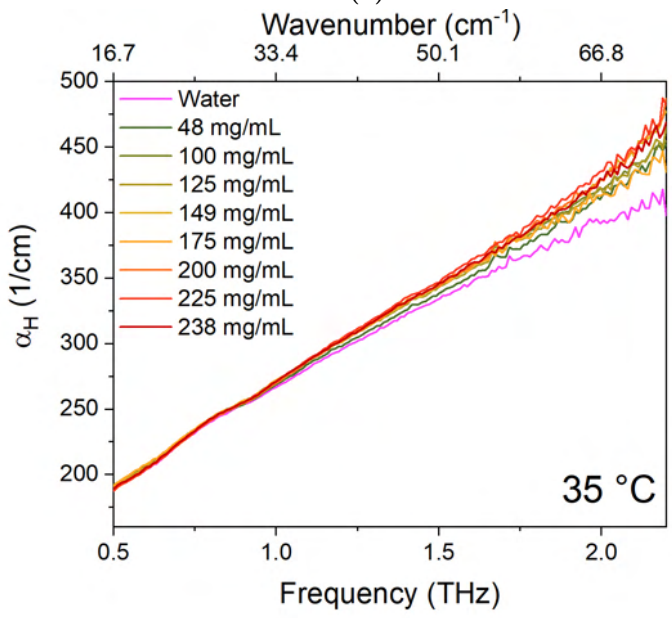

(b)

Figure 3.11. *Absorption coefficients of the hydration water component at different concentrations at 4°C* (a) *and 35°C* (b). *Low temperature measurements show greater dependence on concentration than high-temperature measurements, which are almost constant. In general, an increase in the absorption coefficient is observed as the concentration increases.*

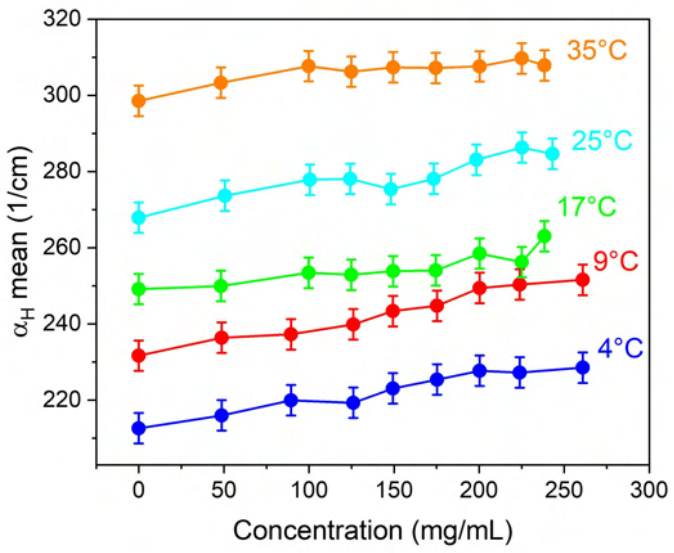

Figure 3.12. *Mean values of the absorption coefficients of the hydration water component, evaluated between 0.5 and 2 THz, are reported as a function of concentration and temperature. It can be observed that, at all temperatures, the absorption coefficient increases linearly with concentration, although this trend becomes less pronounced as the temperature rises.*

which this regime is reached depends on the temperature; specifically, the critical concentration decreases with decreasing temperature (50 mg/mL at 0°C).

It is therefore expected that the total number of clusters in solution will increase proportionally to the increase in concentration, but also that at lower temperatures the structure of the clusters will be more homogeneous than at higher temperatures. Currently, there is no estimate of the extent of the hydration shell of the clusters, but we can assume that at lower temperatures the individual clusters are surrounded by hydration shells of very similar extent, which is less plausible at higher temperatures, where the system has high polydispersity and there are clusters composed of a variable number of lysozyme molecules.

The gradual change in the absorption coefficients of hydration water compared to bulk water at low temperatures may be implicated in the hydration shells of clusters that increasingly overlap as the concentration increases thus modifying the absorption coefficient, while the α_{H} found at high temperature almost independent of concentration can be due to the greater instability of the system linked to temperature, whereby the size of the clusters and their hydration shells vary continuously, thus giving rise to an effective hydration water absorption coefficient that is approximately independent of concentration.

3.5 Conclusion

A spectroscopic investigation was conducted in the THz regime using the TH-TDS technique with an ATR configuration. The samples studied were water-lysozyme solutions at different concentrations, whose properties were studied in a temperature range between 4°C and 35°C. The THz-TDS technique allowed both the absorption coefficients and the refractive index of the solutions to be measured, but the analysis was mainly conducted on the properties of the absorption coefficients.

The high sensitivity of THz spectroscopy to hydration water, combined with the high concentrations used, allowed the concentration dependence of the hydration water absorption coefficients to be measured directly. It was found that at lower temperatures, the α_{H} coefficients are more dependent on concentration variation, while at high temperatures they appear almost constant.

A possible interpretation of this effect can be traced back to the presence of clusters within the solutions, present in high-concentration lysozyme-water solutions. At high temperatures, these have a less stable structure, which can lead to a reshuffling of the hydration shells, thus preventing the effect of the hydration shell overlap linked to the increase in concentration from being observed.

It is important to note that the absorption coefficients associated with hydration water are obtained using a model that is a rough approximation in which the system does not take into account the presence of clusters. In the future, it would be interesting to repeat this type of measurement with other parallel measurements that also allow for a description of the properties of the clusters present in the system, such as Dynamic Light Scattering (DLS) measurements.

Comparing the results obtained from this investigation with the OKE spectroscopy results reported in the previous chapter, in this case no critical discontinuity in the properties of hydration water was observed as the concentration increased and connected in a change in the cluster regime. This may be related to the different physical observable studied in the two experiments: while OKE spectroscopy studies the polarizability of molecules, THz-TDS explores the dipole moment. As already discussed in the introductory chapter of the thesis, the definition of hydration water is strongly dependent on the physical observable under study [10]. In the case of OKE spectroscopy, it is possible to investigate the properties of water strongly influenced by the protein forming the first hydration layer. In this case, however, an extremely extended dynamic hydration shell corresponding to about ten layers is observed. This also demonstrates the need to combine different spectroscopic techniques to study the properties of hydration water.

However, introducing temperature dependence also highlighted an additional effect probably due to the cluster presence on the properties of hydration water. This suggests that OKE spectroscopy measurements should be repeated at different temperatures.

Chapter 4

THz broadband spectroscopy investigation on water-lysozyme solutions

4.1 Introduction

During my PhD programme, I had the opportunity to spend six months in the research group of Professor Martina Havenith at the Ruhr University in Bochum, Germany. During this period, broadband THz absorption measurements were performed with a Fourier-transform infrared (FTIR) spectrometer on the water–lysozyme samples presented in the previous two chapters. This study provided a more comprehensive description of the absorption spectra of the samples, extending the investigated spectral range up to 18 THz.

In this spectral range, the absorption spectrum of liquid water is characterized by two broad bands, peaking at 6–7 THz ($\sim$ 200 cm^{-1}) and 18 THz ($\sim$ 600 cm^{-1}). These spectral features are associated with the stretching vibration of intermolecular HBs, as well as the restricted rotational motion of water molecules within the HBs network, a process generally known as libration [5, 80–82]. The FTIR spectrometer is therefore an extremely effective tool for studying the characteristics of hydration water related to these two dynamics. Recently, Havenith's group has developed a new technique called THz calorimetry, based on experimental data obtained using FTIR spectroscopy [12, 40, 83, 84].

THz calorimetry is a spectroscopic technique that enables the extraction of solvation free-energy changes from low-frequency vibrational spectra. These changes are directly linked to chemical and biological processes, in which subtle variations in solvation enthalpy and entropy dictate stability, folding, aggregation, or phase separation phenomena [84]. Solvation thermodynamics can be described through a two-step thermodynamic cycle [85]. First, a cavity is created in the water HB network to host the solute. Then, the solute is inserted and solute-water interactions are formed. For hydrophilic solutes, insertion restricts orientational dynamics and leads to a Gibbs free energy gain (ΔG_{ins}) mainly of enthalpic origin. For hydrophobic solutes, the free-energy change is instead dominated by entropic contributions.

The solvation free energy can be written as a sum of these two steps [83]:

$$\begin{aligned} &\Delta G_{\text{cav}} + \Delta G_{\text{ins}} = \\ &= \Delta H_{\text{cav}} - T\Delta S_{\text{cav}} + \Delta H_{\text{ins}} - T\Delta S_{\text{ins}} = \\ &= \Delta H_{\text{solv}} - T\Delta S_{\text{solv}} \end{aligned} \tag{4.1}$$

Here, ΔH_{cav}, $-T\Delta S_{\text{cav}}$, ΔH_{ins}, and $-T\Delta S_{\text{ins}}$ represent the partial enthalpic and entropic contributions, according to $\Delta G = \Delta H - T\Delta S$, with T denoting the temperature. ΔG_{cav} accounts for the volume exclusion effect and the resulting perturbation of the surrounding water network wrapped around the solute, while ΔG_{ins} includes attractive intermolecular interactions such as Van der Waals, electrostatic, and hydrogen bonding. Enthalpic and entropic contributions arising from bulk water-water interactions are unaffected and therefore do not contribute to solvation thermodynamics. Consequently, all terms in equation 4.1 exclusively arise from solute–water interactions.

The intermolecular interactions between a solute and its surrounding hydration water molecules can be studied by analysing the THz difference spectra, $\Delta\alpha$, obtained by subtracting the pure water spectrum from that of the solution. The relevant modes lie within the frequency window of the HBs intermolecular stretching vibrations and in the range of water librations. These two spectral regions, can be linked to two characteristic water populations in the thermodynamic cycle [12, 83, 86, 87]: water arranged around the solute-induced cavity and the solute-bound water molecules. The correspondence of these spectroscopic signatures with the underlying local solvation motifs can be established by combining experimental data with simulations and theoretical THz spectroscopy. In the frequency domain, the so-called cavity-wrap (hydrophobic) population, which corresponds to the two-dimensional HBs network enveloping the solute-induced cavity (first step of the thermodynamic cycle), displays a characteristic THz band centred at 150-160 cm^{-1}. This band is red-shifted with respect to the bulk intermolecular HBs stretching peak ($\sim$195 cm^{-1}). The cavity spanning HBs differ spectroscopically, structurally, and dynamically from those in bulk water. In particular, the HBs forming the wrap exhibit a reduced number of accessible configurations compared to the bulk, leading to a weakening of the HBs network due to diminished cooperativity [83, 86]. As a result, the intermolecular stretch frequency shifts to lower values, reflecting the reduced effective HBs strength. The larger the perturbation of the water network required to accommodate the solute, the more intense this band becomes in the THz difference spectrum. Hence, the appearance of a feature at 150-160 cm^{-1} in the difference spectra relative to the bulk serves as a fingerprint of how compatibly a solute integrates into the water network.

In the second step of the thermodynamic cycle, corresponding to the water molecules hydrogen bonded to polar moieties of the solutes, the region of interest is the one covered from the librational regime of water (300-700 cm^{-1}). In this domain, soft librations appear at lower frequencies ($\sim$400 cm^{-1}), whereas harder, more constrained librations are observed at higher frequencies (400-600 cm^{-1}), indicating progressively hindered orientational motions of water molecules. The distinctive spectral fingerprint of the bound population in this range arises from steric restrictions on the rotational dynamics of water induced by proximity to solutes

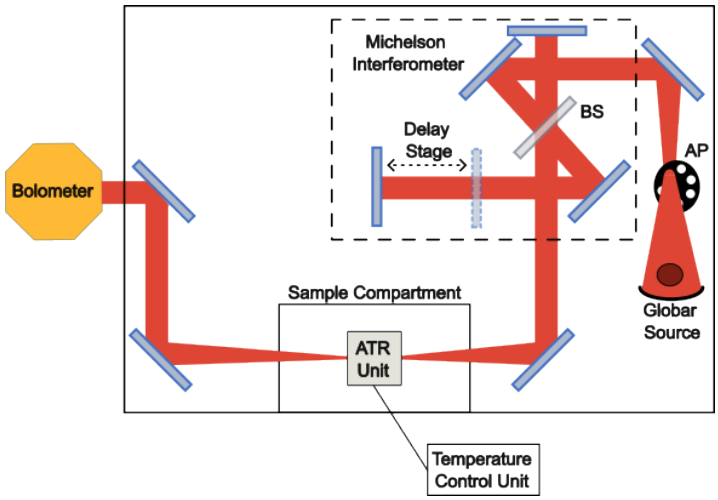

Figure 4.1. *Optical path in the Fourier Transform spectrometer Bruker-80v. The THz sourced used ia a standard Globar (silicon carbide blackbody) source. An aperture wheel (AP) is used to select the numerical aperture of the beam. First, the beam pass through a Michelson interferometer. A mylar multilayer is used as Beam Splitter (BS). From the exit of the Michelson interferometer, the beam is focused inside the ATR unit. Finally, the beam is detected by means of a helium-cooled silicon bolometer. Figure adapted from [89].*

and direct HBs interactions [8, 86, 88]. This manifests as a reduced intensity at the soft librational mode and an enhanced amplitude at the higher-frequency librations compared to bulk water, resulting in a negative $\Delta\alpha$ below 400 cm^{-1} and a positive $\Delta\alpha$ between 400 and 600 cm^{-1}. Altogether, the THz difference spectra reveal a characteristic, nearly linear increase in intensity above 400 cm^{-1}. This trend reflects the attractive solute-hydration water interactions that stabilize solvation through a favourable enthalpic contribution. The effect can be quantified by the slope $\Delta\alpha/\Delta\nu$ obtained from linear fits to the difference amplitude in the 400-600 cm^{-1} window.

Based on this context, THz calorimetry was applied to the absorption spectra of water-lysozyme samples as the concentration varied, with the aim of characterising the variation in free solvation energy in a cluster regime. To confirm the clustering state of the samples, Dynamic Light Scattering (DLS) measurements were also performed, which allowed the size of the aggregates present in the samples at different concentrations to be estimated.

4.2 Methods

4.2.1 FTIR-THz setup

In figure 4.1 is reported the FTIR spectrometer optical setup. The FTIR spectrometer (Vertex 80v; Bruker, Billerica, MA) is based on a high-stability Michelson interferometer fully enclosed in a vacuum chamber to suppress the strong absorption of water vapour and carbon dioxide in the far-infrared and THz regions. A standard Globar (silicon carbide blackbody) sources is used to produce the THz

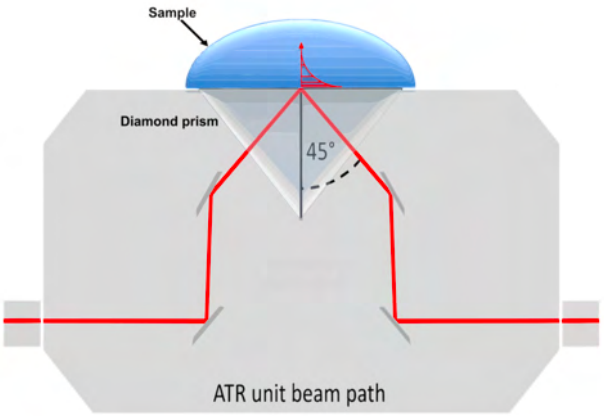

Figure 4.2. *Optical path of the beam inside the ATR unit. The beam it's totally internally reflected form the interface between the sample and the diamond prism. This generate an evanescent wave that decay exponentially with the distance from the surface. The decay constant depends on the wavelength of the beam. Figure from [89].*

radiation. An aperture wheel (AP) is used to select the numerical aperture of the beam. The experiment has been conducted using an aperture of 4 mm. The frequency resolution of the instrument is 2 cm^{-1} in the 30-650 cm^{-1} range. For the measurements, an ATR unit with a temperature controlled diamond prism of 500 μm diameter (MVP-Pro; Harrick Scientific, Pleasantville, NY) has been used. In figure 4.2 is reported a graphical representation of the optical path of the THz beam inside the ATR unit. A sample drop of approximately 100 μL is pipetted onto the surface of the prism and the sample compartment was constantly purged with nitrogen at atmospheric pressure. The evanescent field penetrating the crystal decay exponentially with the distance from the surface of the diamond prism. The characteristic distances of decay (penetration depth d_p) are dependent on the wavelength of the beam (Eq. 4.3). An helium-cooled silicon bolometer (Infrared Laboratories, Tucson, AZ) is used as a detector. The data acquired are the average over 64 scans in 2 min. The THz absorption spectrum $\Delta\alpha$ was calculated from the intensity I by Beer-Lambert's law [40]:

$$\alpha(\nu) \approx -\frac{1}{d_p} \ln\left(\frac{I(\nu)}{I_{ref}(\nu)}\right) \tag{4.2}$$

$$d_p = \frac{\lambda}{2\pi \cdot \sqrt{n^2_{diamond} \cdot \sin^2(\theta) - n^2_{sample}}} \tag{4.3}$$

where appear the penetration depth d_p and an angle θ of 45°is considered. The refraction index of the diamond is $n_{diamond} = 2.38$, while for the sample $n_{sample} = 1.5$ is assumed. The symbol $\approx$ appearing in the equation 4.2 is due to the fact that Beer-Lambert's law, as written, would measure the optical density of the sample. However, this can be considered comparable to the absorption coefficient, assuming the condition n_{sample} is constant, an assumption considered valid in previous similar

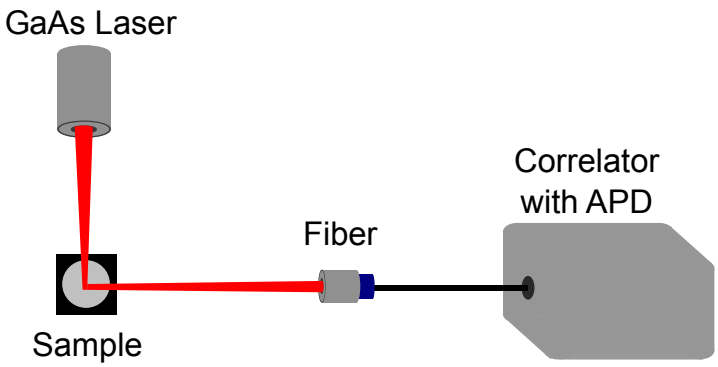

Figure 4.3. *Schematic representation of the DLS measurement setup. The laser source is GaAs laser. The detection system is composed of a single-photon counting module to record time-dependent fluctuations of the scattering signal combined with an Avalanche Photodiode (APD). This transmits the photon counts to a high-speed digital correlator for data analysis. The detector operates at 90° scattering angles.*

studies of aqueous protein solutions [12, 90, 91]. Nevertheless, given that this is also an approximation, it would be incorrect to use the equality symbol.

4.2.2 Dynamic Light Scattering

The hydrodynamic radius (R_h) of a macromolecule in solution is determined from its translational diffusion coefficient (D_t), which can be obtained from dynamic light scattering (DLS) measurements. DLS relies on the time fluctuations of scattered light intensity: smaller macromolecules diffuse faster and generate more rapid intensity fluctuations compared to larger ones. The relationship between R_h and D_t is described by the Stokes–Einstein equation [92]:

$$R_h = \frac{k_B T}{6\pi\eta D_t} \tag{4.4}$$

where k_B is the Boltzmann constant, T is the absolute temperature, and η is the solvent viscosity.

DLS experiments were carried out in the DynaPro NanoStar instrument. Figure 4.3 reports a schematic representation of the optical setup. The laser source is GaAs laser operating at a nominal wavelength of 658 nm with 95 mW delivered to the sample cell. The DLS detector employs a single-photon counting module to record time-dependent fluctuations of the scattering signal. DLS detector is an actively quenched, solid state Single Photon Counting Module (SPCM), which contains an Avalanche Photodiode (APD). This high-speed detector operates at frequencies up to 30 MHz and transmits the photon counts to a high-speed digital correlator for data analysis. The detector operates at 90° scattering angles. The translational diffusion coefficient D_t of the molecules in the sample is determined from the decay of the intensity autocorrelation data.

4.2.3 Samples preparation

HEWL was purchased from Carl Roth (12650-88-3). The samples were prepared by dissolving the lyophilised HEWL in milli-Q water to create a stock solution at the highest concentration. Complete dissolution was obtained using Vortex mixing. Samples at lower concentrations were obtained by diluting the stock solution. Three sets of samples were prepared starting from three different stock solutions. The stock solutions were filtered using a $0.22\,\mu m$ pore size syringe filter to prevent the introduction of dust or undissolved protein. The final concentration of the samples has been tested using an UV-VIS spectrometer, probing the absorption peak at $281\,nm$.

4.3 Results

THz spectra in the range between 50 - 650 cm^{-1} ($\sim$ 1.5-19.5 THz) have been collected to monitor the changes in hydration of lysozyme with increasing concentrations. In figure 4.4 are reported absorption coefficients from one of the three set of samples measured. The low and high frequency region are showed separated to a better visualization of the results. Figure 4.4 (a) shows the spectra between 75 and 250 cm^{-1} while figure 4.4 (b) between 400 and 600 cm^{-1}. In the first region the intermolecular stretching vibrational mode of water is visible, while in the second the librational mode lies. A comparison of the two measurements reveals a different trend as a function of protein concentration. In the lower frequency region, the absorption coefficient decreases as the concentration increases, while in the higher frequency region, this behaviour is reversed, increasing as the amount of protein in solution increases.

To perform the analysis of the results the spectra of the water-lysozyme solutions had been subtracted of the bulk water spectrum. This spectrum is acquired from a measure on a pure water sample. All the measurements has been conducted at a constant temperature of 25°C with a temperature stability of 0.1 °C.

In Figure 4.5 are reported the difference absorption spectra $\Delta\alpha$ of the lysozyme solutions at different concentration. It's visible a negative band at around 125 cm^{-1} for lysozyme solutions. This band is the one connected to the intermolecular stretching of the HBs water network. It's appear redshifted compared to bulk water at 190 cm^{-1}. This behaviour is consistent with what has been previously measured in studies on proteins undergoing LLPS, such as alpha-elastin or FUS [12, 40, 91]. However, comparing the results, in the case of lysozyme the band appears to be shifted further towards the red than in the previous cases, where a central wavelength of $\sim$ 150 cm^{-1} is reported. This could be attributed to the slower translational and re-orientational dynamics of water molecules around hydrophobic parts in lysozyme due to constrained dynamics at hydrophobic patches, which are buried inside in the case of a globular protein. As lysozyme is a globular protein, hydrophobic patches are not as exposed, and this could explain the lower intensity of the band compared to the intensity of the wrap water band for alcohols or intrinsically disordered proteins. The negative peak of wrap water became deeper with the increase of protein concentration. The intensity of the wrap water band is found to be directly correlated instead to the number of water molecules hydrating

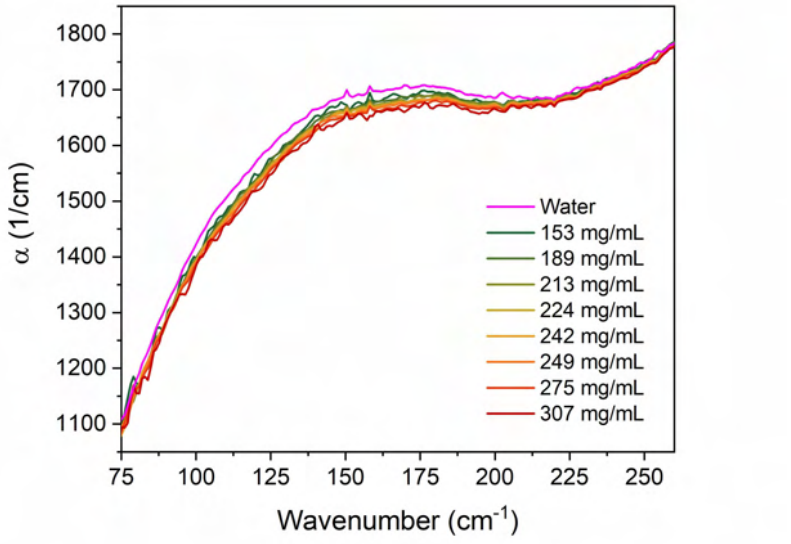

(a)

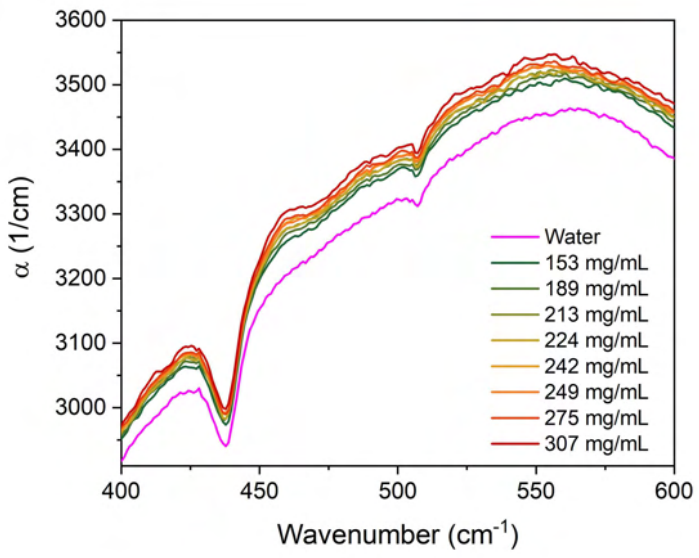

(b)

Figure 4.4. (a) *Absorption coefficients between 75 and 250 cm^{-1} ($\sim$ 2.25-7.5 THz) of water-lysozyme solutions in a concentration range between $\sim$ 150 mg/mL and $\sim$ 300 mg/mL at a temperature of 25°C. In this spectral region leis the intermolecular stretching vibrational mode of water.* (b) *Same spectra of* (a) *but in the frequencies region between 400 and 600 cm^{-1} ($\sim$ 12-18 THz). In this spectral region leis the librational mode of water. Comparing the two spectral regions can be observed a reversal in the absorption coefficient trend with concentration.*

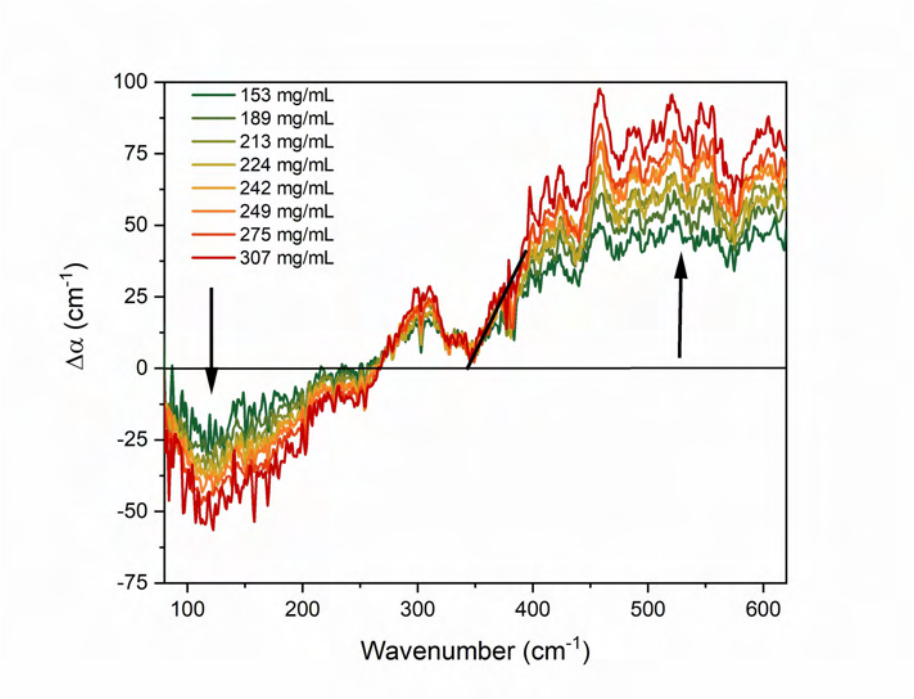

Figure 4.5. *Absorption spectra of lysozyme solutions at different concentrations, after subtraction of the bulk water spectrum. The distinct trends of the wrap water band (∼125 cm^{-1}) and the bound water band (>300 cm^{-1}) are highlighted by the black arrows. With increasing protein concentration, the intensity of the wrap water band decreases, while the slope of the bound water band (black line) increases.*

hydrophobic parts of the protein and to how much the hydration water network is perturbed by the solute [83]. Hence, this decrease could denote the release of wrap water.

The second characteristic feature at > 300 cm^{-1} is in the region related to the dynamics of water librations. The band has a different shape, appearing broader and much steeper than the wrap water one. Moreover, with increasing concentrations the slope of the bound water band increases. The slope of the band from 400 to 600 cm^{-1} has been proven to be a quantitative measure of bound water population [12, 84] and the increase in slope denotes the increased bound water contribution.

Maintaining the comparison with previous THz calorimetry measurements, the shape and positions of these bands vary greatly as compared to phase-separating proteins, indicating a different phenomenon. Additionally, all solutions prepared did not show any kind of aspect of phase separation, and the environment properties guaranteed the stability of the protein [93]. The decrease in the intensity of the wrap water band and the increase in the bound water could instead be an indication of the monomers/dimers coming together to form bigger clusters. The subunits of these clusters are not strongly bonded to each other, but are just closely associated [34, 63]. This would still decrease the number of wrap water molecules, as water in the vicinity of hydrophobic patches or buried in the grooves could be lost first, resulting in an entropic gain. The number of bound water molecules interacting

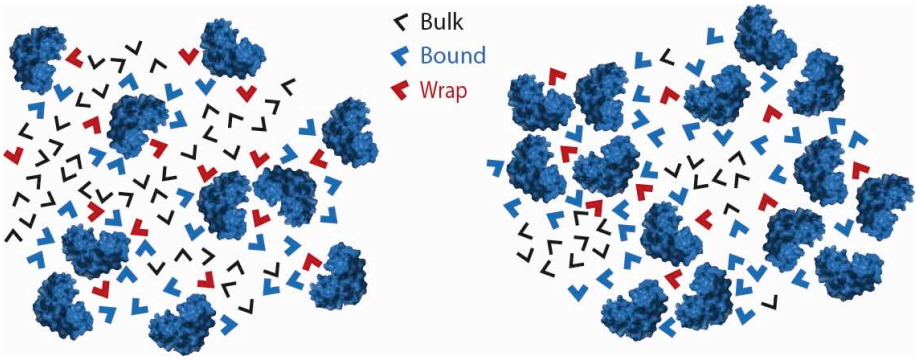

Figure 4.6. *Graphical representation of the water–lysozyme system at different concentrations. The left panel illustrates the low-concentration regime, while the right panel depicts the high-concentration regime. Bound hydration water molecules are shown in blue, wrap hydration water molecules in red, and bulk water molecules in black. At higher concentrations, larger and more numerous protein clusters are formed, and the reorganization of proteins within the solution modifies the balance between the two hydration water components.*

with hydrophilic groups mostly on the surface of the protein, increases as these clusters grow in size. A graphic illustration of this has been shown in Figure 4.6.

To confirm the presence of clusters in the samples and characterise their features such as size or number, an analysis was also performed using DLS measurements. These measurements reveal three characteristic cluster sizes after cumulant fit analysis: $R_1 \sim 1.5\,\text{nm}$, associated with lysozyme monomers; $R_2 \sim 25\,\text{nm}$, attributed to small clusters; and R_3, whose values are reported in Fig. 4.7. For R_3, the clusters appear highly dispersive, indicating the formation of larger aggregates as concentration increases. Moreover, the DLS data show that the cluster-size distribution broadens with increasing concentration, suggesting the progressive formation of larger clusters from monomers or smaller aggregates due to enhanced short-range attractive interactions relative to electrostatic repulsions. These measurements confirm the existence of a cluster regime change within the water-lysozyme solutions at a critical concentration, consistent with the OKE spectroscopy measurements shown in the first chapter of the thesis.

4.4 Discussion

Having established that the variation in wrap and bound water contributions is linked to a reorganisation of proteins within the solvent, i.e. to the presence of clusters that are always larger as the concentration increases, it becomes interesting to compare this result with previous studies on protein systems. In particular, it is possible to combine this result with other critical phenomena such as LLPS and Liquid-Solid Phase Separation (LSPS). Variations in the overall ΔG are obtained from the amplitude of the cavity-wrap feature or the slope of the bound-water response. From here on, these two observables will be referred to as $\Delta\alpha_{\text{wrap}}$ and $\frac{\Delta\alpha_{\text{bound}}}{\Delta\nu}$ respectively. A linear correlation was identified between $\Delta\alpha_{\text{wrap}}$ and $\frac{\Delta\alpha_{\text{bound}}}{\Delta\nu}$, and the variations in the excess mixing entropy, ΔS_{cav}, and enthalpy, ΔH_{ins}, respectively. Conse-

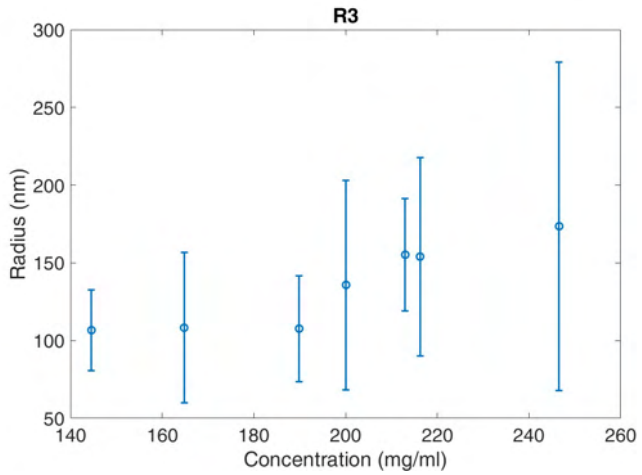

Figure 4.7. *Hydrodynamic radius of large clusters (R_3) in water–lysozyme solutions obtained from DLS measurements. The bars indicate the polydispersity values provided by the cumulant analysis. With increasing protein concentration, the average cluster radius grows, accompanied by a pronounced increase in polydispersity.*

quently, the individual free-energy contributions for cavity formation and solute insertion can be expressed as linear functions of the corresponding spectroscopic observables, scaled by the appropriate factors [84]:

$$\Delta G_{\mathrm{cav}} \approx -T\Delta S_{\mathrm{cav}} = -T\frac{\Delta\alpha_{\mathrm{wrap}}}{\mathrm{cm}^{-1}}\bar{S}_{\mathrm{wrap}} \tag{4.5}$$

with

$$\bar{S}_{\mathrm{wrap}} = -4.4 \pm 0.3\,\mathrm{J\,mol^{-1}K^{-1}}$$

and

$$\Delta G_{\mathrm{ins}} \approx \Delta H_{\mathrm{ins}} = \frac{\Delta\alpha_{\mathrm{bound}}}{\Delta\nu}\bar{H}_{\mathrm{bound}} \tag{4.6}$$

with

$$\bar{H}_{\mathrm{bound}} = -320 \pm 35\ \mathrm{kJ\,mol^{-1}}.$$

The linear correlation factors $\bar{S}_{\mathrm{wrap}}$ and $\bar{H}_{\mathrm{bound}}$ are solute-independent scaling quantities. Their values were fitted to reproduce the results of calorimetry measurements on a set of alcohols [83] and glycerol of different temperatures and concentrations [87]. The thermodynamic values derived from THz calorimetry are excess properties referenced to the pure liquid states, since spectroscopically are measured differences between solution and neat liquid references. In this way, the spectroscopic observables provide direct quantitative access to excess thermodynamic properties as functions of solute concentration, solute size, temperature, and also during biological processes (such as liquid–liquid phase separation, LLPS) [84].

This analysis allow to realize a THz phase diagram (figure 4.8), where the variation in the intensity of the wrap-water band is plotted on the x-axis, and the variation of the parameter associated with bound water is reported on the y-axis. The data shown in figure 4.8 can be combined in a diagram reporting values from previous studies to allow comparison between different phases. The diagram is

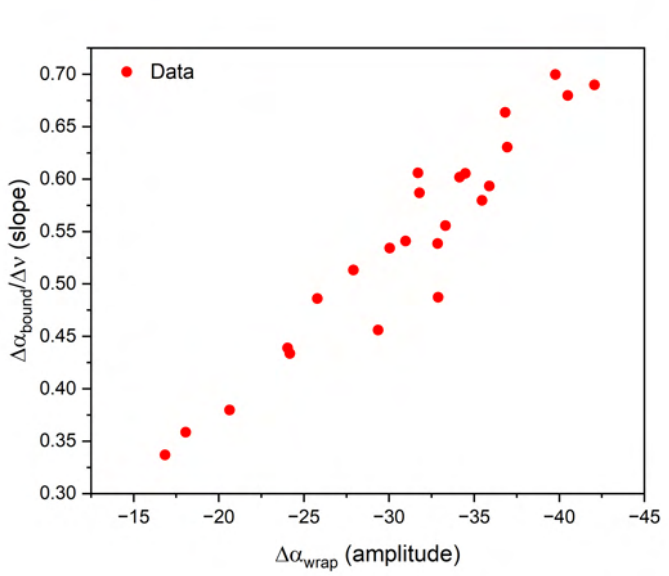

Figure 4.8. *THz phase diagram for water–lysozyme solutions in the cluster regime. The diagram shows the slope of the bound band, used as a parameter characterising its behaviour, plotted as a function of the intensity of the wrap band.*

presented here in figure 4.9, where are shown: the data from the cluster regime measured in this work in red, results from an experiment on α-elastin undergoing LLPS as the system temperature changes [12] in blue, and data from another experiment in which an intrinsically disordered protein undergoes LLPS [90] in green. Each of the three critical behaviours occupy a different region in the phase diagram. The cluster regime appears to cover a region of the phase diagram intermediate between LLPS and LSPS.

Previous studies have suggested the possible existence of equilibrium clusters at these concentrations [34, 63]. In particular, stable equilibrium lysozyme clusters have been reported to arise from a subtle balance between electrostatic repulsion and short-range attractive forces. In this study, the presence of such clusters was not only confirmed, but their hydration water dynamics and size distribution were also investigated in detail. From the phase diagram, it is clearly seen that there is a possibility of intermediate equilibrium states between different types of phase separations. Small changes in variables such as temperature or pH can be used to alter the hydration structure, which can help control the formation of any of these states. This emphasizes the need for further experimental and theoretical investigations aimed at identifying, characterizing, and classifying these intermediate and metastable states, with particular attention to their hydration properties, both in model proteins such as lysozyme and in intrinsically disordered proteins undergoing phase separation.

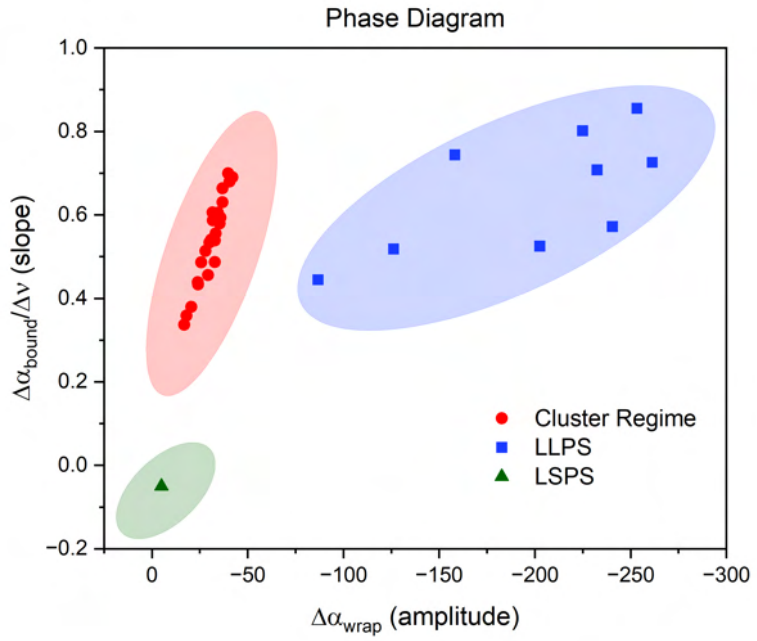

Figure 4.9. *THz phase diagram for different critical behaviours in protein solutions. Data from the present work on the lysozyme clustering regime are shown in red, data from S. Pezzotti et al. [12] describing the LLPS transition are reported in blue, and data from S. Ramos et al. [90] describing the LSPS transition are in green. The three phenomena occupy distinct regions of the phase diagram, highlighting the effectiveness of THz calorimetry in probing the impact of protein reorganization on water.*

4.5 Conclusion

A spectroscopic study was conducted using FTIR spectroscopy in the THz regime of water-lysozyme solutions at increasing concentrations. The absorption spectra obtained were analysed using THz calorimetry to obtain the characteristic parameters of the so-called bound and wrap water in the specific system studied. To better characterize the properties of the water-lysozyme solution also DLS measurements have been performed, clearing showing the presence of cluster of varying size depending from protein concentration. The presence of clusters made it possible to map the $\Delta\alpha_{\text{wrap}}$ and $\Delta\alpha_{\text{bound}}$ parameters to construct a THz phase diagram specific to the cluster regime. The results indicate that the dynamics and release of water molecules around hydrophobic patches of lysozyme (wrap water) slow down as smaller clusters merge into larger ones or as their size increases. At the same time, the population of water molecules interacting with the hydrophilic patches of lysozyme (bound water) grows, reflecting an increasing number of interactions with the protein hydrophilic groups exposed on the cluster surfaces.

By comparing the results obtained with previous measurements of this type on protein samples that perform critical phenomena such as LLPS and LSPS, it was observed that the different regimes occupy well-separated areas of the phase

diagram. This confirms the effectiveness of THz calorimetry, which proves to be a tool capable of distinguishing different critical phenomena that occur in the samples.

The results obtained in this investigation extend the range of frequencies studied in the previous chapter. Using the THz-TDS technique with PCAs as sources and detectors, it is not possible to obtain THz pulses with spectra above 4.5 THz ($\sim$ 150 cm^{-1}), and in particular, the signal-to-noise ratio of the measurements allowed investigation only up to approximately 2.5 THz ($\sim$ 65 cm^{-1}). The spectral region observed with THz-TDS is therefore that in which the initial part of the absorption band associated with the intramolecular stretching vibration of water lies, i.e., the rise of the first peak observable using the FTIR technique.

Comparing the previous measurements at 25°C with those presented here, the trend in the concentration of the absorption coefficient observed is consistent in both measurements. As in the case of THz-TDS measurements, no discontinuity in this trend is evident in FTIR measurements, as was the case in OKE spectroscopy measurements. In the higher frequency band linked to the librational motion of water the behaviour with concentration is reversed, but even here no critical concentrations are observed. This discrepancy with the OKE measurements and the agreement with the THz-TDS measurements once again highlights how studying different physical observables provides access to different properties of hydration water.

This experiment completes the series of measurements conducted on water and lysozyme samples. The results obtained have made it possible to describe various aspects of the collective dynamics of protein hydration water when proteins are placed in an extremely crowded environment.

Chapter 5

Optical Pump-THz Probe study on heme proteins solutions

5.1 Introduction

During the six months research period conducted in Professor Martina Havenith's research group, non-linear spectroscopy techniques were employed to investigate and study the properties of the protein solvation environment. The results presented in this chapter were obtained during the specified period and led to the publication of the paper *A. Buchmann et al.* [94] on which content this chapter is based. The technique employed is known as Optical Pump-THz Probe (OPTP) spectroscopy. In summary, it is a pump-probe experiment in which the sample is excited using a pump beam with a wavelength in the optical range (400 nm), while the response of the system is probed using a probe beam in the THz range. The technical specifications of the experimental setup are explained in the dedicated section of this chapter (see section 5.2.1).

This technique enables the observation of energy coupling between solute and solvent by studying the changing of the THz absorption spectra of the samples after the optical pumping. In this study, the reported data specifically refer to the analysis of samples of myoglobin and cytochrome *c* dissolved in H_2O and D_2O. Heme protein are characterized by a strong absorption peak at around 400 nm, called *Soret band*. The energy absorbed by the heme group after the 400 nm pump pulse, is redistributed to the surrounding protein moiety via intramolecular vibrational relaxation until it reaches the surrounding solvent. The study of the propagation through the sample of the THz probe beam as a function of its time delay relative to the optical pulse, enables the measurement of the characteristic times of energy transport through the protein and its coupling with the solvent.

In living systems, proteins must efficiently dissipate excess energy in order to prevent damage induced by radiation [95]. The capacity of proteins to conduct energy is fundamentally linked to their highly flexible nature, characterised by continuous conformational fluctuations on timescales ranging from picoseconds to microseconds [96]. This intrinsic flexibility provides multiple pathways for dissipating the energy absorbed by photoexcitation.

In heme proteins, these dynamics can be selectively triggered by photodisso-

ciation of bound carbon monoxide in a process known as the "protein quake", a phenomenon that has been extensively studied and debated for decades [97–103]. Despite significant effort, the molecular details of internal energy redistribution and its coupling to the solvent remain incompletely understood [104]. It has been proposed that energy relaxation proceeds in a quake-like manner via a hierarchical, glass-like structural network [105]. The high conformational flexibility of proteins and their strong coupling with the solvent have so far made it difficult to directly observe energy flow, making it highly dependent on the specific technique used.

Transient absorption studies in the Soret band revealed oscillations in the band intensity corresponding to heme deformation upon NO dissociation, persisting for approximately 1 ps [104]. The heme's properties are found to be strongly influenced by protein folding, as evidenced by significant changes in UV-Vis absorption [106] and electron transfer capacity [107]. Investigation on the anti-Stokes intensity of the $\nu 4$ band in myoglobin, reporting biphasic population decay with time constants of 1.9 ± 0.6 ps and 16 ± 9 ps for vibrational relaxation, and 3.0 ± 1.0 ps and 25 ± 1 ps for cooling of the photolyzed heme via energy transfer to the solvent bath [101].

A direct probe of the solvent, monitoring the bending-libration combination band of D_2O at 1800 cm^{-1} after photoexcitation at 580 nm allowed to observe that a solvent heating signal manifested, with a rise time of approximately 4 ps, which could be fitted with a biexponential function. The slower component (∼20 ps, 40±10 nm amplitude) was attributed to diffusive energy transfer from the heme to the solvent. In contrast, the faster component (7 ± 2 ps for myoglobin) was too rapid to be explained by classical diffusion. It was hypothesised that this faster component involved collective protein motions [108].

A study on the transient absorption spectroscopy of cytochrome *c* revealed distinct relaxation components corresponding to heme vibrational relaxation (1.8 ± 0.5 ps) and protein relaxation (11.0 ± 0.5 ps) in the oxidized state. However, it was not possible to resolve the ferrous state that was utilised in this study [102]. The focus of this study is to ascertain which vibrational modes mediate ultrafast energy transfer in proteins. The question of whether energy transport is ballistic or diffusive in nature remains a subject of scientific debate. The temporal parameters within which dissipation into the solvent occurs must be established.

Molecular dynamics simulations have identified three principal pathways for dissipation of excess heme energy, each of which contributes to the overall relaxation (∼ 5 ps). The three different mechanisms are: through-projectile transfer, facilitated by interactions between the dissociated ligand and protein side chains; through-space transfer, driven by interactions between the heme and surrounding residues; through-bond transfer, involving the bond between the heme iron and the proximal histidine (His93). The predominant mechanism in native myoglobin is the energy 'funnelling' through the heme propionate side chains into the solvent via electrostatic interactions [109].

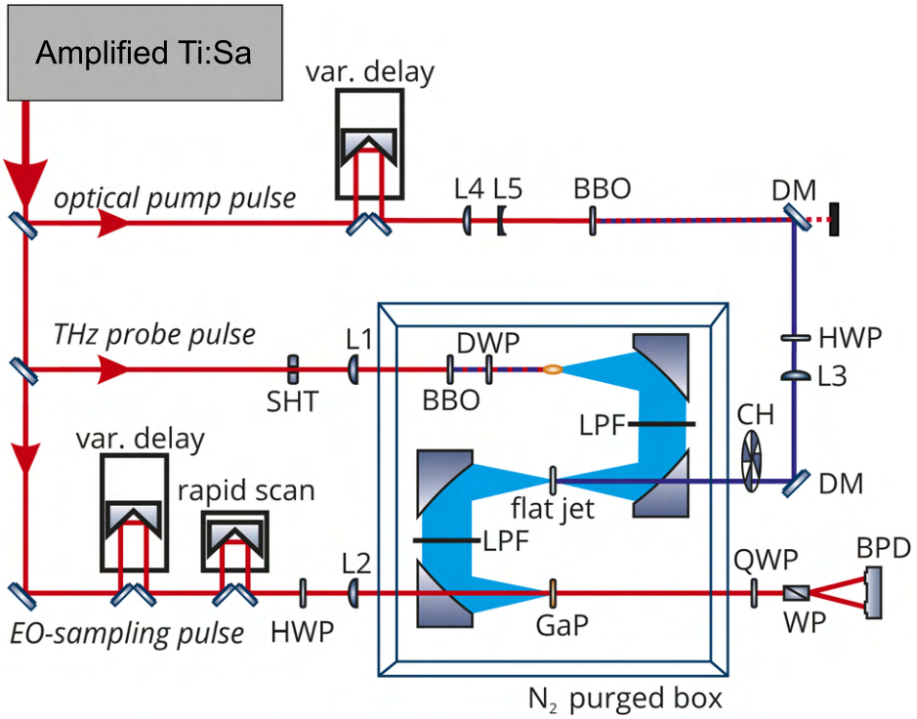

Figure 5.1. *Sketch of the OPTP experimental setup. An amplified Ti:Sapphire (800 nm, 50 fs, 1 kHz, 5.5 mJ) provides the laser pulsed source. The output is split into three branches: the optical pump beam, the THz probe beam, and the electro-optic sampling (EOS) beam for the THz pulse detection. In the pump arm, the 800 nm beam is frequency doubled by a BBO crystal to generate 400 nm pulses, the residual 800 nm is removed by the dichroic mirror DM. The time delay of the pump pulse is controlled by a translation stage. Second harmonic beam is chopped at a frequency of 500 Hz for shot-to-shot comparison of pumped and unpumped states. THz probe pulses are generated by two-colour plasma filamentation. Residual fundamental light is blocked by a 0.5 mm thin high resistivity silicon plate, whilst the THz beam is focused onto the sample and finally refocused onto the detection crystal by means of classic four off-axis parabolic mirrors THz-TDS configuration. The entire path of THz beam is enclosed in a nitrogen-purged box. Detection is performed by electro-optic sampling. A fraction of the 800 nm beam overlapped with the THz field in a 100 µm GaP crystal. The polarization of the optical beam, after being made circular by a quarter wave plate, is analysed by a Wollaston polariser. The horizontal and vertical polarization intensity are then measured by a balance photodiode. A slow moving stage is used to match the temporal overlap in the crystal, while a rapid moving stage varies the delay in a small time window. Figure from [110]*

5.2 Methods

5.2.1 OPTP experimental setup

This section describes the OPTP spectrometer employed in this work. Figure 5.1 shows a scheme of the experimental optical setup. The laser source is a Ti:Sapphire amplified laser (Solstice Ace, Spectra Physics) operating at 800 nm with 50 fs pulses at 1 kHz and a pulse energy of 5.5 mJ. The output is split into three branches: the optical-pump beam, the THz-probe beam, and the electro-optic sampling (EOS) beam. The 800 nm beam is frequency doubled by 500 μm BBO crystal to generate 400 nm pulses. Residual 800 nm light is removed with a dichroic mirror DM, and the pulse energy is adjusted to a pump fluence of 13 mJ/cm^{-2}. Polarization is set to the magic angle (54.7°) with a half-wave plate. A delay stage controls the time delay between pump and THz probe pulses (up to 1 ns). A chopper is setted at the repetition rate 500 Hz, enabling direct shot-to-shot comparison of pumped and unpumped states. The pump spot size at the sample is $\sim$ 400 μm.

THz radiation is generated via two-colour plasma filamentation. The air-induced plasma produces short (190 fs full-width at half maximum) broadband THz probe pulses with a spectral content spanning the 0.5–10 THz (17–334 cm^{-1}) range with an intensity maximum at around 1–2 THz 33–67 cm^{-1}). Residual fundamental light is removed by a 0.5 mm thin silicon plate, and the THz beam is focused onto the sample by a couple of off-axis parabolic mirrors. After transmission, the radiation is collected and refocused onto the detection crystal. The THz beam path is enclosed in a nitrogen purged box to prevent water vapour absorption.

Electro-optic sampling with a 100 μm GaP crystal is used to detect the THz field. A fraction of the 800 nm beam is overlapped with the THz pulse inside the crystal. The polarization of the optical beam became circular after passing trough a quarter-wave plate and is analysed by a Wollaston polariser. The intensity difference between vertical ad horizontal polarization is detected by a balanced photodiodes and sent to a Lock-In Amplifier. A first slow moving motorised stage is used to obtain the pump-probe temporal overlap into the crystal, while a fast-scanning stage samples the full THz waveform [111].

Conventional cuvettes limit OPTP spectroscopy due to absorption of window materials and heating effects. Even diamond windows can distort signals through exciton generation. To overcome this problem, a thin, flat jet of the sample liquid is produced using a 3D-printed nozzle thus enabling the excitation and probing processes without any interference from solid windows. The thickness of the jet was determined to be 28 μm for cytochrome *c* and myoglobin in water and 25 μm for myoglobin in D_2O. For cytochrome *c* in D_2O, it's used a nozzle with a thickness of 13 μm. A temperature controlled reservoir and circulating pump refreshed the sample volume during the period between one excitation pulse and the next, while a syringe pump compensated for evaporation. The reservoir is maintained at a stable temperature of 0°C.

5.2.2 Sample preparation

Equine myoglobin and cytochrome *c* were obtained commercially and used without further purification. Protein solutions (20.0 mg/mL) were prepared in potassium

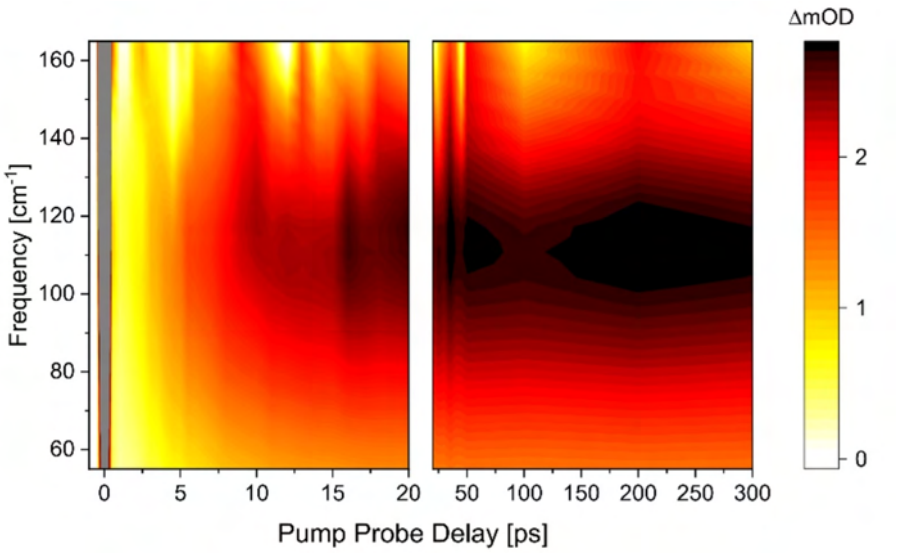

Figure 5.2. *OPTP measurements of an aqueous cytochrome c solution as a function of pump–probe time delay. Figure adapted from [94]*

phosphate buffer (0.05 M, pH 7.3) and filtered through 20 μm syringe filters to remove particulates. For isotope substitution experiments, D_2O was used as solvent, and the pH was adjusted to match the protonated samples (pD = pH + 0.4).

5.3 Results

5.3.1 Experimental Data

The transmitted THz field was recorded as a function of pump-probe delay between 0.5 and 300 ps. The first 0.5 ps of the signal are excluded because they are affected by the Raman response of the sample, which decays within 0.25 ps. The recorded field traces are analysed by Fourier transformation. The differential optical density of the sample ΔmOD, was computed by subtracting the unpumped signal. A positive ΔmOD corresponds to reduced THz transmission, consistent with increased absorption due to local heating of the solvent. The reported errors are extracted from the analysis of 50 consecutive measurements.

Figure 5.2 shows in a 2D map the transient THz differential absorption spectrum as a function of frequency and of pump-probe delay for the cytochrome *c* in water solution. A clear increase in absorption is observed, centred initially near 120 cm^{-1} and shifting to 110 cm^{-1} as a plateau is approached. For a quantitative analysis, spectra at each time delay were fitted with a Gaussian function, and the resulting amplitude was plotted as a function of time delay. The temporal evolution was modelled using a single exponential rise function. Figure 5.3(a) reports some vertical slices of the map and the Gaussian fit of the signal at different time delays. In black it's also plotted the difference in absorption for bulk water in the case of an increase of temperature ΔT=0.2 K. Figure 5.3(b) displays, as function of the delay time, the maximum amplitudes extracted by fitting with a Gaussian the OPTP signal.

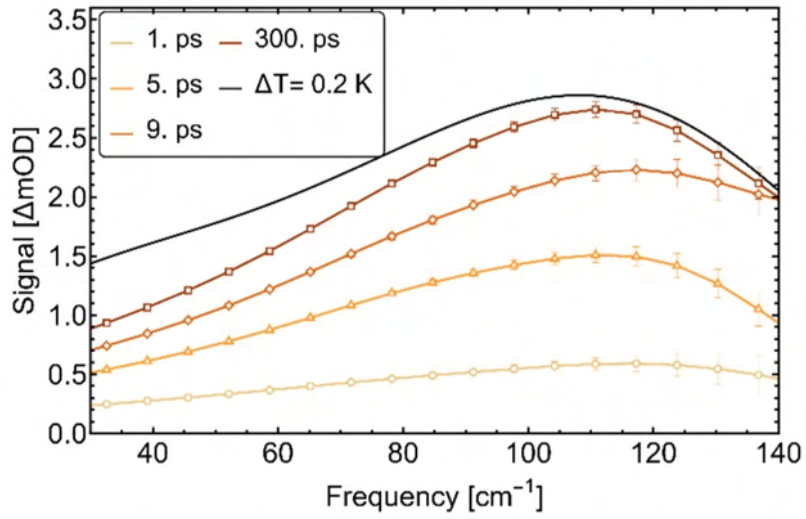

(a)

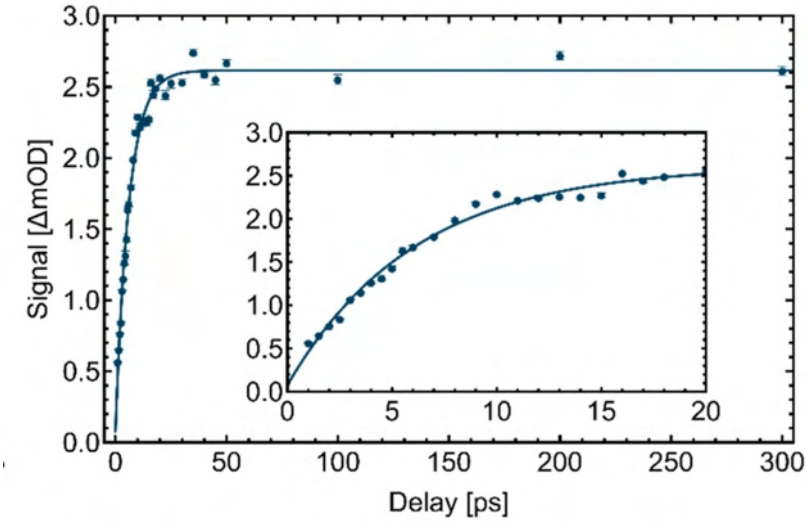

(b)

Figure 5.3. (a) *Transient THz spectra (vertical slices of the map) at representative delays of 1, 5, 9, and 300 ps. For comparison, the differential absorption of bulk water upon a 0.2 K temperature increase is shown in black.* (b) *Maximum amplitudes extracted by fitting a Gaussian to the OPTP spectra ΔmOD at different delays. The solid line represents the fit function, yielding a decay time of* 6.1 ± 0.3 *ps. The inset provides a zoom of the early time region between 1 and 20 ps. Figure adapted from [94].*

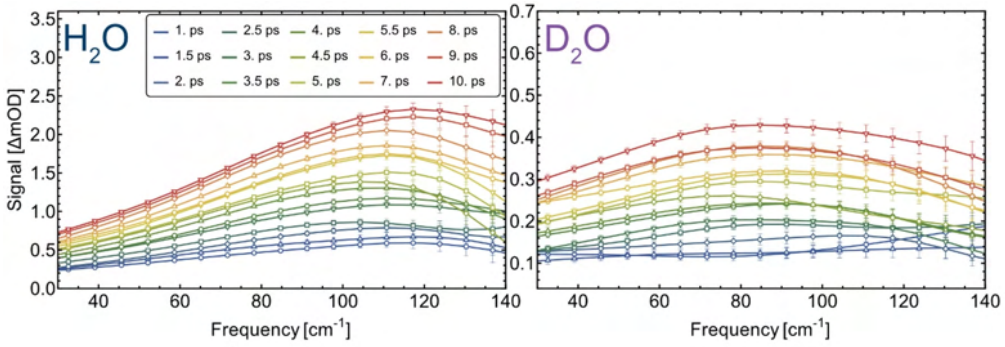

Figure 5.4. *Transient OPTP spectra of cytochrome c at representative pump–probe time delays between 1 and 10 ps in H_2O (left) and D_2O (right). Figure adapted from [94]*

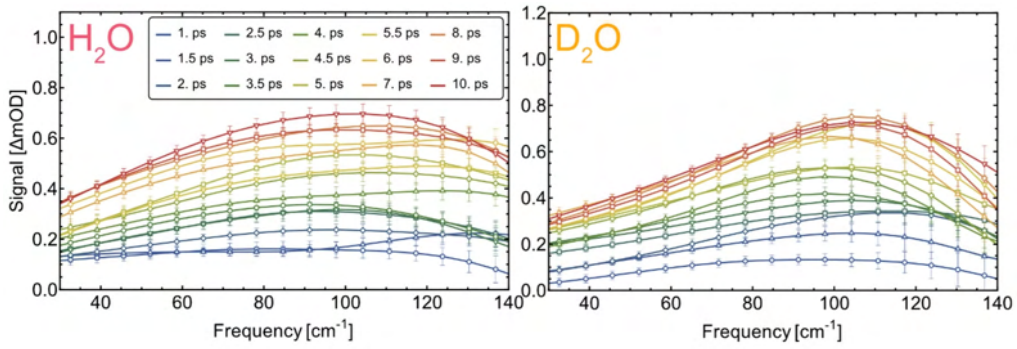

Figure 5.5. *Transient OPTP spectra of myoglobin at representative pump–probe time delays between 1 and 10 ps in H_2O (left) and D_2O (right). Figure adapted from [94]*

The amplitudes values increase with the time delay until it reaches a plateau after around 30 ps. It's possible fit this trend using the equation

$$A(t_{\text{pp}}) = C_{\text{offset}} - A_G e^{-\frac{t_{pp}}{\tau}} \tag{5.1}$$

with C_{offset} the value of amplitude when the plateau is reached, A_G the maximum amplitude and τ the time constant that it's used to describe the dynamic of the system. The estimated time constants for the four samples are reported in the table 5.1. For the cytochrome c in H_2O it is found a single exponential rise with time constant $\tau = 6.1 \pm 0.3$ ps . Repeating the experiment in D_2O yields a slightly longer time constant $\tau = 7.1 \pm 0.3$ ps.

In Figure 5.4 the transient OPTP spectra of the two samples are reported in a time delays range between 1 and 10 ps. Figure 5.5 shows analogous results for myoglobin in water and D_2O. From the exponential fit, the extracted rise time in H_2O is $\tau = 7.3 \pm 0.4$ ps, noticeably longer than for cytochrome c. Substitution of H_2O with D_2O leads to a pronounced increase to $\tau = 10.3 \pm 0.7$ ps, corresponding to a $\approx 40\%$ slowdown.

The absolute amplitudes of the signals are dependent on the thickness of the liquid jet, which is influenced by the viscosity of the sample and the nozzle used. However, this has not effect on the extrapolation of time constants.

Table 5.1. *Fitted rise time constants and comparison with diffusion model predictions.*

Sample	τ (ps)	τ_{mod} (ps)
Cytochrome c (H_2O)	6.1 ± 0.3	5.8
Cytochrome c (D_2O)	7.1 ± 0.3	6.1
Myoglobin (H_2O)	7.3 ± 0.4	7.7
Myoglobin (D_2O)	10.3 ± 0.7	8.2

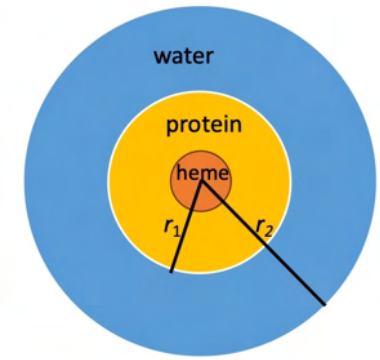

Figure 5.6. *Schematic model of a protein in solvent, with the heat source (heme) located at the centre. Here, r_1 denotes the protein radius and r_2 the distance from the protein centre to the edge of the hydration shell. Figure from [94]*

5.3.2 Modelling

To interpret the experimental data, a model of the flow of thermal energy from the heme throw the protein to the surrounding solvent has been implemented from professor D. M. Leitner. The model assume, for simplicity, a spherical protein where the heat sources (the heme) lies at the centre (figure 5.6). Both experimental and computational studies suggest that the energy flow in a protein is primarily diffusive [95, 112, 113]. Solving the diffusion equation for the temperature $T(r,t)$:

$$\frac{\partial T(r,t)}{\partial t} = D(r)\frac{1}{r}\frac{\partial^2}{\partial r^2}(rT(r,t)) + g(r,t) \tag{5.2}$$

it's possible to compute the evolution of the solvent temperature in time $T(t)$ (figure 5.7). In equation 5.2 r is the distance from the centre of the protein, t the time, $D(r)$ the thermal diffusivity and $g(r,t)$ the heat source. The latter has the form:

$$g(r,t) = \frac{\Delta T}{\tau_H} e^{-\frac{r^2}{2\sigma^2}} e^{-\frac{t}{\tau_H}} \tag{5.3}$$

Here ΔT correspond to the rise in temperature of the heme due to optical excitation, τ_H is the time constant for the decay of the excess thermal energy from the heme into the protein and σ is taken to be an effective radius for the heating source. The solution $T(t)$ can be fitted with the relation:

$$T(t) = T_\infty + (T(0) - T_\infty)e^{-\frac{t}{\tau_{\mathrm{mod}}}} \tag{5.4}$$

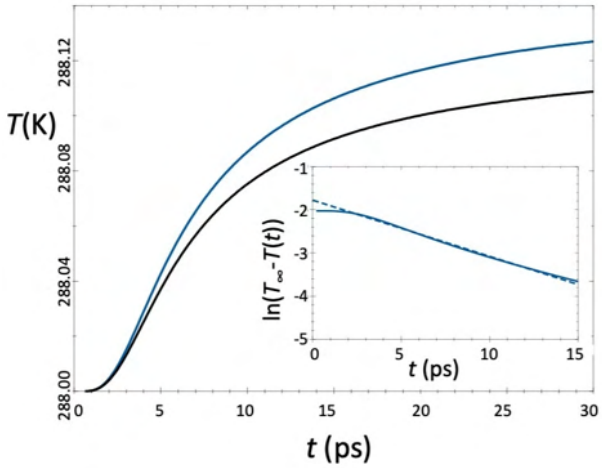

(a)

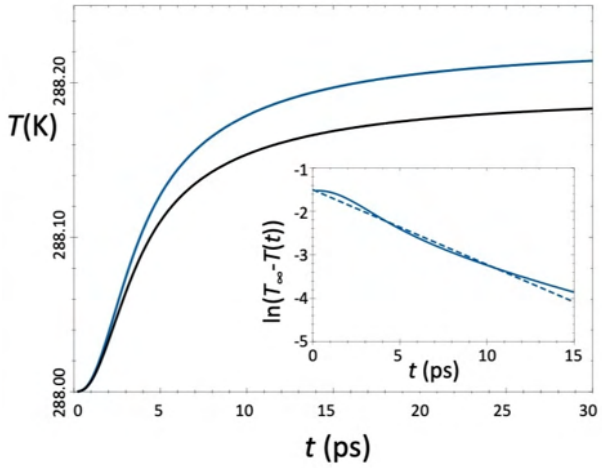

(b)

Figure 5.7. (a) *Computed temperature evolution for H_2O (blue) and D_2O (black) surrounding myoglobin. The inset shows the fit used to extract the solvent heating time τ_{mod} for H_2O (τ_{mod} for D2O is analogous), where $T\infty$ represents the asymptotic long-time temperature.* (b) *Computed temperature evolution for H_2O (blue) and D_2O (black) surrounding cytochrome c. The inset shows the fit used to obtain τ_{mod} for H_2O (the procedure for D_2O is similar). Figure from [94]*

where T_∞ is the temperature at long times and τ_{mod} is the heating time of the solvent. In this way the expected values of the time constants are obtained. These values are reported in tab 1 as τ_{mod}. More details on the model are reported in *A. Buchmann et al.* [94]

5.4 Conclusions

For myoglobin in D_2O, it's possible to observe an excellent agreement between experimental and predicted relaxation times, which are 10.3 ± 0.7 ps and 8.3 ps, respectively. These time constants are also consistent with the 7.5 ps constant reported by *T. Lian et al.* [108] for the combination band of the bending and librational modes of D_2O. They also reported a slower component ($\sim$ 20 ps). Within the experimental uncertainty of data, there is no evidence for such a slower component. This observation suggests that energy transfer into the low-frequency vibrational modes of the protein, followed by relaxation into the modes of the hydration shell (centred around 50–80 cm^{-1}), constitutes the dominant relaxation pathway. Energy dissipation into the mid-infrared modes and librational band proceeds more slowly, on the order of ∼20 ps, and is detectable in the *T. Lian et al.* experiments but lies outside the frequency range probed in this measurement.

Upon photoexcitation in the Soret band, both myoglobin and cytochrome *c* undergo electronic excitation of the heme group, followed by intramolecular vibrational relaxation, which transfers energy into the protein matrix within ∼1 ps. Here, new results on the molecular mechanism governing energy flow into the solvent are presented. Notably, it's been observed that the relaxation time of the larger myoglobin matrix is longer compared to that of the smaller cytochrome *c* protein. In the model, the decay constant for the dissipation of excess thermal energy from the heme into the protein matrix is set to 1 ps, with an effective heating radius of 3.5 Å. The thermal diffusivity $D(r)$ is assumed to be identical for both proteins, with effective radii of 1.9 nm for myoglobin and 1.4 nm for cytochrome *c*. The thermal conductance at the protein–water interface is taken from previous computational studies for myoglobin–water and cytochrome *c*–water systems. The predicted relaxation times of 5.8 ps for cytochrome *c* and 7.7 ps for myoglobin are in excellent agreement with these experimental values of 6.1 ± 0.3 ps and 7.3 ± 0.4 ps, respectively, confirming that energy flow from the hot heme group through the protein matrix is predominantly diffusive, rather than directional or protein-specific.

This finding challenges the hypothesis that rapid kinetic energy relaxation of the heme in native myoglobin results from directed ''funneling'' of energy through the propionate side chains into the solvent via electrostatic interactions [98, 114]. In cytochrome *c*, the propionate side chains are less solvent-exposed compared to myoglobin, yet the measured relaxation time is shorter. These results therefore indicate that the timescale of energy transfer is primarily governed by intramolecular redistribution of energy within the protein matrix for both proteins.

Evidence for mechanistic differences between cytochrome *c* and myoglobin is found. Substitution of H_2O with D_2O produces a more pronounced isotope effect for myoglobin. This suggests that, whereas intramolecular vibrational relaxation dominates in cytochrome *c*, the protein-water thermal conductance plays a more

significant role in myoglobin due to its larger solvent-exposed surface area. For myoglobin, the relaxation time increases from 7.3 ± 0.4 ps in H_2O to 10.3 ± 0.7 ps in D_2O, a ∼40% increase, significantly exceeding the ∼15% increase predicted by simplified model applied here. This discrepancy probably stems from the fact that the model neglects the details of coupling at the molecular level, which may depend on the energy matching between the low frequency modes of the propionate groups and those of H_2O/D_2O.

In summary, OPTP spectroscopy provides a highly sensitive probe of energy relaxation from the protein interior into the surrounding solvent, complementing more localized techniques such as Raman and infrared spectroscopy. The combination of OPTP measurements and theoretical modelling has enabled the revelation of a hierarchical energy flow pathway in heme proteins. This pathway involves the ultrafast transfer of energy from the hot heme into the protein matrix within 1 ps, followed by thermal diffusion through the matrix to the protein surface, which is completed within 15 ps. The final coupling to the solvent, governed by the protein–water thermal boundary conductance, appears to be protein-specific. It is proposed that the observed increase in relaxation time by a factor of 1.41 ± 0.08 for myoglobin, compared to a smaller factor of 1.16 ± 0.06 for cytochrome *c*, is attributable to differences in the boundary conductance of the propionate side chains, which are more solvent exposed in myoglobin.

Chapter 6

Conclusion and Future Prospective

During the three years of the PhD programme, various spectroscopic investigations were conducted on water-protein samples. The main work focused on studying the collective dynamics of hydration water in high-concentration water-lysozyme solutions. The highly crowded environment in which proteins are found gives rise to the formation of clusters, a form of aggregate in which proteins reorganise themselves within the solution to form groups of varying numbers of proteins that are in close proximity to each other maintaining their native state [34, 36, 45, 62, 63]. The structural properties of these clusters depend on both protein concentration and temperature [63].

Starting from the OKE measurements, it was possible to verify that a change in the nature of the clusters can have effects on the spectroscopic properties of hydration water. Using the OKE spectroscopy technique, it was possible to access two structural dynamics and two vibrational intermolecular dynamics of hydration water. Unexpectedly, the amplitude of these showed a trend with concentration that deviated from the expected linear trend, due to a discontinuity at the critical concentration of 200 mg/ml. This critical concentration result in the crossing point between a phase in which cluster formation becomes energetically favoured and a phase in which a monodisperse solution is maintained.

Subsequent measurements using THz-TDS made it possible to extract the refractive index and absorption coefficients of water-lysozyme solutions between 0.1 and 3 THz as both the protein concentration and temperature varied. THz spectroscopy is recognised as one of the most sensitive techniques for detecting hydration water, allowing extremely extensive hydration shells to be defined. This property, combined with the study of high-concentration solutions, has made it possible to extract the absorption coefficient associated with the hydration water present in the samples and to study its behaviour as concentration and temperature vary. It has been found that at higher temperatures, the absorption coefficient of hydration water appears to be less dependent on concentration than when measured at lower temperatures. As the temperature decreases, a growing trend with increasing concentration becomes evident. A possible interpretation of this behaviour can again be attributed to the presence of clusters in solution. At lower temperatures, these

clusters are composed of a number of proteins that vary less than at higher temperatures. This can result at higher temperature, in different hydration shells that are less affected by the overlap effect caused by increasing concentration.

During the research period conducted abroad, at Professor Martina Havenith's research group in Bochum (GER), a second spectroscopic investigation in the THz regime was conducted using an FTIR spectrometer combined with a bolometer used as a detector. This allowed the spectral window of investigation to be extended to $\sim$ 18 THz, giving access to the absorption peak given by the intermolecular stretching vibrational band and the water librational mode. The data show that the absorption coefficients exhibit different trends at low and high frequencies: in the first case, they decrease linearly as concentration increases, while in the second case, they increase. By interpreting the spectra using THz calorimetry, it was possible to construct a phase diagram characteristic of the cluster regime, also demonstrating the effectiveness of this interpretation of the data in distinguishing between critical phenomena of different types, such as LLPS and LSPS.

Various aspects of the collective dynamics of protein hydration water in a crowded environment were successfully described by this series of experiments. By comparing the results of the three investigations, it was observed that the presence of clusters in solution manifests differently depending on the type of experiment conducted. The work presented here once again demonstrates the complexity of addressing the issue of protein hydration water, an issue further complicated by the extremely crowded environment investigated in this study. Importantly, the work carried out has enabled the development of analytical techniques that can be adapted in the future to study other phenomena related to protein aggregation processes, such as LLPS or amyloid aggregate formation.

The results reported here clearly confirm the existence of a strong link between critical phenomena of this nature and hydration water. THz spectroscopy has already yielded excellent results in this regard especially on LLPS phenomena [12, 40, 91], the OKE technique has so far been rarely employed. Moreover, the shown results demonstrate that a single technique may not be sufficient to describe such complex processes.

The last part of the thesis also presented the results of an OPTP spectroscopy was employed to investigate ultrafast energy transport in heme proteins (myoglobin and cytochrome *c*). This technique directly tracks the flow of vibrational energy from the optically excited heme group through the protein matrix to the surrounding solvent. The measured relaxation times, ranging from 6 to 10 ps and showing a clear isotope effect between H_2O and D_2O, are in excellent agreement with diffusive energy transfer models. These results reveal that thermal energy dissipation occurs predominantly through vibrational diffusion within the protein matrix, followed by coupling to the hydration shell.

In the future, OKE measurements on samples undergoing LLPS will be of great interest, as will studies of amyloid-type aggregate phases and hydrogel formation. Unfortunately, the OKE technique is severely limited by sample turbidity, making direct measurements of the LLPS phase unfeasible. However, it has been demonstrated here that the effect of protein reorganisation within the solvent on the surrounding hydration water can be observed, thus enabling the investigation of pre-transitional phases.

Furthermore, both OKE and THz-TDS can in the future be combined with emerging methods that enable the study of transient phases in samples. An example is ASOPS (Asynchronous Optical Sampling), which has recently been implemented in the ultrafast spectroscopy laboratories at LENS. This pump–probe technique enables high-speed scans over time delays on the order of nanoseconds, without the need for a mechanical delay stage. Specifically, two nearly identical model locked laser sources are used, differing only by a small offset in repetition rate. Owing to these characteristics, the technique can be applied to study samples even when they are out of equilibrium. Similar systems include, for example, the formation of lysozyme amyloid gels, which occurs on a timescale of a few hours [31]. The ASOPS technique has already been applied to THz-TDS measurements [115, 116], whereas no results have yet been reported for OKE spectroscopy combined with ASOPS.

Experiments of the type shown, involving highly concentrated protein solutions, are inherently challenging. A major difficulty arises from the instability of the samples under such critical conditions, particularly when transitions such as LLPS are triggered. In addition, the high cost of obtaining the large protein quantities needed to prepare adequate solution volumes poses a further limitation.

During the final period of my PhD, I focused on the possibility of studying alternative systems to protein–water solutions. Aqueous solutions of zwitterionic polymers have proven to be particularly interesting. Although these polymers are overall electrically neutral, they are characterised by a large dipole moment arising from the arrangement of numerous charged groups along the polymer chain [117]. Numerous applications are possible, but in this case the most interesting aspect is their potential use as systems that mimic the properties of protein–water solutions, including notable phenomena such as LLPS [118, 119].

An initial investigation of samples of this type was recently initiated as part of a collaboration with Professor Paolo Arosio at ETH Zurich, who supplied zwitterionic polymers based on poly(sulfobetaine-*co*-sulfabetaine). These polymers exhibit LLPS behaviour, and in particular, the transition point can be tuned by adjusting the ratio between the two components [119].

At present, only preliminary studies have been conducted to define the LLPS phase diagram of these samples, mainly using microscopy and light-scattering techniques. Once the critical points of the phase diagram have been clearly defined, a series of spectroscopic measurements similar to those presented here can be carried out to investigate the hydration water properties of the system. The decision to switch from proteins to polymers makes it possible to work with samples that are more reliable and reproducible, as well as significantly less expensive.

Appendix A

Additional data from the THz-TDS measurements

In this appendix additional data from THz-TDS measurements are reported. Figure A.1 shows the absorption coefficients of the water-lysozyme solutions at 9°C, 17°C and 25°C. A decrease in the absorption coefficient with increasing concentration is observed at all three temperatures. Figure A.2 shows the absorption coefficients assigned of the hydration water components of the α showed in A.1. As discussed in the main text, dependence on concentration decreases as temperature increases.

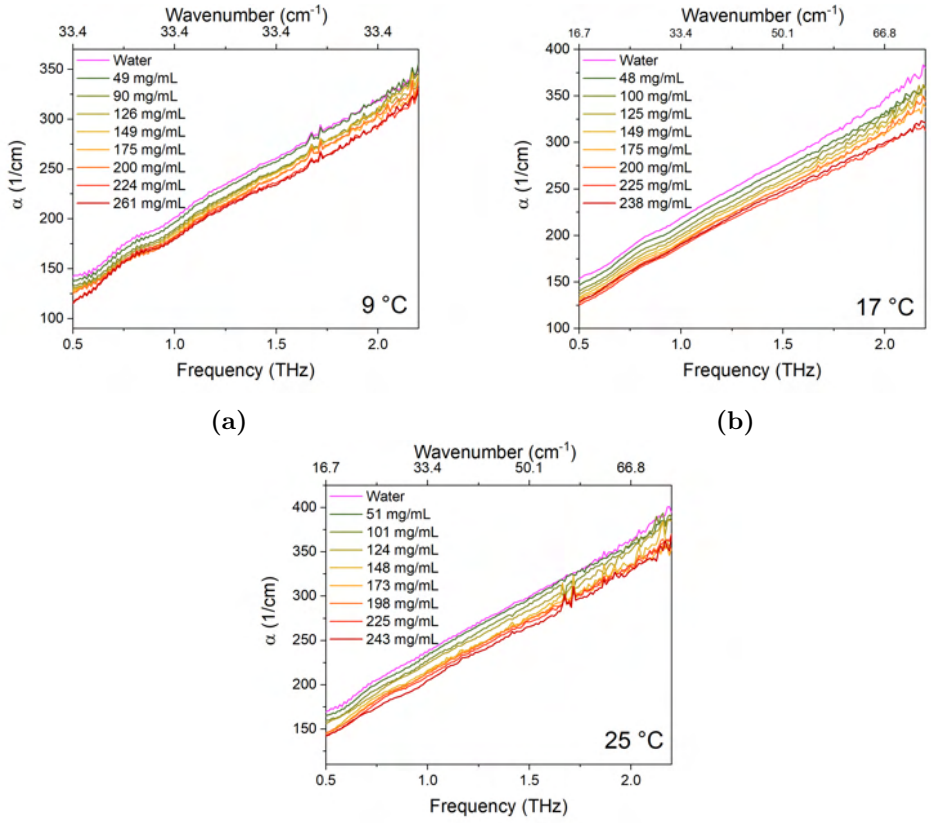

Figure A.1. *Absorption coefficients of the water-lysozyme solutions at 9°C* (a), *17°C*(b) *and 25°C* (c)

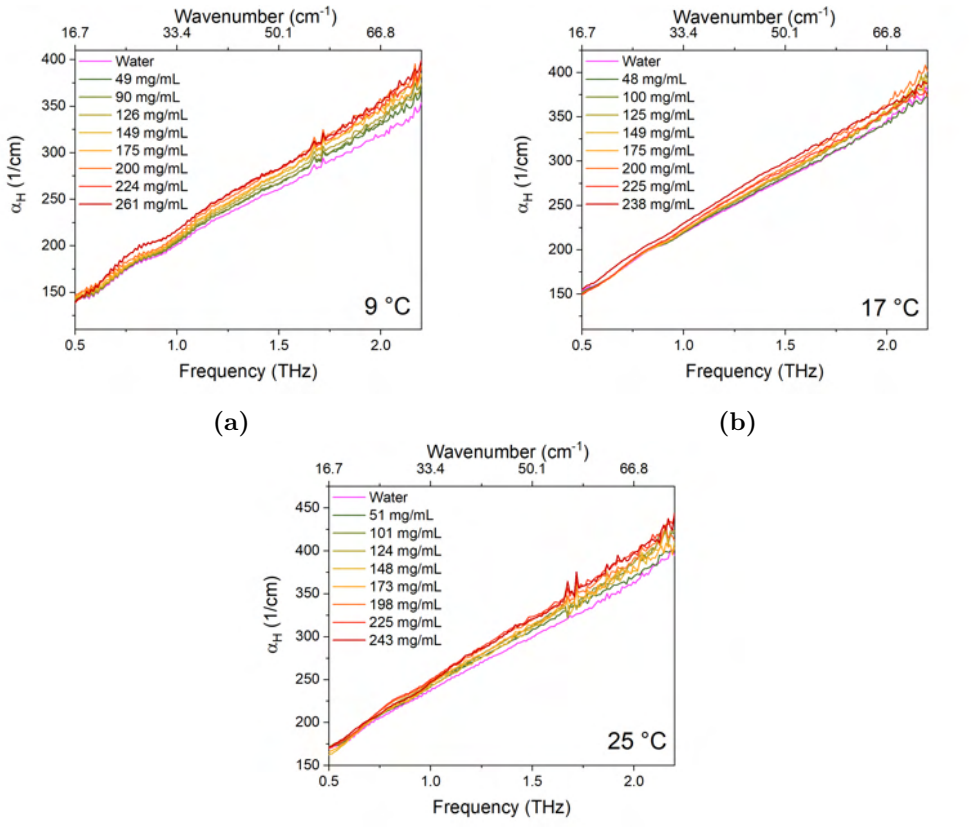

Figure A.2. *Absorption coefficients assigned at the hydration water components of the water-lysozyme solutions at 9°C* (a), *17°C*(b) *and 25°C* (c)

Bibliography

[1] H. J. Bakker and J. L. Skinner. "Vibrational Spectroscopy as a Probe of Structure and Dynamics in Liquid Water". In: *Chemical Reviews* 110.3 (2010), pp. 1498–1517. DOI: 10.1021/cr9001879.

[2] Fivos Perakis et al. "Vibrational Spectroscopy and Dynamics of Water". In: *Chemical Reviews* 116.13 (2016), pp. 7590–7607. DOI: 10.1021/acs.chemrev.5b00640.

[3] Thomas Fransson et al. "X-ray and Electron Spectroscopy of Water". In: *Chemical Reviews* 116.13 (2016), pp. 7551–7569. DOI: 10.1021/acs.chemrev.5b00672.

[4] Hongyi Ge et al. "Recent Advances in THz Detection of Water". In: *International Journal of Molecular Sciences* 24.13 (2023), p. 10936. DOI: 10.3390/ijms241310936.

[5] Matthias Heyden et al. "Dissecting the THz spectrum of liquid water from first principles via correlations in time and space". In: *Proceedings of the National Academy of Sciences* 107.27 (2010), pp. 12068–12073. DOI: 10.1073/pnas.0914885107.

[6] Tao Li et al. "Ab Initio Vibrational Spectroscopy of Water and Aqueous Solutions in a Wide Pressure–Temperature Range". In: *WIREs Computational Molecular Science* 15.3 (2025), e70017. DOI: 10.1002/wcms.70017.

[7] José Teixeira. "Recent experimental aspects of the structure and dynamics of liquid and supercooled water". In: *Molecular Physics* 110.5 (2012), pp. 249–258. DOI: 10.1080/00268976.2011.645894.

[8] Damien Laage and James T. Hynes. "A Molecular Jump Mechanism of Water Reorientation". In: *Science* 311.5762 (2006), pp. 832–835. DOI: 10.1126/science.1122154.

[9] A. Taschin et al. "Evidence of two distinct local structures of water from ambient to supercooled conditions". In: *Nature Communications* 4.1 (2013), p. 2401. DOI: 10.1038/ncomms3401.

[10] Damien Laage, Thomas Elsaesser, and James T. Hynes. "Water Dynamics in the Hydration Shells of Biomolecules". In: *Chemical Reviews* 117.16 (2017). Publisher: American Chemical Society (ACS), pp. 10694–10725. DOI: 10.1021/acs.chemrev.6b00765.

[11] Lada Biedermannová and Bohdan Schneider. "Hydration of proteins and nucleic acids: Advances in experiment and theory. A review". In: *Biochimica et Biophysica Acta (BBA) - General Subjects* 1860.9 (2016), pp. 1821–1835. DOI: 10.1016/j.bbagen.2016.05.036.

[12] Simone Pezzotti et al. "Liquid–Liquid Phase Separation? Ask the Water!" In: *The Journal of Physical Chemistry Letters* 14.6 (2023). Publisher: American Chemical Society (ACS), pp. 1556–1563. DOI: 10.1021/acs.jpclett.2c02697.

[13] Aoife C. Fogarty and Damien Laage. "Water Dynamics in Protein Hydration Shells: The Molecular Origins of the Dynamical Perturbation". In: *The Journal of Physical Chemistry B* 118.28 (2014), pp. 7715–7729. DOI: 10.1021/jp409805p.

[14] Marie-Claire Bellissent-Funel et al. "Water Determines the Structure and Dynamics of Proteins". In: *Chemical Reviews* 116.13 (2016), pp. 7673–7697. DOI: 10.1021/acs.chemrev.5b00664.

[15] G. Camisasca et al. "Two structural relaxations in protein hydration water and their dynamic crossovers". In: *The Journal of Chemical Physics* 145.4 (2016), p. 044503. DOI: 10.1063/1.4959286.

[16] Simon Ebbinghaus et al. "An extended dynamical hydration shell around proteins". In: *Proceedings of the National Academy of Sciences* 104.52 (2007), pp. 20749–20752. DOI: 10.1073/pnas.0709207104.

[17] D. I. Svergun et al. "Protein hydration in solution: Experimental observation by x-ray and neutron scattering". In: *Proceedings of the National Academy of Sciences* 95.5 (1998), pp. 2267–2272. DOI: 10.1073/pnas.95.5.2267.

[18] Bertil Halle and Monika Davidovic. "Biomolecular hydration: From water dynamics to hydrodynamics". In: *Proceedings of the National Academy of Sciences* 100.21 (2003), pp. 12135–12140. DOI: 10.1073/pnas.2033320100.

[19] Franci Merzel and Jeremy C. Smith. "Is the first hydration shell of lysozyme of higher density than bulk water?" In: *Proceedings of the National Academy of Sciences* 99.8 (2002), pp. 5378–5383. DOI: 10.1073/pnas.082335099.

[20] Jordan W. Bye et al. "Analysis of the Hydration Water around Bovine Serum Albumin Using Terahertz Coherent Synchrotron Radiation". In: *The Journal of Physical Chemistry A* 118.1 (2014), pp. 83–88. DOI: 10.1021/jp407410g.

[21] Daniel R. Martin and Dmitry V. Matyushov. "Hydration shells of proteins probed by depolarized light scattering and dielectric spectroscopy: Orientational structure is significant, positional structure is not". In: *The Journal of Chemical Physics* 141.22 (2014), p. 22D501. DOI: 10.1063/1.4895544.

[22] Song-Ho Chong and Sihyun Ham. "Impact of chemical heterogeneity on protein self-assembly in water". In: *Proceedings of the National Academy of Sciences* 109.20 (2012), pp. 7636–7641. DOI: 10.1073/pnas.1120646109.

[23] Matthias Heyden and Douglas J. Tobias. "Spatial Dependence of Protein-Water Collective Hydrogen-Bond Dynamics". In: *Physical Review Letters* 111.21 (2013), p. 218101. DOI: 10.1103/PhysRevLett.111.218101.

[24] W. J. Ellison. "Permittivity of Pure Water, at Standard Atmospheric Pressure, over the Frequency Range –25THz and the Temperature Range –100°C". In: *Journal of Physical and Chemical Reference Data* 36.1 (2007), pp. 1–18. DOI: 10.1063/1.2360986.

[25] Kristina E. Furse and Steven A. Corcelli. "The Dynamics of Water at DNA Interfaces: Computational Studies of Hoechst 33258 Bound to DNA". In: *Journal of the American Chemical Society* 130.39 (2008), pp. 13103–13109. DOI: 10.1021/ja803728g.

[26] Stefania Perticaroli et al. "Dynamics of Hydration Water in Sugars and Peptides Solutions". In: *The Journal of Physical Chemistry B* 117.25 (2013), pp. 7729–7736. DOI: 10.1021/jp403665w.

[27] A. Oleinikova, P. Sasisanker, and H. Weingärtner. "What Can Really Be Learned from Dielectric Spectroscopy of Protein Solutions? A Case Study of Ribonuclease A". In: *The Journal of Physical Chemistry B* 108.24 (2004), pp. 8467–8474. DOI: 10.1021/jp049618b.

[28] Shuji Kaieda and Bertil Halle. "Internal Water and Microsecond Dynamics in Myoglobin". In: *The Journal of Physical Chemistry B* 117.47 (2013), pp. 14676–14687. DOI: 10.1021/jp409234g.

[29] Nikita V. Penkov. "Terahertz spectroscopy as a method for investigation of hydration shells of biomolecules". In: *Biophysical Reviews* 15.5 (2023), pp. 833–849. DOI: 10.1007/s12551-023-01131-z.

[30] Sara Catalini et al. "Probing Globular Protein Self-Assembling Dynamics by Heterodyne Transient Grating Experiments". In: *Applied Sciences* 9.3 (2019), p. 405. DOI: 10.3390/app9030405.

[31] Sara Catalini et al. "Amyloid Self-Assembly of Lysozyme in Self-Crowded Conditions: The Formation of a Protein Oligomer Hydrogel". In: *Biomacromolecules* 22.3 (2021). Publisher: American Chemical Society (ACS), pp. 1147–1158. DOI: 10.1021/acs.biomac.0c01652.

[32] Sara Catalini et al. "Multi-length scale structural investigation of lysozyme self-assembly". In: *iScience* 25.7 (2022), p. 104586. DOI: 10.1016/j.isci.2022.104586.

[33] Rajaram Swaminathan et al. "Lysozyme". In: *Advances in Protein Chemistry and Structural Biology*. Vol. 84. Elsevier, 2011, pp. 63–111. DOI: 10.1016/B978-0-12-386483-3.00003-3.

[34] Anna Stradner et al. "Equilibrium cluster formation in concentrated protein solutions and colloids". In: *Nature* 432.7016 (2004). Publisher: Springer Science and Business Media LLC, pp. 492–495. DOI: 10.1038/nature03109.

[35] Lionel Porcar et al. "Formation of the Dynamic Clusters in Concentrated Lysozyme Protein Solutions". In: *The Journal of Physical Chemistry Letters* 1.1 (2010). Publisher: American Chemical Society (ACS), pp. 126–129. DOI: 10.1021/jz900127c.

[36] Frédéric Cardinaux et al. “Cluster-Driven Dynamical Arrest in Concentrated Lysozyme Solutions”. In: *The Journal of Physical Chemistry B* 115.22 (2011), pp. 7227–7237. DOI: 10.1021/jp112180p.

[37] Victor G. Taratuta et al. “Liquid-liquid phase separation of aqueous lysozyme solutions: effects of pH and salt identity”. In: *The Journal of Physical Chemistry* 94.5 (1990), pp. 2140–2144. DOI: 10.1021/j100368a074.

[38] Martin Muschol and Franz Rosenberger. “Liquid–liquid phase separation in supersaturated lysozyme solutions and associated precipitate formation/crystallization”. In: *The Journal of Chemical Physics* 107.6 (1997). Publisher: AIP Publishing, pp. 1953–1962. DOI: 10.1063/1.474547.

[39] Fajun Zhang et al. “The role of cluster formation and metastable liquid—liquid phase separation in protein crystallization”. In: *Faraday Discussions* 159.0 (2012). Publisher: The Royal Society of Chemistry, pp. 313–325. DOI: 10.1039/C2FD20021J.

[40] Jonas Ahlers et al. “The key role of solvent in condensation: Mapping water in liquid-liquid phase-separated FUS”. In: *Biophysical Journal* 120.7 (2021), pp. 1266–1275. DOI: 10.1016/j.bpj.2021.01.019.

[41] Saumyak Mukherjee and Lars V. Schäfer. “Thermodynamic forces from protein and water govern condensate formation of an intrinsically disordered protein domain”. In: *Nature Communications* 14.1 (2023), p. 5892. DOI: 10.1038/s41467-023-41586-y.

[42] Saumyak Mukherjee et al. “Entropy Tug-of-War Determines Solvent Effects in the Liquid–Liquid Phase Separation of a Globular Protein”. In: *The Journal of Physical Chemistry Letters* 15.15 (2024), pp. 4047–4055. DOI: 10.1021/acs.jpclett.3c03421.

[43] Luigi Caminiti et al. “Protein Crowding Effects on Hydration Water Dynamics”. In: *The Journal of Physical Chemistry Letters* 16.9 (2025). Publisher: American Chemical Society (ACS), pp. 2340–2347. DOI: 10.1021/acs.jpclett.4c03391.

[44] Stefania Perticaroli et al. “Broadband Depolarized Light Scattering Study of Diluted Protein Aqueous Solutions”. In: *The Journal of Physical Chemistry B* 114.24 (2010), pp. 8262–8269. DOI: 10.1021/jp101896f.

[45] S. Perticaroli et al. “Hydration and aggregation of lysozyme by extended frequency range depolarized light scattering”. In: *Journal of Non-Crystalline Solids* 407 (2015). Publisher: Elsevier BV, pp. 472–477. DOI: 10.1016/j.jnoncrysol.2014.07.017.

[46] Vitaly Kocherbitov et al. “Hydration of Lysozyme Studied by Raman Spectroscopy”. In: *The Journal of Physical Chemistry B* 117.17 (2013), pp. 4981–4992. DOI: 10.1021/jp4017954.

[47] Gerard Giraud and Klaas Wynne. “Time-Resolved Optical Kerr-Effect Spectroscopy of Low-Frequency Dynamics in Dialanine, Polyalanine, and Lysozyme in Solution”. In: *Journal of the American Chemical Society* 124.41 (2002), pp. 12110–12111. DOI: 10.1021/ja027801h.

[48] Gerard Giraud, Jan Karolin, and Klaas Wynne. "Low-Frequency Modes of Peptides and Globular Proteins in Solution Observed by Ultrafast OHD-RIKES Spectroscopy". In: *Biophysical Journal* 85.3 (2003), pp. 1903–1913. DOI: 10.1016/S0006-3495(03)74618-9.

[49] Kamila Mazur, Ismael A. Heisler, and Stephen R. Meech. "Water Dynamics at Protein Interfaces: Ultrafast Optical Kerr Effect Study". In: *The Journal of Physical Chemistry A* 116.11 (2012), pp. 2678–2685. DOI: 10.1021/jp2074539.

[50] David A. Turton et al. "Terahertz underdamped vibrational motion governs protein-ligand binding in solution". In: *Nature Communications* 5.1 (2014), p. 3999. DOI: 10.1038/ncomms4999.

[51] Gaia Camisasca et al. "Structure and slow dynamics of protein hydration water". In: *Journal of Molecular Liquids* 268 (2018). Publisher: Elsevier BV, pp. 903–910. DOI: 10.1016/j.molliq.2018.07.104.

[52] Fabio Sterpone et al. "Water Hydrogen-Bond Dynamics around Amino Acids: The Key Role of Hydrophilic Hydrogen-Bond Acceptor Groups". In: *The Journal of Physical Chemistry B* 114.5 (2010), pp. 2083–2089. DOI: 10.1021/jp9119793.

[53] Roberto Righini. "Ultrafast Optical Kerr Effect in Liquids and Solids". In: *Science* 262.5138 (1993), pp. 1386–1390. DOI: 10.1126/science.262.5138.1386.

[54] P Bartolini et al. "Optical kerr effect measurements on supercooled water: The experimental perspective". In: *Journal of Physics: Conference Series* 177 (2009), p. 012009. DOI: 10.1088/1742-6596/177/1/012009.

[55] A. Taschin et al. "Optical Kerr effect of liquid and supercooled water: The experimental and data analysis perspective". In: *The Journal of Chemical Physics* 141.8 (2014), p. 084507. DOI: 10.1063/1.4893557.

[56] Chiara Calvagna et al. "Modification of local and collective dynamics of water in perchlorate solution, induced by pressure and concentration". In: *Journal of Molecular Liquids* 337 (2021). Publisher: Elsevier BV, p. 116273. DOI: 10.1016/j.molliq.2021.116273.

[57] Giorgio Schirò and Martin Weik. "Role of hydration water in the onset of protein structural dynamics". In: *Journal of Physics: Condensed Matter* 31.46 (2019). Publisher: IOP Publishing, p. 463002. DOI: 10.1088/1361-648X/ab388a.

[58] Raffaele Sinibaldi et al. "Preferential hydration of lysozyme in water/glycerol mixtures: A small-angle neutron scattering study". In: *The Journal of Chemical Physics* 126.23 (2007). Publisher: AIP Publishing. DOI: 10.1063/1.2735620.

[59] A Taschin et al. "Supercooling and freezing processes in nanoconfined water by time-resolved optical Kerr effect spectroscopy". In: *Journal of Physics: Condensed Matter* 27.19 (2015). Publisher: IOP Publishing, p. 194107. DOI: 10.1088/0953-8984/27/19/194107.

[60] Samir Kumar Pal and Ahmed H. Zewail. "Dynamics of Water in Biological Recognition". In: *Chemical Reviews* 104.4 (2004), pp. 2099–2124. DOI: 10.1021/cr0206891.

[61] Luyuan Zhang et al. "Mapping hydration dynamics around a protein surface". In: *Proceedings of the National Academy of Sciences* 104.47 (2007), pp. 18461–18466. DOI: 10.1073/pnas.0707647104.

[62] C. Cametti, S. Marchetti, and G. Onori. "Lysozyme Hydration in Concentrated Aqueous Solutions. Effect of an Equilibrium Cluster Phase". In: *The Journal of Physical Chemistry B* 117.1 (2013). Publisher: American Chemical Society (ACS), pp. 104–110. DOI: 10.1021/jp308863h.

[63] A. Baumketner and W. Cai. "Clusters of lysozyme in aqueous solutions". In: *Physical Review E* 98.3 (2018). Publisher: American Physical Society (APS). DOI: 10.1103/physreve.98.032419.

[64] Andrea Taschin et al. "A comparative study on bulk and nanoconfined water by time-resolved optical Kerr effect spectroscopy". In: *Faraday Discussions* 167 (2013). Publisher: Royal Society of Chemistry (RSC), p. 293. DOI: 10.1039/c3fd00060e.

[65] L. Genzel et al. "Low-frequency Raman spectra of lysozyme". In: *Biopolymers* 15.1 (1976), pp. 219–225. DOI: 10.1002/bip.1976.360150115.

[66] Anna V. Frontzek (Neé Svanidze) et al. "Study of the phase transition in lysozyme crystals by Raman spectroscopy". In: *Biochimica et Biophysica Acta (BBA) - General Subjects* 1860.2 (2016), pp. 412–423. DOI: 10.1016/j.bbagen.2015.10.020.

[67] Benjamin Born et al. "The terahertz dance of water with the proteins: the effect of protein flexibility on the dynamical hydration shell of ubiquitin". In: *Faraday Discuss.* 141 (2009), pp. 161–173. DOI: 10.1039/B804734K.

[68] Fabio Novelli et al. "Time-Domain THz Spectroscopy Reveals Coupled Protein–Hydration Dielectric Response in Solutions of Native and Fibrils of Human Lysozyme". In: *The Journal of Physical Chemistry B* 121.18 (2017). Publisher: American Chemical Society (ACS), pp. 4810–4816. DOI: 10.1021/acs.jpcb.7b02724.

[69] Daniel R. Martin and Dmitry V. Matyushov. "Terahertz absorption of lysozyme in solution". In: *The Journal of Chemical Physics* 147.8 (2017). Publisher: AIP Publishing. DOI: 10.1063/1.4989641.

[70] Hendrik Vondracek et al. "THz absorption spectroscopy of solvated -lactoglobulin". In: *The Journal of Chemical Physics* 141.22 (2014), p. 22D534. DOI: 10.1063/1.4903237.

[71] Matthias Heyden, Douglas J. Tobias, and Dmitry V. Matyushov. "Terahertz absorption of dilute aqueous solutions". In: *The Journal of Chemical Physics* 137.23 (2012), p. 235103. DOI: 10.1063/1.4772000.

[72] Amin Soltani et al. "Attenuated Total Reflection Terahertz Time-Domain Spectroscopy: Uncertainty Analysis and Reduction Scheme". In: *IEEE Transactions on Terahertz Science and Technology* 6.1 (2016), pp. 32–39. DOI: 10.1109/TTHZ.2015.2505909.

[73] A. Soltani et al. "Error from Delay Drift in Terahertz Attenuated Total Reflection Spectroscopy". In: *Journal of Infrared, Millimeter, and Terahertz Waves* 35.5 (2014), pp. 468–477. DOI: 10.1007/s10762-014-0054-3.

[74] Yun-Shik Lee, ed. *Principles of Terahertz Science and Technology*. SpringerLink Bücher. Boston, MA: Springer-Verlag US, 2009. DOI: 10.1007/978-0-387-09540-0.

[75] Withawat Withayachumnankul. "Engineering Aspects of Terahertz Time-Domain Spectroscopy". PhD thesis. The University of Adelaide, 2009.

[76] L. Duvillaret et al. "Analytical modeling and optimization of terahertz time-domain spectroscopy experiments, using photoswitches as antennas". In: *IEEE Journal of Selected Topics in Quantum Electronics* 7.4 (2001), pp. 615–623. DOI: 10.1109/2944.974233.

[77] Cecilie Ro/nne et al. "Investigation of the temperature dependence of dielectric relaxation in liquid water by THz reflection spectroscopy and molecular dynamics simulation". In: *The Journal of Chemical Physics* 107.14 (1997), pp. 5319–5331. DOI: 10.1063/1.474242.

[78] J.K. Vij, D.R.J. Simpson, and O.E. Panarina. "Far infrared spectroscopy of water at different temperatures: GHz to THz dielectric spectroscopy of water". In: *Journal of Molecular Liquids* 112.3 (2004), pp. 125–135. DOI: 10.1016/j.molliq.2003.12.014.

[79] Joanna Krakowiak, Magdalena Krajewska, and Jarosław Wawer. "Monitoring of lysozyme thermal denaturation by volumetric measurements and nanoDSF technique in the presence of N-butylurea". In: *Journal of Biological Physics* 45.2 (2019), pp. 161–172. DOI: 10.1007/s10867-019-09521-9.

[80] Fabio Novelli et al. "Nonlinear TeraHertz Transmission by Liquid Water at 1 THz". In: *Applied Sciences* 10.15 (2020), p. 5290. DOI: 10.3390/app10155290.

[81] Janne Savolainen, Saima Ahmed, and Peter Hamm. "Two-dimensional Raman-terahertz spectroscopy of water". In: *Proceedings of the National Academy of Sciences* 110.51 (2013), pp. 20402–20407. DOI: 10.1073/pnas.1317459110.

[82] Sho Imoto and Dominik Marx. "Pressure response of the THz spectrum of bulk liquid water revealed by intermolecular instantaneous normal mode analysis". In: *The Journal of Chemical Physics* 150.8 (2019), p. 084502. DOI: 10.1063/1.5080381.

[83] Simone Pezzotti et al. "Spectroscopic Fingerprints of Cavity Formation and Solute Insertion as a Measure of Hydration Entropic Loss and Enthalpic Gain". In: *Angewandte Chemie International Edition* 61.29 (2022), e202203893. DOI: 10.1002/anie.202203893.

[84] Simone Pezzotti et al. “Terahertz calorimetry spotlights the role of water in biological processes”. In: *Nature Reviews Chemistry* 9.7 (2025). Publisher: Springer Science and Business Media LLC, pp. 481–494. DOI: 10.1038/s41570-025-00712-8.

[85] David Chandler and Patrick Varilly. “Lectures on Molecular- and Nano-scale Fluctuations in Water”. In: *Proceedings of the International School of Physics “Enrico Fermi”* 176 (Complex Materials in Physics and Biology 2012), pp. 75–111. DOI: 10.3254/978-1-61499-071-0-75. arXiv: 1101.2235[cond-mat].

[86] V. Conti Nibali et al. “Wrapping Up Hydrophobic Hydration: Locality Matters”. In: *The Journal of Physical Chemistry Letters* 11.12 (2020), pp. 4809–4816. DOI: 10.1021/acs.jpclett.0c00846.

[87] Debasish Das Mahanta et al. “Local solvation structures govern the mixing thermodynamics of glycerol–water solutions”. In: *Chemical Science* 14.26 (2023), pp. 7381–7392. DOI: 10.1039/D3SC00517H.

[88] Damien Laage, Guillaume Stirnemann, and James T. Hynes. “Why Water Reorientation Slows without Iceberg Formation around Hydrophobic Solutes”. In: *The Journal of Physical Chemistry B* 113.8 (2009), pp. 2428–2435. DOI: 10.1021/jp809521t.

[89] Sanjiana Nalige. “Probing Hydration Water Dynamics of Carbon Nanotubes and HeLa Cells using THz Spectroscopy”. PhD thesis. Ruhr University Bochum, 2025.

[90] Sashary Ramos et al. “Hydration makes a difference! How to tune protein complexes between liquid–liquid and liquid–solid phase separation”. In: *Physical Chemistry Chemical Physics* 25.41 (2023). Publisher: Royal Society of Chemistry (RSC), pp. 28063–28069. DOI: 10.1039/d3cp03299j.

[91] Benedikt König et al. “Real-time measure of solvation free energy changes upon liquid-liquid phase separation of -elastin”. In: *Biophysical Journal* 123.11 (2024). Publisher: Elsevier BV, pp. 1367–1375. DOI: 10.1016/j.bpj.2023.07.023.

[92] Jörg Stetefeld, Sean A. McKenna, and Trushar R. Patel. “Dynamic light scattering: a practical guide and applications in biomedical sciences”. In: *Biophysical Reviews* 8.4 (2016), pp. 409–427. DOI: 10.1007/s12551-016-0218-6.

[93] Filip Hasecke et al. “Origin of metastable oligomers and their effects on amyloid fibril self-assembly”. In: *Chemical Science* 9.27 (2018). Publisher: Royal Society of Chemistry (RSC), pp. 5937–5948. DOI: 10.1039/c8sc01479e.

[94] Adrian Buchmann et al. “Internal vibrational energy redistribution precedes energy dissipation into the solvent upon photoexcitation of heme proteins”. In: *Physical Chemistry Chemical Physics* 27.18 (2025). Publisher: Royal Society of Chemistry (RSC), pp. 9470–9477. DOI: 10.1039/d5cp00797f.

[95] David M. Leitner. “Energy Flow in Proteins”. In: *Annual Review of Physical Chemistry* 59.1 (2008). Publisher: Annual Reviews, pp. 233–259. DOI: 10.1146/annurev.physchem.59.032607.093606.

[96] Guanghong Wei et al. "Protein Ensembles: How Does Nature Harness Thermodynamic Fluctuations for Life? The Diverse Functional Roles of Conformational Ensembles in the Cell". In: *Chemical Reviews* 116.11 (2016), pp. 6516–6551. DOI: 10.1021/acs.chemrev.5b00562.

[97] Xiong Ye, Andrey Demidov, and Paul M. Champion. "Measurements of the Photodissociation Quantum Yields of MbNO and MbO_2 and the Vibrational Relaxation of the Six-Coordinate Heme Species". In: *Journal of the American Chemical Society* 124.20 (2002), pp. 5914–5924. DOI: 10.1021/ja017359n.

[98] Ying Gao et al. "Time-resolved Raman evidence for energy 'funneling' through propionate side chains in heme 'cooling' upon photolysis of carbonmonoxy myoglobin". In: *Chemical Physics Letters* 429.1 (2006), pp. 239–243. DOI: 10.1016/j.cplett.2006.07.085.

[99] Thomas R. M. Barends et al. "Direct observation of ultrafast collective motions in CO myoglobin upon ligand dissociation". In: *Science* 350.6259 (2015), pp. 445–450. DOI: 10.1126/science.aac5492.

[100] Misao Mizuno and Yasuhisa Mizutani. "Role of atomic contacts in vibrational energy transfer in myoglobin". In: *Biophysical Reviews* 12.2 (2020). Publisher: Springer Science and Business Media LLC, pp. 511–518. DOI: 10.1007/s12551-020-00681-w.

[101] Yasuhisa Mizutani and Teizo Kitagawa. "Direct Observation of Cooling of Heme Upon Photodissociation of Carbonmonoxy Myoglobin". In: *Science* 278.5337 (1997), pp. 443–446. DOI: 10.1126/science.278.5337.443.

[102] Cristina Consani et al. "Energy transfer and relaxation mechanisms in Cytochrome c". In: *Chemical Physics* 396 (2012), pp. 108–115. DOI: 10.1016/j.chemphys.2011.09.002.

[103] Leyun Zhu, J. Timothy Sage, and Paul M. Champion. "Observation of Coherent Reaction Dynamics in Heme Proteins". In: *Science* 266.5185 (1994). Publisher: American Association for the Advancement of Science, pp. 629–632. DOI: 10.1126/science.7939716.

[104] Huiyu Li, Shanshan Wu, and Ao Ma. "Origin of Protein Quake: Energy Waves Conducted by a Precise Mechanical Machine". In: *Journal of Chemical Theory and Computation* 18.9 (2022), pp. 5692–5702. DOI: 10.1021/acs.jctc.2c00514.

[105] A Ansari et al. "Protein states and proteinquakes." In: *Proceedings of the National Academy of Sciences* 82.15 (1985), pp. 5000–5004. DOI: 10.1073/pnas.82.15.5000.

[106] A. A. Moosavi-Movahedi. "Formation of the Molten Globule-Like State of Cytochrome c Induced by n-Alkyl Sulfates at Low Concentrations". In: *Journal of Biochemistry* 133.1 (2003), pp. 93–102. DOI: 10.1093/jb/mvg008.

[107] A. A. Moosavi-Movahedi et al. "Electrochemical Evidence for the Molten Globule States of Cytochrome c Induced by N-Alkyl Sulfates at Low Concentrations". In: *Journal of Protein Chemistry* 22.1 (2003), pp. 23–30. DOI: 10.1023/A:1023011609931.

[108] Tianquan Lian et al. “Energy Flow from Solute to Solvent Probed by Femtosecond IR Spectroscopy: Malachite Green and Heme Protein Solutions”. In: *The Journal of Physical Chemistry* 98.45 (1994). Publisher: American Chemical Society (ACS), pp. 11648–11656. DOI: 10.1021/j100096a005.

[109] Diane E. Sagnella and John E. Straub. “Directed Energy “Funneling” Mechanism for Heme Cooling Following Ligand Photolysis or Direct Excitation in Solvated Carbonmonoxy Myoglobin”. In: *The Journal of Physical Chemistry B* 105.29 (2001), pp. 7057–7063. DOI: 10.1021/jp0107917.

[110] Claudius Hoberg et al. “Caught in the act: real-time observation of the solvent response that promotes excited-state proton transfer in pyranine”. In: *Chemical Science* 14.15 (2023). Publisher: Royal Society of Chemistry (RSC), pp. 4048–4058. DOI: 10.1039/d2sc07126f.

[111] C. Hoberg, P. Balzerowski, and M. Havenith. “Integration of a rapid scanning technique into THz time-domain spectrometers for nonlinear THz spectroscopy measurements”. In: *AIP Advances* 9.3 (2019). Publisher: AIP Publishing. DOI: 10.1063/1.5080653.

[112] Virgiliu Botan et al. “Energy transport in peptide helices”. In: *Proceedings of the National Academy of Sciences* 104.31 (2007). Publisher: Proceedings of the National Academy of Sciences, pp. 12749–12754. DOI: 10.1073/pnas.0701762104.

[113] Xin Yu and David M. Leitner. “Anomalous diffusion of vibrational energy in proteins”. In: *The Journal of Chemical Physics* 119.23 (2003), pp. 12673–12679. DOI: 10.1063/1.1626636.

[114] David Arnlund et al. “Visualizing a protein quake with time-resolved X-ray scattering at a free-electron laser”. In: *Nature Methods* 11.9 (2014), pp. 923–926. DOI: 10.1038/nmeth.3067.

[115] Simone Peli et al. “Simplifying asynchronous optical sampling: an experimental approach toward industrial integration exploiting lock-in acquisition”. In: *Applied Optics* 63.23 (2024), p. 6086. DOI: 10.1364/AO.525546.

[116] M. Jewariya et al. “Evaluation of spectral resolution and accuracy in ASOPS THz time-domain spectroscopy”. In: *2011 International Conference on Infrared, Millimeter, and Terahertz Waves*. 2011 36th International Conference on Infrared, Millimeter, and Terahertz Waves (IRMMW-THz 2011). Houston, TX, USA: IEEE, 2011, pp. 1–2. DOI: 10.1109/irmmw-THz.2011.6104859.

[117] Keyu Qu et al. “Structures, properties, and applications of zwitterionic polymers”. In: *ChemPhysMater* 1.4 (2022), pp. 294–309. DOI: 10.1016/j.chphma.2022.04.003.

[118] Mattia Sponchioni et al. “Biodegradable zwitterionic nanoparticles with tunable UCST-type phase separation under physiological conditions”. In: *Nanoscale* 11.35 (2019), pp. 16582–16591. DOI: 10.1039/C9NR04311J.

[119] Umberto Capasso Palmiero et al. “Programmable Zwitterionic Droplets as Biomolecular Sorters and Model of Membraneless Organelles”. In: *Advanced Materials* 34.4 (2022), p. 2104837. DOI: 10.1002/adma.202104837.

Acknowledgements

At the end of this three-year PhD programme, I feel it is deeply important to express my gratitude to all the people who have contributed to and supported me along the way.

My heartfelt thanks go to my supervisor, Professor Renato Torre, for guiding me over these years, for introducing me to the world of research, and for the trust he has always placed in me.

I am especially grateful to Dr. Paolo Bartolini and Dr. Andrea Taschin, with whom I shared my daily work in the laboratory. They have been excellent mentors and invaluable guides since my master's thesis, as well as generous friends.

I would also like to warmly thank Dr. Alice Boschetti, who has always been a source of crucial support and inspiration. Further thanks go to the other current and former members of Professor Torre's research group whom I have had the pleasure to meet over the years: Dr. Sara Catalini, Dr. Pamela Cinfrignini, and the newcomer Dr. Andrea Betti.

A thank also to the other LENS researchers who helped me in studying the biological and polymeric samples: Dr. Claudia Capitini, Dr. Martino Calamai, Dr. Sara Venturi, Dr. Francesca Torrini and Dr. Marta Rojas Rodrìguez.

I am deeply grateful to Professor Martina Havenith for giving me the opportunity to join her research group in Bochum for six months, an experience that was extremely formative and had a significant impact on the completion of my PhD. In this regard, I would like to thank all the members of Professor Havenith's group for welcoming me and making me feel part of the team. Special thanks go to Dr. Adrian Buchmann, with whom I had the pleasure of working on the OPTP measurements, and to Dr. Sanjiana Nalige, with whom I collaborated on the FTIR measurements.

These acknowledgements would not be complete without mentioning the group of PhD students from LENS and the Department of Physics, with whom I shared the challenges and efforts of the PhD journey. Among them, I have found great friends and people of remarkable value.

Finally, I would like to thank my family, who, despite the geographical distance that separates us, have always been by my side, supporting and encouraging me in the most difficult moments.